TotalControl

Advanced integrated supervisory and wind turbine control for optimal operation of large Wind Power Plants

Controller adaptation for varying conditions and ancillary services
Deliverable no. D3.2

Delivery date: 31.10.2019
Lead beneficiary: DNV
Dissemination level: Public

Author(s) information (alphabetical):		
Name	**Organisation**	**Email**
Albert Meseguer Urban	DTU	amur@dtu.dk
Marc de Battista	DNV GL	marc.debattista@dnvgl.com
Harald G Svendsen	SINTEF	harald.svendsen@sintef.no
Salvatore D'Arco	SINTEF	salvatore.darco@sintef.no
Santiago Sanchez	SINTEF	santiago.sanchez@sintef.no

Acknowledgements/Contributions:
Name
Alan Wai Hou Lio, DTU

Document information

Version	Date	Description		
		Prepared by	Reviewed by	Approved by
1	28/10/2019	The authors	Ervin Bossanyi	Ervin Bossanyi

TABLE OF CONTENTS

1 EXECUTIVE SUMMARY

This report describes work carried out as part of TotalControl tasks 3.1.2 and 3.1.3, which are concerned with modification of the active power output of the wind turbine for the purposes of wind farm control and providing ancillary services to the grid system to help with increased penetration of renewables.

The first part of this report develops a strategy for de-rated operation, which is then implemented in the controller software of the 7MW Levenmouth turbine, ready for field testing in the coming year. The second part of the report explores changes to the inverter control which could be used to provide a fast frequency response capability to help stabilise grid frequency.

2 INTRODUCTION

This report covers two types of modification to the operation of the turbine control which are likely to become essential in the context of wind farm control, both involving changing the active power output of the turbine.

De-rated operation, whereby the turbine generates less power than is actually available, serves two main purposes: one is to reduce the severity of wake effects on downstream turbines in a wind farm, with the potential to increase overall wind farm production and decrease fatigue loading, and the other is to comply with grid requests for power reduction or curtailment which may be necessary to help with the operation of the grid system as a whole. Such de-rating can be done relatively gradually, on a timescale of minutes.

The second modification involves rapid changes to the active power production, in a timescale of seconds or less, in response to variations in the grid frequency (fast frequency response). This is likely to be needed to help stabilise the grid frequency, by allowing the turbine rotor inertia to compensate to the total inertia of the grid system inertia.

The first part of the report develops a strategy for de-rated operation, which is then implemented in the controller software of the 7MW Levenmouth turbine, ready for field testing in the coming year. The second part of the report explores changes to the inverter control which could be used to provide the fast frequency response capability.

2.1 TURBINE DE-RATING

Large wind turbines in a wind farm are often curtailed or down-regulated for the purposes of stabilising the power grid or improving the power and load performance of wind farms. For example, the power references for turbines is set to comply with the orders of the power grid operators or down-regulation of the upstream turbines could improve the power production and load performance of the entire wind farm. Typically, in normal operations, the control objective of a wind

turbine is to maximise its power production in the below-rated wind conditions and operate at the rated power in the above-rated wind conditions. The control inputs (pitch angles and generator torque) and rotor speed set-point are pre-defined, leaving limited room to manoeuvre. In contrast, in derated operations, wind turbines operate at a lower efficiency compared to nominal operation, thus, it allows the turbine controller to interpret the power set-point, with more freedom, using different combinations of control inputs and allow both rotor speed and pitch angle to be changed. Consequently, this motivates the development of derating control strategies that not only can track the power set-point, but also take into account other factors such as the fatigue of key turbine components and the generated downstream wake.

Section 3 in this report aims to address the load analysis of turbines under different down-regulating strategies, as part of Task 3.1 of TotalControl. The objective of this study is to understand how the de-rating strategies could affect the Samsung 7MW turbine under various wind operating conditions. In addition, this study also considers both extreme and fatigue loads. In the first part of Section 3, the baseline model comparison is presented, showing the Bladed model of the Samsung 7MW is in good agreement with HAWC2 model. In the second part of Section 3, simulation results are presented under different de-rating strategies and various wind conditions.

In Section 4, this control logic, having been tested in HAWC2 simulations, is implemented into the actual controller code of the 7MW Levenmouth turbine, and Bladed simulations are used to confirm that it operates correctly, and to give confidence that it can be deployed for field testing on that turbine.

2.2 FAST FREQUENCY RESPONSE

With increasing penetration of renewable generation on the grid system, technical issues may arise due to the perceived difficulty of scheduling wind energy production and the loss of direct system inertia linked to non-synchronous production through power converters. However, wind turbines may contribute to the mitigation of some of these problems if suitably configured and controlled. Grid operators are developing markets in ancillary services whereby generators are remunerated for contributing to grid stability and operational efficiency, for example by providing voltage and frequency regulation services. Moreover, it is increasingly being recognised that wind power plants can actively provide some of these services, thereby earning additional revenue. Some of these services are best provided at the wind farm control level as considered in WP2 and WP4, but the high-speed response required for grid frequency support is well handled by the turbine controller. Wind power plants will increasingly have to control their active power output in response to demands from the grid system, through power curtailment and through fast frequency response.

The ability to provide fast frequency response through modifications to the wind turbine converter control system is the focus of Task 3.1.3 in the TotalControl project, and described in sections 0 to 8 of this report. The objective of these investigations is to adapt the virtual synchronous machine (VSM) concept to wind turbine levels and demonstrate its feasibility in numerical simulations. Also, the potential for converters to allow turbine overpowering by temporarily exceeding

converter current ratings is investigated and discussed based on simulation results. The scope of these studies includes the modelling of an offshore wind power plant connected to shore, with detailed representations of the converter circuits and controllers. The study is on a generic level and the main purpose. The final tuning and optimisation of controllers to achieve the best performance is not within the scope of the study. Neither is the thorough testing of the performance in different operating conditions.

Section 0 presents the virtual synchronous machine concept and adaptations of previously developed implementation schemes for wind turbine applications. Section 6 describes a reference model consisting of an offshore wind power plant connected via subsea cables to an onshore grid. This model has been used for numerical analyses of the proposed VSM control schemes for fast frequency response. Section 7 summarizes and discusses the results from these simulations. Section 8 examines the idea of temporary converter overpowering in order to allow additional frequency support.

3   BASELINE HAWC2-BLADED COMPARISON AND LOAD ANALYSIS IN DIFFERENT DOWN-REGULATION STRATEGIES

3.1   BACKGROUND

This section covers part of Task 3.1 of the Total Control project - controller adaptation for varying conditions and ancillary services,

DTU needs to provide to DNV-GL the definition and load analysis of the de-rating strategies to be implemented in the Samsung 7 MW turbine. This section presents the HAWC2-Bladed model baseline comparison based on the available information provided to DTU. Two de-rating strategies and its load analysis are also presented.

Deliverable 3.1. includes an overall description of the Samsung 7 MW turbine and its Design Load Case. In the document "7MW turbine model and reference loadset" it is possible to find the overall wind turbine characteristics as the speed limits, foundation stiffness, mass and damping representative matrices, drive-train characteristics or system natural frequencies. However, tabulated structural and aerodynamic data of the tower and blades are not provided. The provided information was not sufficient to define the aero-servo-elastic model in the in-house tool used by DTU, HAWC2.

In order to enable DTU's task, ORE Catapult shared the Bladed model and a preliminary implementation of the 7MW turbine in HAWC2. DTU decided not to continue with ORE's Catapult implementation in HAWC2 because the model was incomplete, the transformation from the Bladed model unclear and most of the parameters were taken from the reference open-source DTU 10 MW wind turbine. The results presented in this document are based on the

transformation from the Bladed model made by DTU. Additional information was required for further model tuning as steady state operation or power-loss model to complete the turbine.

The original Bladed controller was provided along with the Bladed and HAWC2 model. An attempt to create an interface between the HAWC2 model and the Bladed controller was done by ORE Catapult but its implementation never succeeded. DTU has decided not to continue with the interface implementation due to time limitations and lack of accessibility to the source code, which will raise a problem later on in the implementation of the de-rating strategies.

3.2 MODEL COMPARISON

The standstill frequencies ensure that the principal stiffness and mass properties of the wind turbine are correctly capture. Table 1 presents the first 10 natural frequencies comparison of the Bladed and HAWC2 model.

TABLE 1: STANDSTILL NATURAL FREQUENCY COMPARISON BLADED - HAWC2

Mode Number + ID	Bladed Model	HAWC2 Model	Difference [%]
1 – Tower Fore-aft	0.348	0.357	2.5
2 – Tower Side-side	0.351	0.362	3.1
3 – Flapwise BF sine cyclic	0.529	0.522	-1.92
4 – Flapwise cosine cyclic	0.552	0.547	-1.56
5 – Flapwise collective	0.568	0.574	0.43
6 – Edgewise sine cyclic	0.821	0.846	1.19
7 – Edgewise cosine cyclic	0.831	0.854	0.90
8 – 2nd Flapwise sine cyclic	1.297	1.318	1.10
9 – Edgewise collective	1.410	1.426	-0.67
10 – 2nd flapwise cosine cyclic	1.435	1.475	2.02

The difference between models is contain within the ± 3 % difference. The largest modelling error is present in the tower modes. The jacket structure is not modelled as beam elements since it is included as an "M-C-K" external system. Considering the good agreement for the rest of the nodes, it is possible that the coupling of the jacket structure with the turbine differs between HAWC2 and Bladed. No further investigation has been conducted since the evaluation of the de-rating performance is done with the HAWC2 model and its controller.

ORE Catapult also provided the steady state information. The comparison is shown in Figure 1.
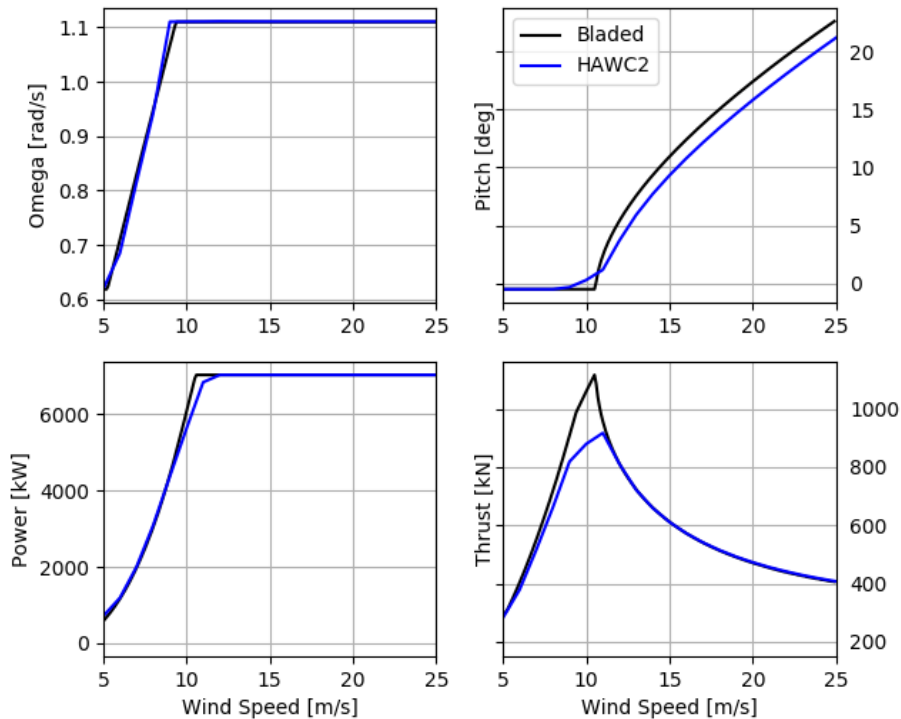
FIGURE 1: STEADY-STATE COMPARISON ROTOR SPEED, PITCH, POWER AND THRUST

The rotor speed and power channels presented in Figure 1 show good agreement. On the other hand, thrust loading present a difference of 18% on the peak-to-peak value. The difference can be explained by the different control strategy applied, note that the HAWC2 controller pitch out when rated rotor speed is achieved while the Bladed model does not.

It is unclear how Ore Catapult has run the steady simulations. DNV-GL suggested that the results might not include the actual control logic of the 7MW controller, which does not include a fine pitch schedule. In order to include fine pitch tuning on the controller, dynamic simulations are needed. This can be easily verified in the future if needed.

Based on the standstill frequencies and the steady-state response comparison, it is agreed that the HAWC2 model represents the overall dynamics of the Samsung 7MW turbine. It is important to keep in mind that the de-rating strategies will use as baseline the HAWC2 model thus, even if model discrepancies with the Bladed model exist on the model, they will be present in both controller operation modes (de-rating and normal).

9

3.3   DESIGN OF THE DOWN-REGULATION CONTROLLER

The DTU down-regulation control strategies are mainly based on the work by [13] and [14], where two different control strategies (max rotation, constant rotation)were proposed. These de-rating strategies are characterised by possessing different rotor speed set-point, representing different operating points in the power (Cp) and thrust (Ct) curve.

As its name suggests, the "max rotation" strategy indicates that in de-rating operations, the rotor speed can reach maximum or rated value when the wind condition is allowed. This is a torque-based down-regulation strategy. In contrast, the "constant rotation" strategy lets the rotor reaches a pre-defined rotor speed set-point. This is achieved by defining the rotor speed set-point based on the de-rating power demand and computing the maximum generator torque accordingly.

Both strategies change the nominal power-set point, thus, the strategies are not adequate for delta-control. The proposed strategies are robust and have a straightforward implementation in the existing controller. DTU can simulate more complex strategies but, due to time constraints and higher implementation difficulty, this report only includes the two presented de-rate strategies.

The actual implementation on the DTU open source controller can be found in a git repository (https://gitlab.windenergy.dtu.dk/OpenLAC/BasicDTUController/blob/master/src/dtu_we_controller/turbine_controller.f90#L254). The implementation of max rotation and constant rotation can be seen in the git repository link provided above. Three de-rate percentages are simulated: 90%, 80% and 70%. For each strategy, the results of the unsteady simulation for control-related channels can be seen in Figure 2 and Figure 3.
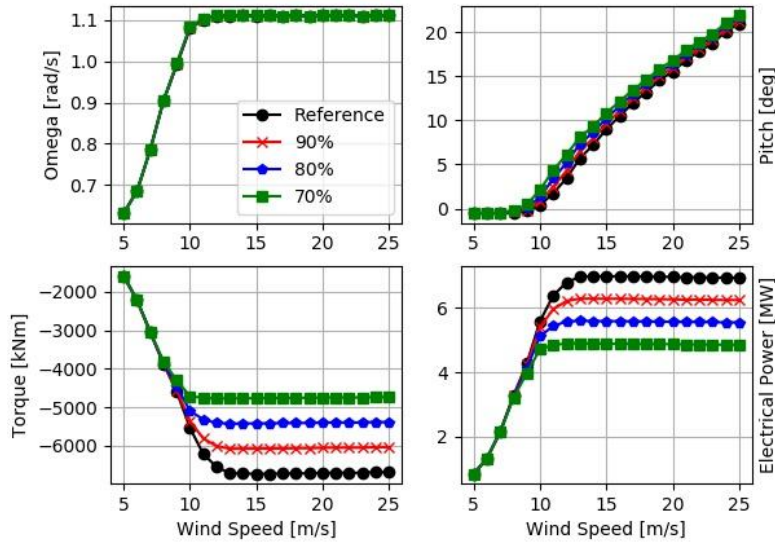
FIGURE 2 UNSTEADY OPERATION COMPARISON MAX. ROTATION DE-RATE STRATEGY
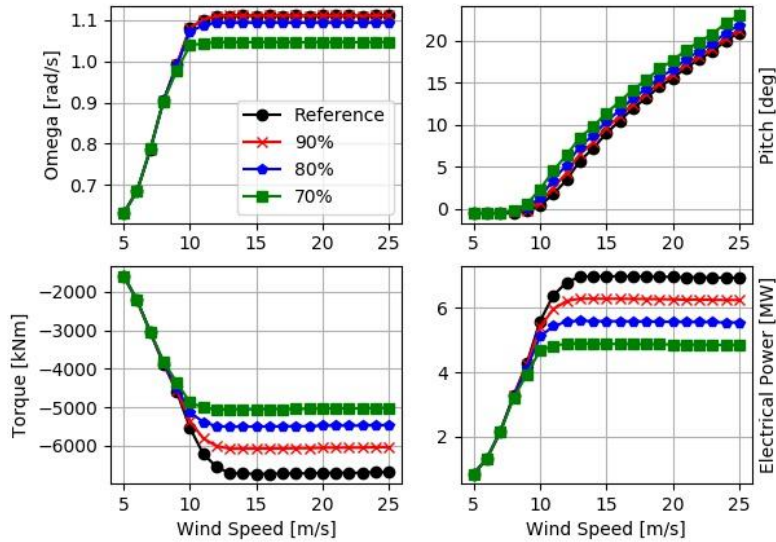
FIGURE 3 UNSTEADY OPERATION COMPARISON CONSTANT ROTATION DE-RATE STRATEGY

In the following subsections, we present the theoretical background of the Basic DTU Wind Energy Controller and down-regulation control strategies.

11

3.3.1 DTU BASIC CONTROLLER – NORMAL OPERATION

Figure 4 shows the operational regions of a typical turbine that use the Basic DTU Wind Energy controller. The nominal controller is defined as follows:

$$\tau_{\mathrm{g}}(t) = \begin{cases} f_{\mathrm{PID}}(\omega(t) - \omega_{\mathrm{min}}), & \omega \leq \frac{1}{2}(\omega_{\mathrm{min}} + \omega_{\mathrm{rated}}) \ \wedge \ \theta(t) \leq \theta_{\mathrm{s}}, \\ f_{\mathrm{PID}}(\omega(t) - \omega_{\mathrm{rated}}), & \omega > \frac{1}{2}(\omega_{\mathrm{min}} + \omega_{\mathrm{rated}}) \ \wedge \ \theta(t) \leq \theta_{\mathrm{s}}, \\ \frac{P_{\mathrm{rated}}}{\omega(t)} \ \text{or} \ \tau_{\mathrm{g,rated}}, & \theta(t) > \theta_{\mathrm{s}}, \end{cases}$$

$$\tau_{\mathrm{g}}(t) \in \begin{cases} [0, K_{\mathrm{opt}}\omega_{\mathrm{min}}^2 \epsilon^+], & \omega(t) \leq \omega_{\mathrm{min}}\epsilon^+ \ \wedge \ \theta(t) \leq \theta_{\mathrm{s}}, \\ [K_{\mathrm{opt}}\omega^2(t), K_{\mathrm{opt}}\omega^2(t)], & \omega_{\mathrm{min}}\epsilon^+ < \omega(t) \leq \omega_{\mathrm{rated}}\epsilon^- \ \wedge \ \theta(t) \leq \theta_{\mathrm{s}}, \\ [K_{\mathrm{opt}}\omega_{\mathrm{rated}}^2\epsilon^-, K_{\mathrm{opt}}\omega_{\mathrm{rated}}^2], & \omega_{\mathrm{rated}}\epsilon^- < \omega(t) \leq \omega_{\mathrm{rated}} \ \wedge \ \theta(t) \leq \theta_{\mathrm{s}}, \end{cases}$$

$$\theta(t) = f_{\mathrm{PID}}(\omega(t) - \omega_{\mathrm{rated}}) \ \in [0, \theta_{\mathrm{max}}],$$

where τ_g and θ are the generator torque and blade pitch angle to the turbine. As shown in Figure 5, the switching mechanism between the partial and full load region is determined by the pitch angle and θ_s. In partial load region, the torque controller regulates the rotor speed ω to either the minimum ω_{min} or rated value ω_{rated}, dependent on the conditions, using a PID controller with anti-windup scheme f_{PID}. In the full load, region, the torque regulates the power at rated P_{rated} or maintains at the maximum torque $\tau_{g,rated}$.

In addition, in the partial region, a set of limits is imposed on the torque input to ensure smooth transient and power maximization. The optimal C_p tracking factor K_{opt} for maximising the power output is defined as follows:

$$K_{\mathrm{opt}} = \frac{1}{2}\rho\pi r^5 C_{\mathrm{p,max}}\lambda_{\mathrm{opt}}^3$$

where ρ, r are the air density and blade length, whilst $C_{p,max}$ λ_{opt} are the maximum power coefficient and optimal tip-speed ratio for maximising the power. The switching variable denotes $\epsilon^+, \epsilon^- \in [0.9; 1.05]$ and the torque limits are depicted in Figure 5, In addition, the blade pitch controller is active to regulates the rotor speed to its rated value via a PID controller.
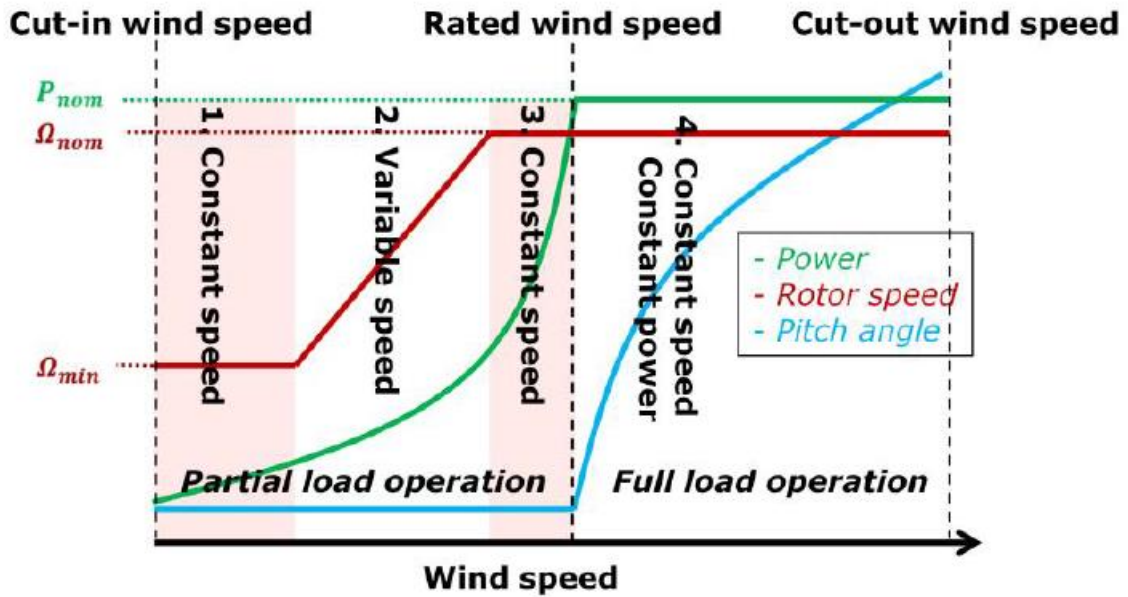
FIGURE 4 OPERATIONAL REGINS OF A TYPICAL TURBINE USING THE BASIC DTU WIND ENERGY CONTROLLER .
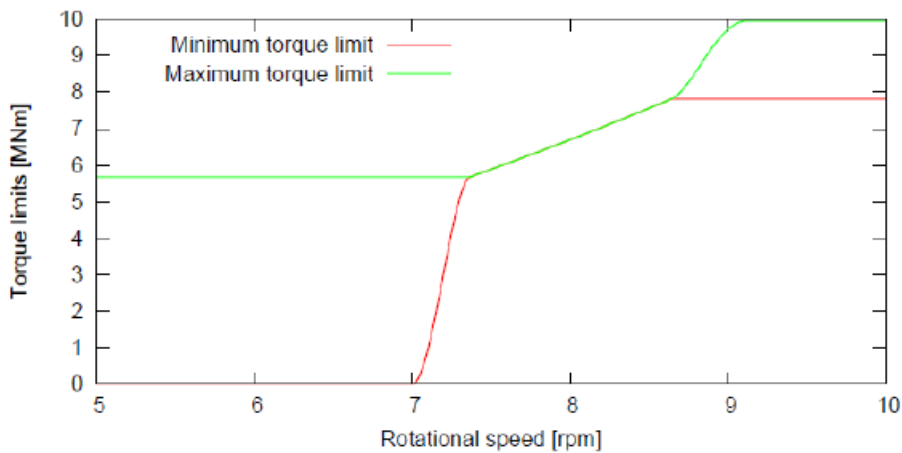
FIGURE 5 THE TORQUE LIMITS IN THE PARTIAL LOAD REGION OF THE DTU10MW REFERENCE

3.3.2 DOWN-REGULATION CONTROL STRATEGIES

The power produced by a turbine is the generator torque times the generator speed. Down-regulation can be achieved by either manipulating the generator torque or rotor speed set-point [14]. Therefore, two types of methods are considered in this work: torque-based and rotor-speed-based down-regulation strategies.

3.3.2.1 MAX ROTATION DOWN-REGULATION STRATEGY

The max rotation strategy is a torque-based strategy, which performs turbine down-regulation by changing the generator torque input solely. One of the benefits of such a strategy is that during

power curtailments, the rotor speed is operating at rated and thus reserving the maximum amount of spinning energy for providing fast frequency response support to the grid. To implement the max rotation strategy, a new maximum torque limit $\bar{\tau}_{g,derated}$ is imposed on the generator torque, defined as follows:

$$\bar{\tau}_{g,\text{derated}} = \frac{P_{\text{derated}}}{\omega_{\text{rated}}},$$

Where $P_{derated}$ denotes the derated power set-point.

3.3.2.2 CONSTANT ROTATION DOWN-REGULATION STRATEGY

In this strategy, down-regulation is performed by defining the rotor speed set-point and the generator torque is updated accordingly. There are numerous advantages to this strategy. For example, the turbines operating in lower rotor speed produce lower noise and also lower fatigue loads on the tower. To perform the rotor-speed-based strategy, the original rated rotor speed and generator torque limit needs to be modified as follows:

$$\omega_{\text{derated}} = \sqrt[3]{\frac{P_{\text{derated}}}{K_{\text{opt}}}}, \quad \bar{\tau}_{g,\text{derated}} = \frac{P_{\text{derated}}}{\omega_{\text{derated}}}$$

3.4 SIMULATION SET-UP

DLC 1.2 is run from cut-in to cut-out every 1 m/s including two misaligned cases, ±10°. Each combination is run for 2 hours, twelve ten-minute simulation, to decrease seed dependency. The total number of simulations, for the normal operation is 756. The same set-up is repeated for each de-rate strategy and de-rate percentage where the same turbulence boxes are used for the de-rate cases to have a direct comparison with the normal operation case. The loads do not include any partial safety factor.

The HAWC2 coordinate system is shown in Figure 6.
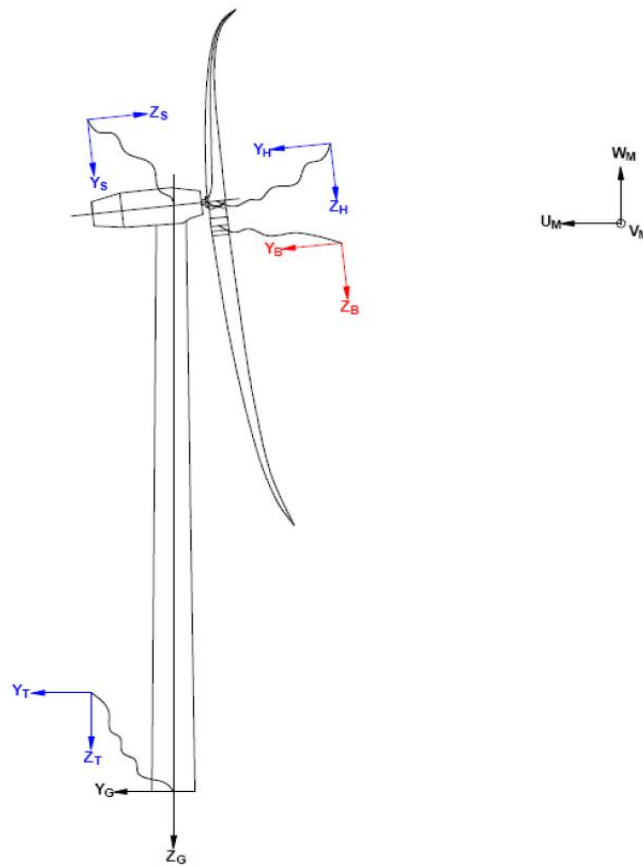
FIGURE 6: HAWC2 COORDINATE SYSTEM

The channels presented in this report and its coordinate system are listed. In case further explanation is needed for the coordinate system please check the HAWC2 manual (www.hawc2.dk). The units of each of the channels are included in the figures, thus, not included here.

- **Omega:** rotor speed at the low-speed shaft of the wind turbine

- **Pitch:** rotation angle taken at the blade bearing

- **Torque:** moment taken from the generator servo model coupled with the controller

- **Electrical Power:** electrical power taken from the generator servo model coupled with the controller

- **TB Fx, Fy, Fz:** Force in (x,y,z) referred to tower local coordinate system at the first tower node.

- **TB Faft, TB S-s, TB Yaw**: Moment in Fore-aft (Faft), Side-side (S-s) and Yaw referred to tower local coordinate system at the first tower node.

- **B Fx, B Fy , B Fz:** Force in (x,y,z) referred to blade local coordinate system at first blade node. All the presented statistics include the three blades.

- **BF, BE and BZ:** Blade Flapwise (BF), Blade Edgewise (BE) and Blade Torsional (BZ) moments referred to blade local coordinate system at first blade node. All the presented statistics include the three blades.

- **S. Tx:** Shaft Torsion (S. Tx) moment referred to shaft local coordinate system at third node (corresponds to generator).

- **Pitch activity:** Standard deviation of pitch angle.

In section 3.5, the mean, extreme and fatigue loads for both strategies are presented as function of wind speed. For control-related outputs, fatigue is not included. The plots provide a quick analysis of the different de-rating strategies in each controller region. The results are divided in control, tower loads, blade loads and shaft torsion and pitch activity. The extreme and fatigue maximum difference over the complete operation is shown in subsection 3.5.4.

It is decided not to compute lifetime equivalent load since the de-rating strategies will not be applied for an extended period. The presented comparison as function of wind speeds aims to provide information on the load variation of the main wind turbine components if a chosen de-rate strategy is applied at certain wind speed.

3.5 RESULTS

3.5.1 OPERATION UNSTEADY WIND TURBINE: MEAN CONTROL

Regarding the steady-state operating points of the turbines under two de-rating strategies, see Figure 2 and Figure 3.

3.5.2 OPERATION UNSTEADY WIND TURBINE: MEAN LOADS

In this section, loads of different sensors are presented for each de-rating strategy.

3.5.2.1 TOWER BASE LOAD CHANNELS
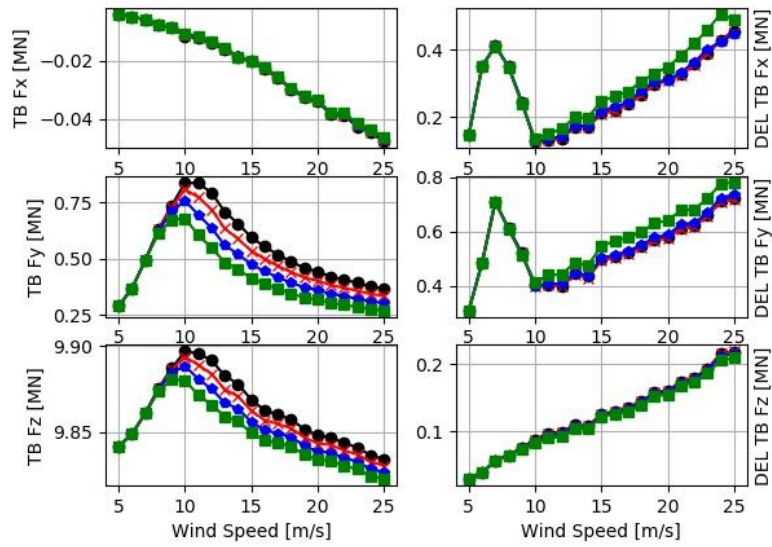
FIGURE 7: UNSTEADY OPERATION COMPARISON CONSTANT ROTATION DE-RATE STRATEGY TOWER FORCES

FIGURE 8: UNSTEADY OPERATION COMPARISON CONSTANT ROTATION DE-RATE STRATEGY TOWER MOMENTS

17

De-rate Max Rotation Tower

FIGURE 9: UNSTEADY OPERATION COMPARISON MAX. ROTATION DE-RATE STRATEGY TOWER FORCES

De-rate Max. Rotation Tower
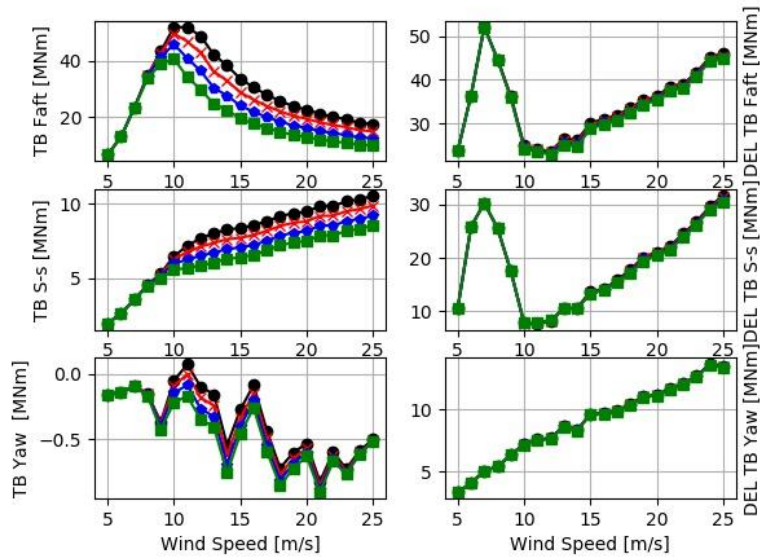
FIGURE 10: UNSTEADY OPERATION COMPARISON MAX. ROTATION DE-RATE STRATEGY TOWER MOMENTS

3.5.2.2 BLADE LOAD CHANNELS
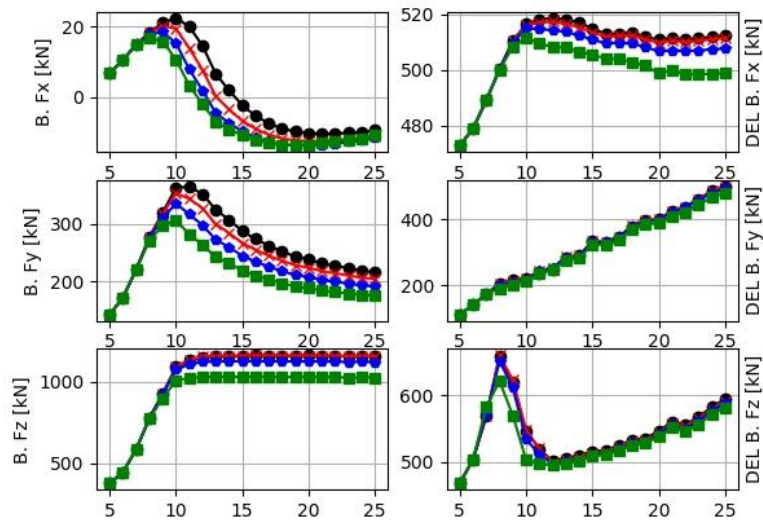
FIGURE 11: UNSTEADY OPERATION COMPARISON CONSTANT ROTATION DE-RATE STRATEGY BLADE FORCES
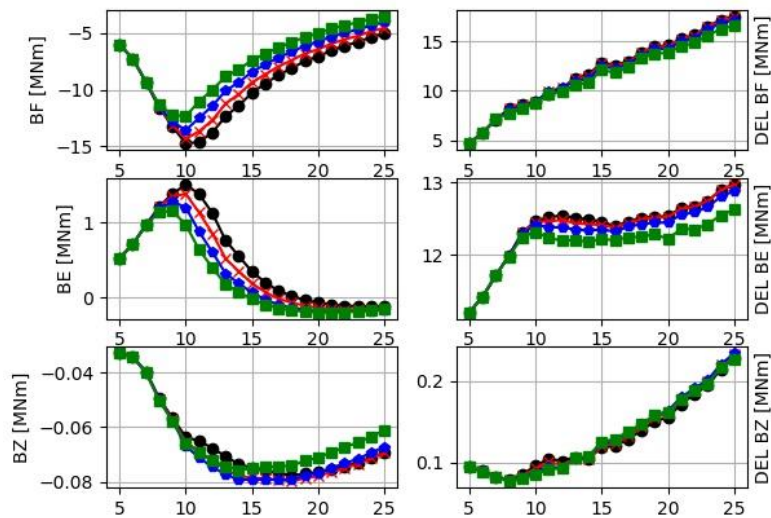
FIGURE 12: UNSTEADY OPERATION COMPARISON CONSTANT ROTATION DE-RATE STRATEGY BLADE MOMENTS

De-rate Max. Rotation Blades
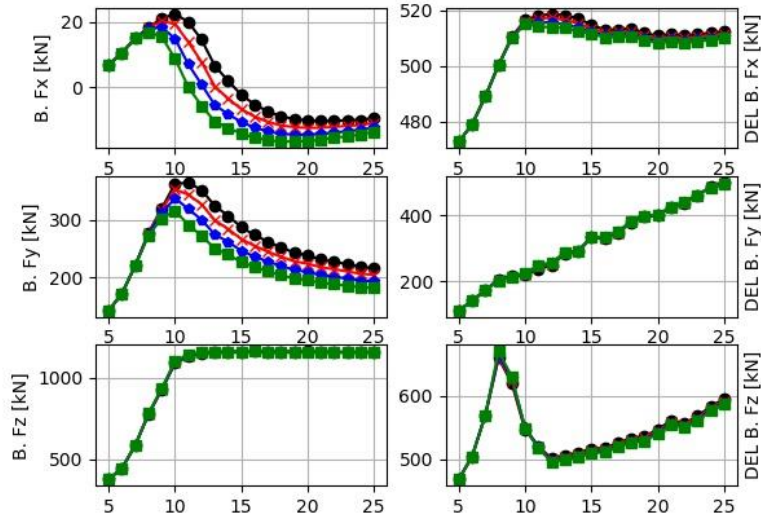
FIGURE 13: UNSTEADY OPERATION COMPARISON MAX. ROTATION DE-RATE STRATEGY BLADE FORCES
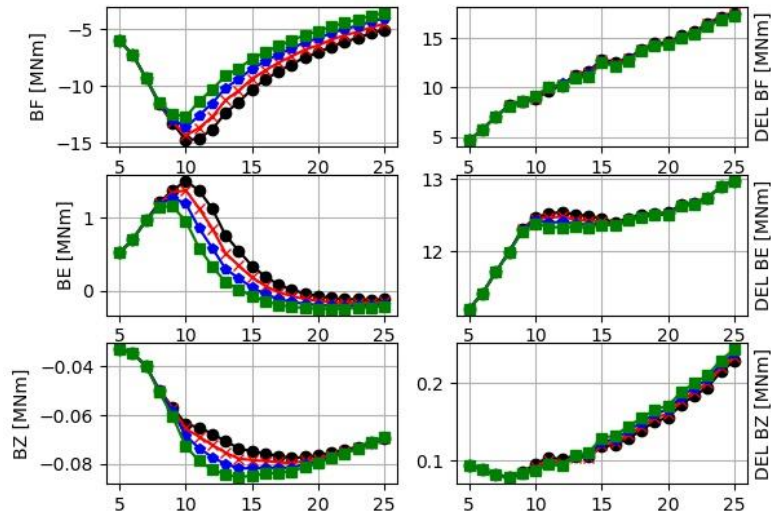
FIGURE 14: UNSTEADY OPERATION COMPARISON MAX. ROTATION DE-RATE STRATEGY BLADE MOMENTS

3.5.2.3 SHAFT TORSION AND PITCH ACTIVITY
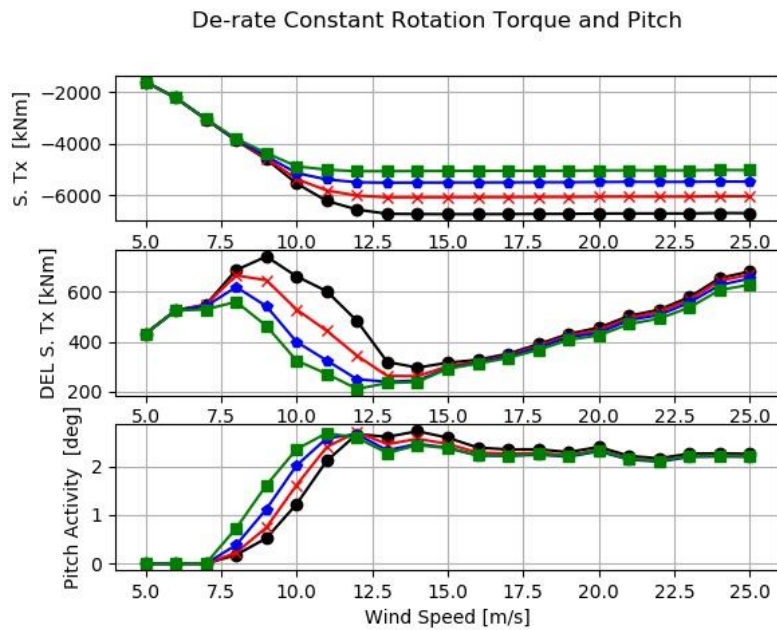
FIGURE 15: UNSTEADY OPERATION COMPARISON CONSTANT ROTATION DE-RATE STRATEGY SHAFT TORSION AND PITCH
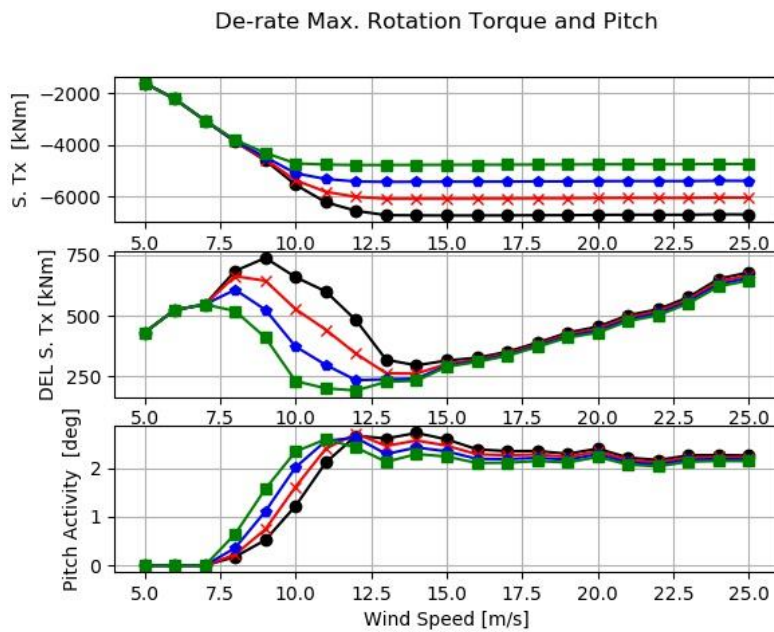
FIGURE 16: UNSTEADY OPERATION COMPARISON MAX. ROTATION DE-RATE STRATEGY SHAFT TORSION AND PITCH

3.5.3 OPERATION UNSTEADY WIND TURBINE: EXTREME LOADS COMPARISON

Now, we consider the extreme loads in this section for both de-rating strategies.

3.5.3.1 TOWER LOAD CHANNELS
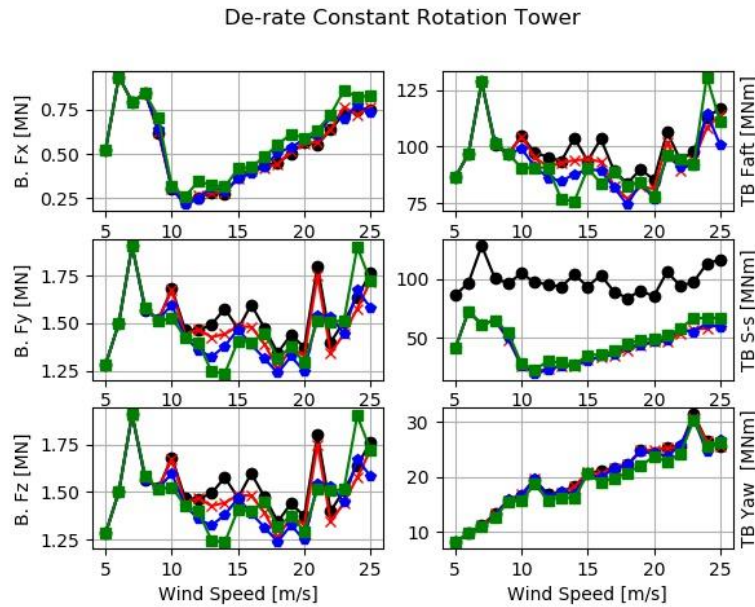
FIGURE 17: UNSTEADY EXTREME COMPARISON CONSTANT ROTATION DE-RATE STRATEGY TOWER LOADS
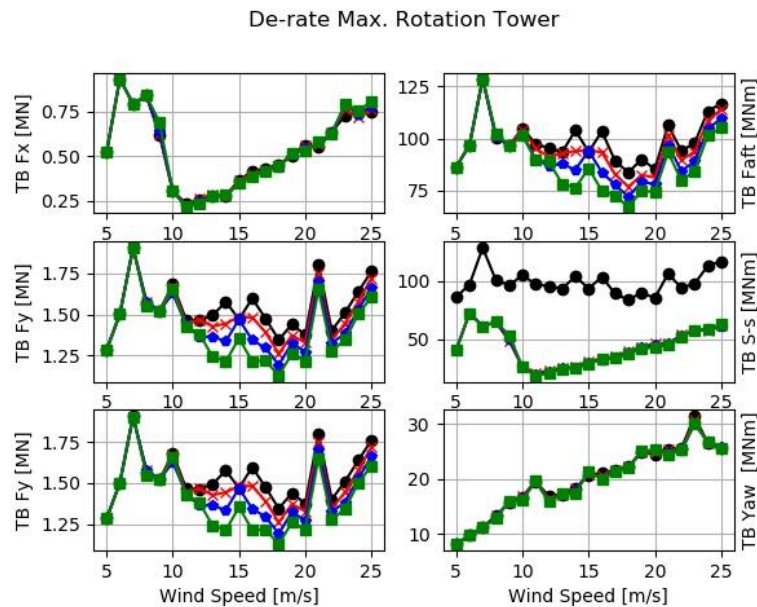
FIGURE 18: UNSTEADY EXTREME COMPARISON MAX. ROTATION DE-RATE STRATEGY TOWER LOADS

3.5.3.2 BLADE LOAD CHANNELS
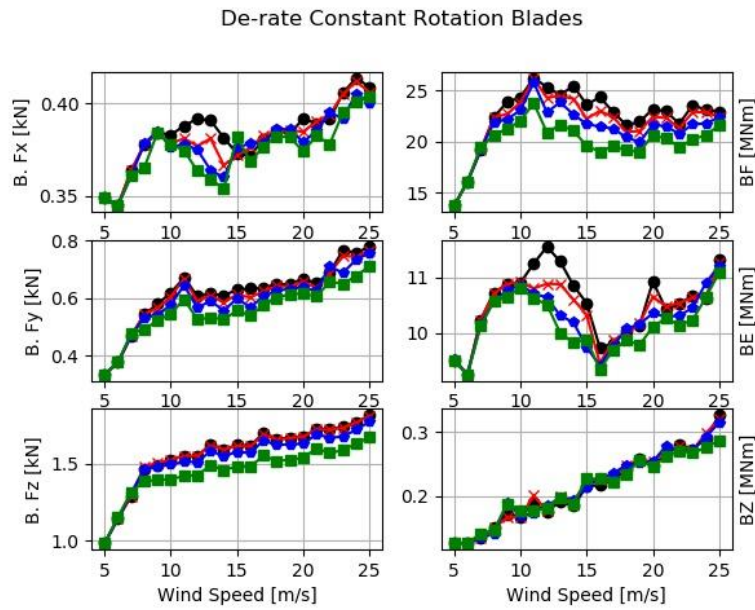
FIGURE 19: UNSTEADY EXTREME COMPARISON CONSTANT ROTATION DE-RATE STRATEGY BLADE LOADS
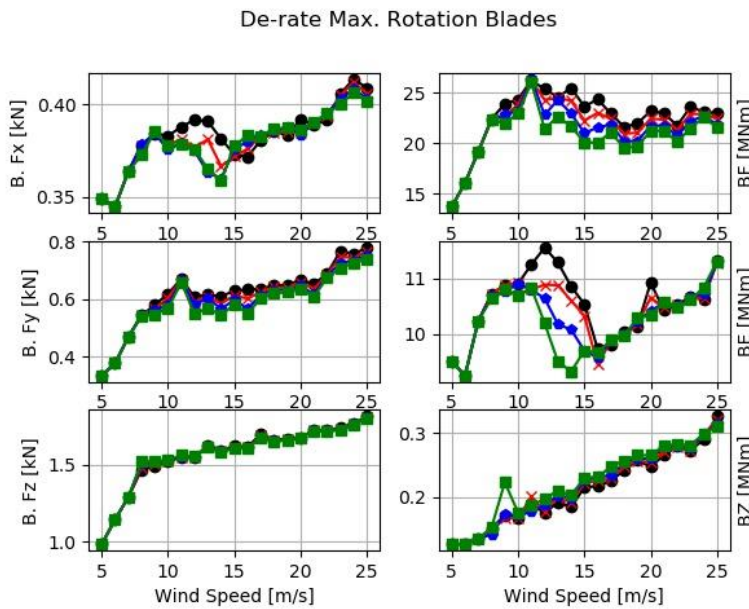
FIGURE 20: UNSTEADY EXTREME COMPARISON MAX. ROTATION DE-RATE STRATEGY BLADE LOADS

23

3.5.3.3 SHAFT TORSION
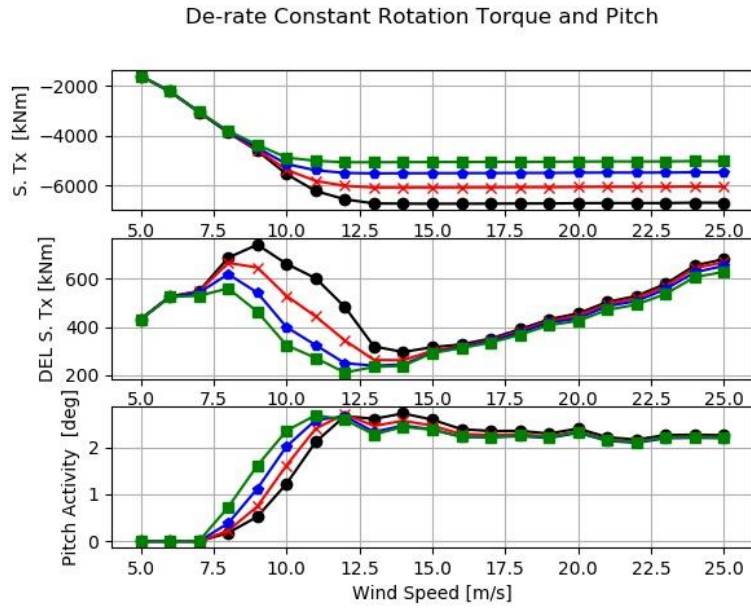
FIGURE 21: UNSTEADY EXTREME COMPARISON CONSTANT ROTATION DE-RATE STRATEGY SHAFT TORSION LOADS
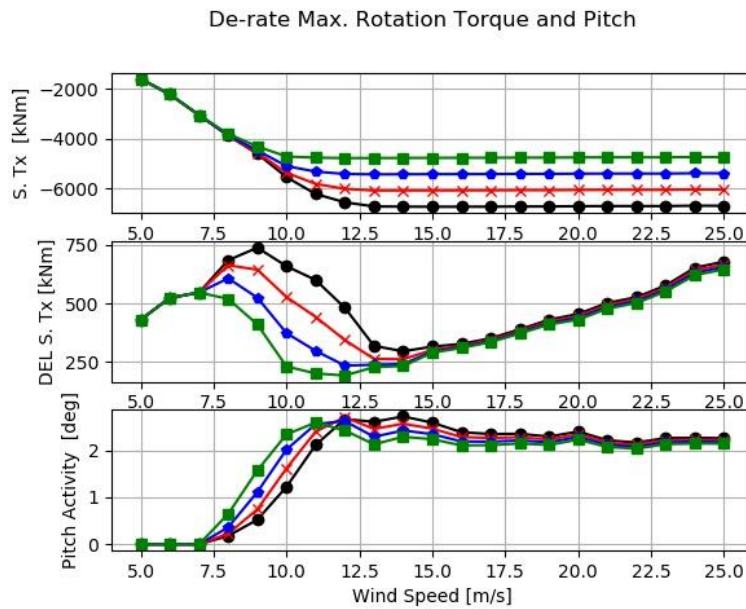
FIGURE 22: UNSTEADY EXTREME COMPARISON MAX. ROTATION DE-RATE STRATEGY SHAFT TORSION LOAD

24

3.5.4   EXTREME AND FATIGUE COMPARISON

In this section, the maximum difference over the complete operation range is plotted. Figure 23 and Figure 24 should be interpreted as: "If a value larger than 1 is found for a given channel, a larger value than the normal operation case at the same wind speed exists". These plots provide a summary of the extreme and fatigue variation as function of wind speed previously presented. The "F" corresponds to fatigue while "E" corresponds to extreme.
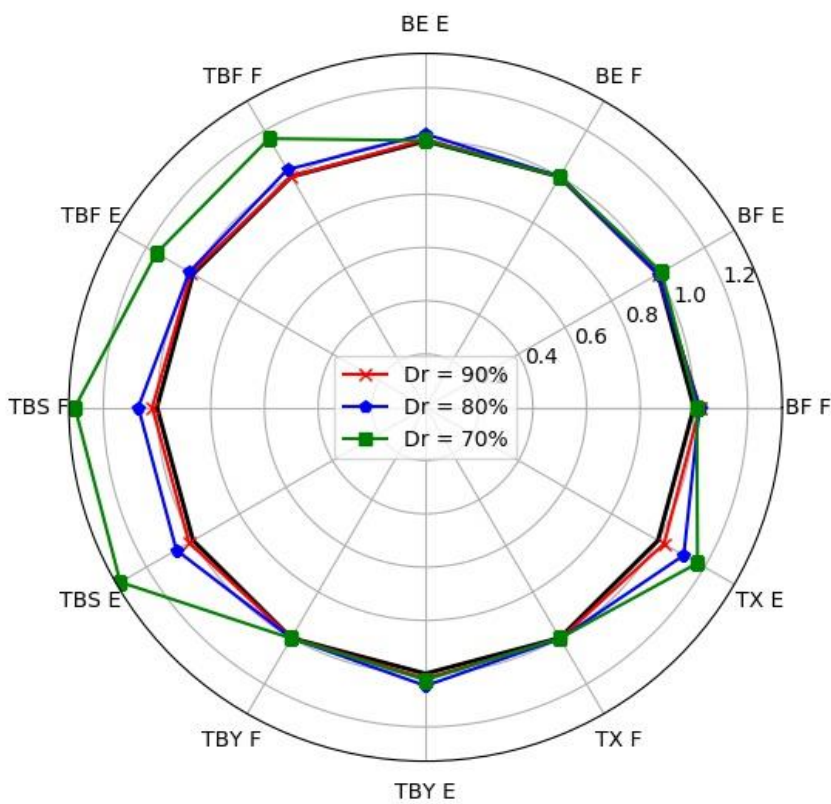
FIGURE 23: COMPARISON EXTREME AND FATIGUE LOADS CONSTANT ROTATION DE-RATE STRATEGY
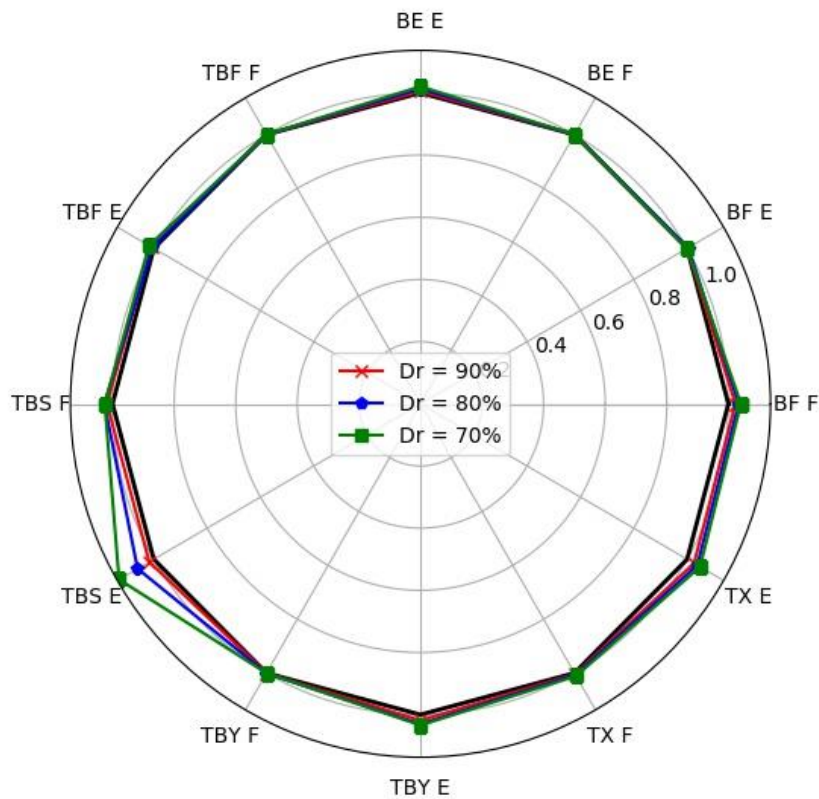
FIGURE 24: COMPARISON EXTREME AND FATIGUE LOADS MAX. ROTATION DE-RATE STRATEGY

3.6 CONCLUSIONS

The first part of the report presents the baseline model comparison where good agreement is found for the standstill frequencies and steady-state turbine response. The peak-to-peak thrust difference is 18%, which indicates that the Bladed model might have not been run with the correct gain scheduling strategy. The de-rating strategies, loads and set-up are also described.

The second part of the report focuses on the comparison of both de-rating strategies at various power set-points with normal operation. The different operation of max rotation and constraint rotation can be seen in **Error! Reference source not found.** and **Error! Reference source not found.** respectively. The max rotation strategy keeps the rotor speed to is nominal value while the constant rotation decreases it as function of de-rate percentage. This has an influence in both blade pitch angle and torque due to the different wind turbine operation. The de-rate power curves look correct for both cases presenting the de-rate power defined by the user (90%, 80% and 70% of rated).

The mean and fatigue tower loads are presented in subsection 3.5.2.1. The operation of the de-rating and normal controller is the same before the constrained power starts which corresponds to around 8-9 m/s for the 70% case. On the fore-aft and side-side direction, an increase of the fatigue can be seen from 6m/s to 9m/s. This phenomenon occurs due to the tower fore-aft and

side-side excitation caused by the 3P. The issue can be solved by including a rotor-speed exclusion zone in the controller. An implementation of such strategy on the controller should attenuate the peak observed in fatigue. This is not relevant for the comparison presented in this report since occurs before the power is constrained (all controller shows the same peak).

The mean tower loads are decreased for both strategies with the produced power. The 70% de-rate percentage presents the lower mean value as function of wind speed. On the other hand, fatigue is increased when the constant rotation is applied, presenting the larger discrepancies on the 70%. This can also be observed in Figure 23 where differences larger than 20% on fatigue and extremes are found for the tower related channels. The maximum rotation speed de-rate strategy generally shows reduction on fatigue and extreme load related channels.

Different behaviour is found for the blades. The constant rotation de-rate strategy reduces both flapwise and edgewise fatigue while the maximum rotation de-rate strategy has barely an impact. The mean and extreme loads are reduced by both strategies. Both strategies also present a decrease on mean and fatigue shaft torsion loading with an increase in pitch activity.

Based on the HAWC2 model of the 7MW Samsung turbine coupled with the open-source DTU controller and considering the modelling limitations DTU had during this time it is possible to conclude that, both control strategies can be used without increasing extreme or fatigue loading when de-rate percentages of 90% and 80% are used. On the other hand, the 70% de-rate for the constant rotation strategy increase the tower-related channels which seems to be related to the previously explained coupling between the 3P and tower natural frequencies.

In the appendix A, the comparison of extreme and fatigue as function of wind speed for each de-rate percentage and de-rate strategy is presented.

4 IMPLEMENTATION IN *BLADED*

4.1 INTRODUCTION

DTU described two derating algorithms in the previous section. These are
1. 'Max Rotation' (see 3.3.2.1)
2. 'Constant Rotation' (see 3.3.2.2)

The 'Max Rotation' power derating strategy simply reduces rated generator torque in line with the derating percentage request. The generator speed setpoint is kept at its rated value for all derating percentages and wind conditions.

The 'Constant Rotation' power derating strategy reduces power by moving the turbine's operating point along the optimal mode gain curve (i.e: generator torque Vs Generator speed steady operating curve). The generator speed setpoint therefore varies between rated generator speed

setpoint (406rpm), and minimum generator speed setpoint (178rpm). The generator torque setpoint is equivalent to the derated power setpoint divided by the derated generator speed set-point.

The Samsung 7MW turbine control algorithm uses three features that are not implemented in the DTU algorithm documented in the previous section:

1. A generator speed exclusion zone (215rpm-344rpm) to avoid exciting the tower first fore-aft mode through a 3P rotational harmonic clash when operating the turbine in the variable speed mode.
2. A fine pitch schedule based on power to reduce thrust forces around rated wind speed by increasing the fine pitch angle as electrical power approaches its rated value.
3. Individual pitch control (IPC) to reduce asymmetrical hub / blade / yaw loads.

The implementation of DTU's derating algorithms was added to the control algorithm software currently deployed on the Samsung 7MW turbine. It was tested by running several simulations in steady and turbulent wind conditions. Derating percentages tested and reported in this section are 20%, 40%, 60%, 80%, 100%.

The testing demonstrates that the derating algorithms operate as expected, and that the turbine does not operate within the generator speed exclusion zone.

4.2 DERATING THE TURBINE

Derating the turbine in the field is done via the following 3 input channels:
- CI_AlgPowerDerateEnable   (0 = disabled, 1 = enabled)
- CI_AlgPowerFractionDTU   (Power fraction [0,1] of rated power)
- CI_AlgPowerDerateAlg   (0 for 'Constant Rotation', 1 for 'Maximum rotation')

Another feature of the current control algorithm is a noise reduction strategy. Power derating according to DTU's strategies is only permitted if the noise reduction strategy is not in use (CI_AlgNoiseModeEnabled = false).

For Win32 simulations in Bladed, the following parameters can be used instead of the CI_XXX channels:
- P_PowerDerateEnable
- P_PowerFractionDTU
- P_PowerDerateAlg

An additional parameter P_PowerFractionDTUafterFaultN09 is provided to both set P_PowerDerateEnable to true and P_PowerFractionDTU to the provided value in P_PowerFractionDTUafterFaultN09 when the emergency stop button linking to safety system #9 is triggered during the simulation. This provides a mechanism to test the transient response of the algorithm.

4.3 MAX ROTATION STRATEGY

4.3.1 STEADY WIND

Steady wind simulations were run from 4m/s to 24 m/s wind speed in 0.5m/s steps.

After 50 seconds the power fraction is decreased from 100% to 80%, 60%, 40% or 20%. The average value of pitch angle, generator speed, generator torque and electrical power is calculated over the last 50 seconds of each 300 second simulations to produce steady state curves.

FIgure 25 to Figure 27: STEADY Torque trajectories FOR MAX ROTATION DERATING STRATEGY below show the results for Electrical power, generator speed and torque, and pitch angle.

As the strategy is Max Rotation, the generator speed remains at the rated speed value, as expected.
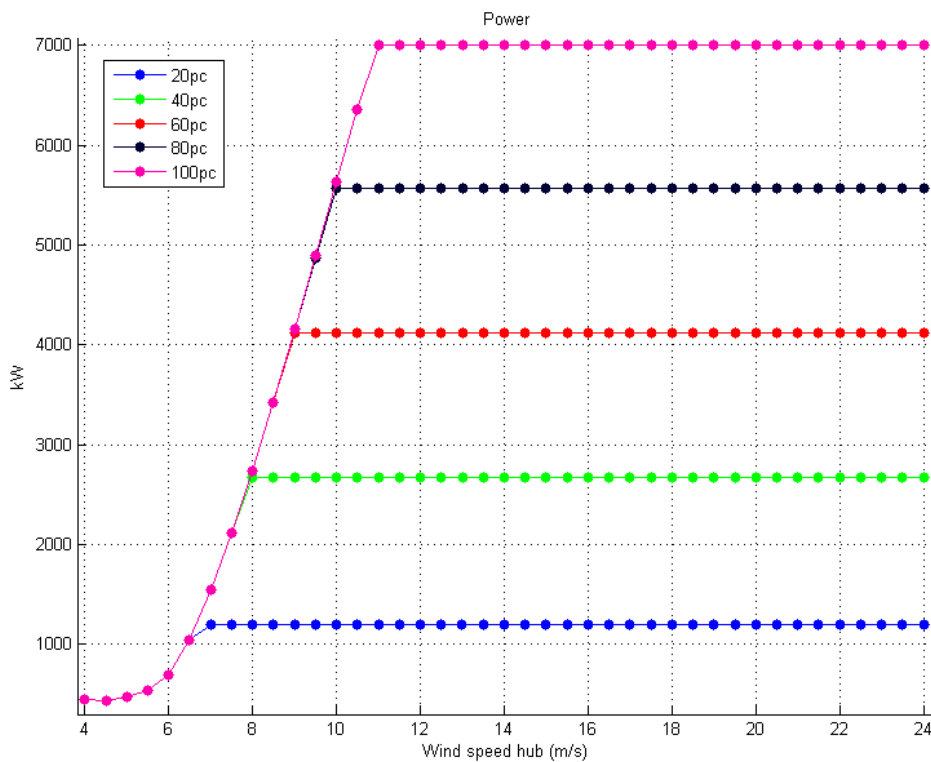
FIGURE 25: STEADY POWER CURVE FOR MAX ROTATION DERATING STRATEGY
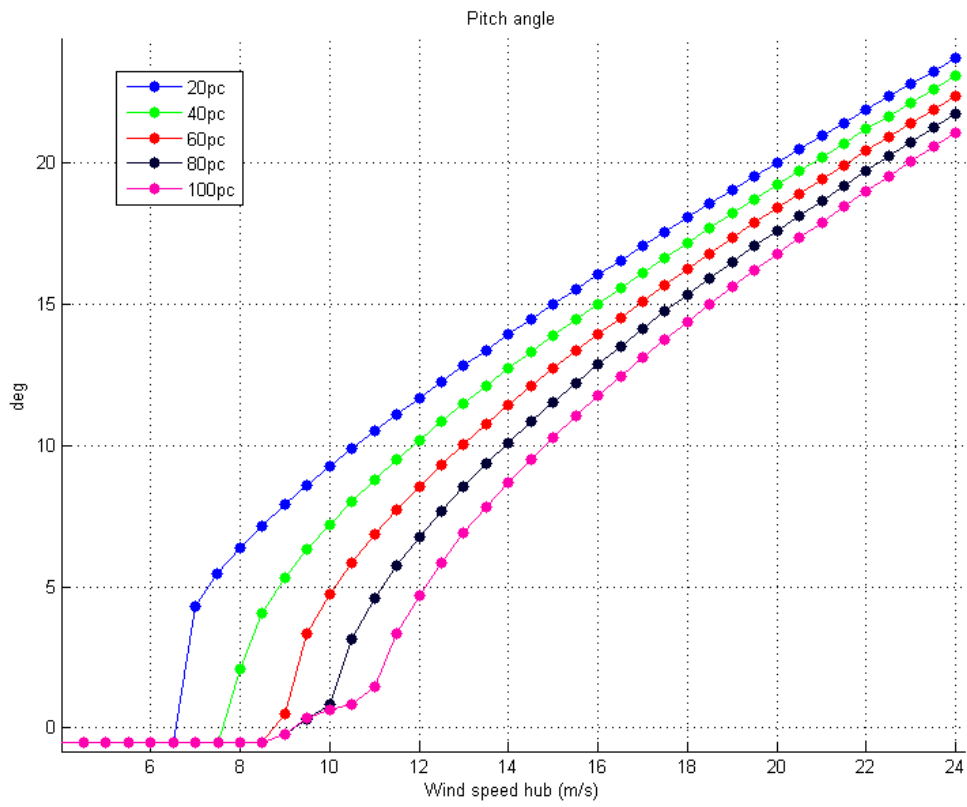
FIGURE 26: STEADY PITCH TRAJECTORIES FOR MAX ROTATION DERATING STRATEGY
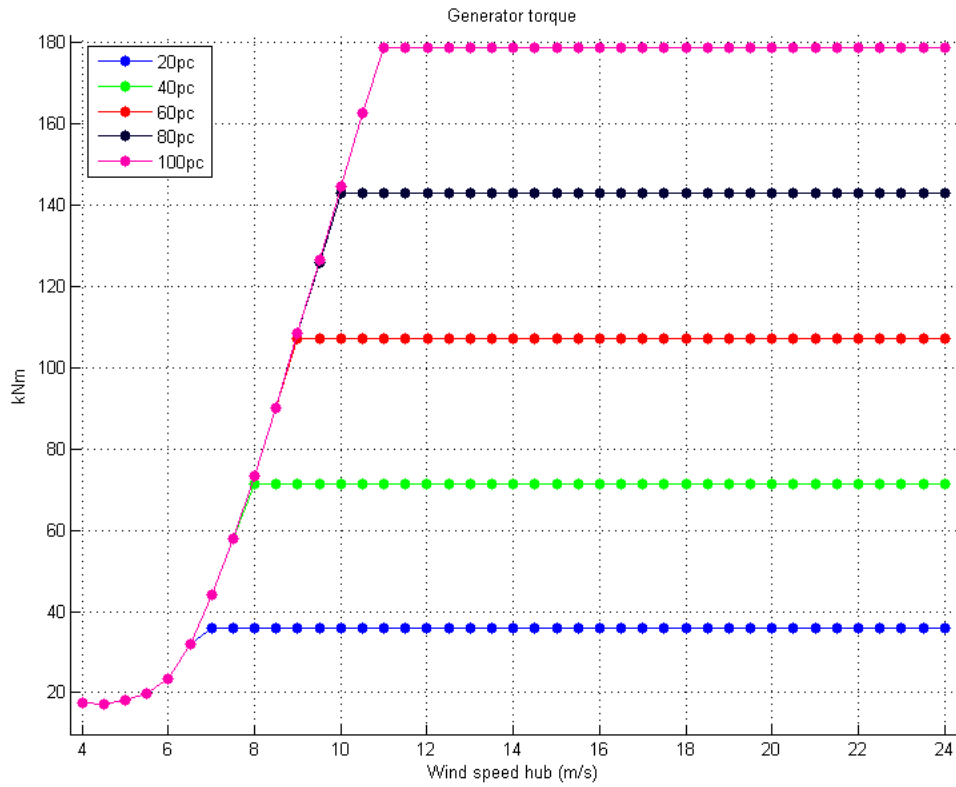
FIGURE 27: STEADY TORQUE TRAJECTORIES FOR MAX ROTATION DERATING STRATEGY
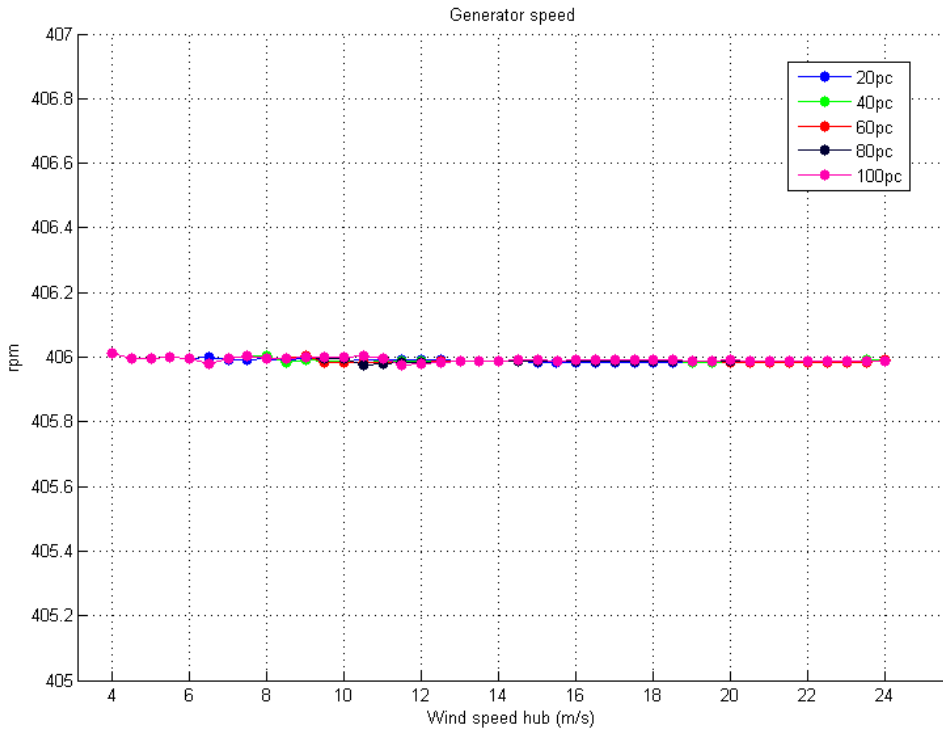
FIGURE 28: STEADY GENERATOR SPEED TRAJECTORIES FOR MAX ROTATION DERATING STRATEGY

4.3.2 TURBULENT WIND

Plots in this section show results when the Max Rotation derating percentage is 80%.

Time histories of Electrical power, generator speed & torque, and pitch angle are presented in Figure 29 to Figure 32 below.

As in the steady wind case, the derating percentage is changed 50 seconds into the simulation.

Figure 33 shows the new torque-speed curve derived when instantaneous generator torque is plotted against the generator speed, for all wind conditions and derating percentages. The data shown on that plot is from 250 seconds to the end of simulations, to avoid transients occurring at the beginning of each simulation. As expected, the turbine only operates at rated generator speed by varying generator torque between rated value and 0 Nm.
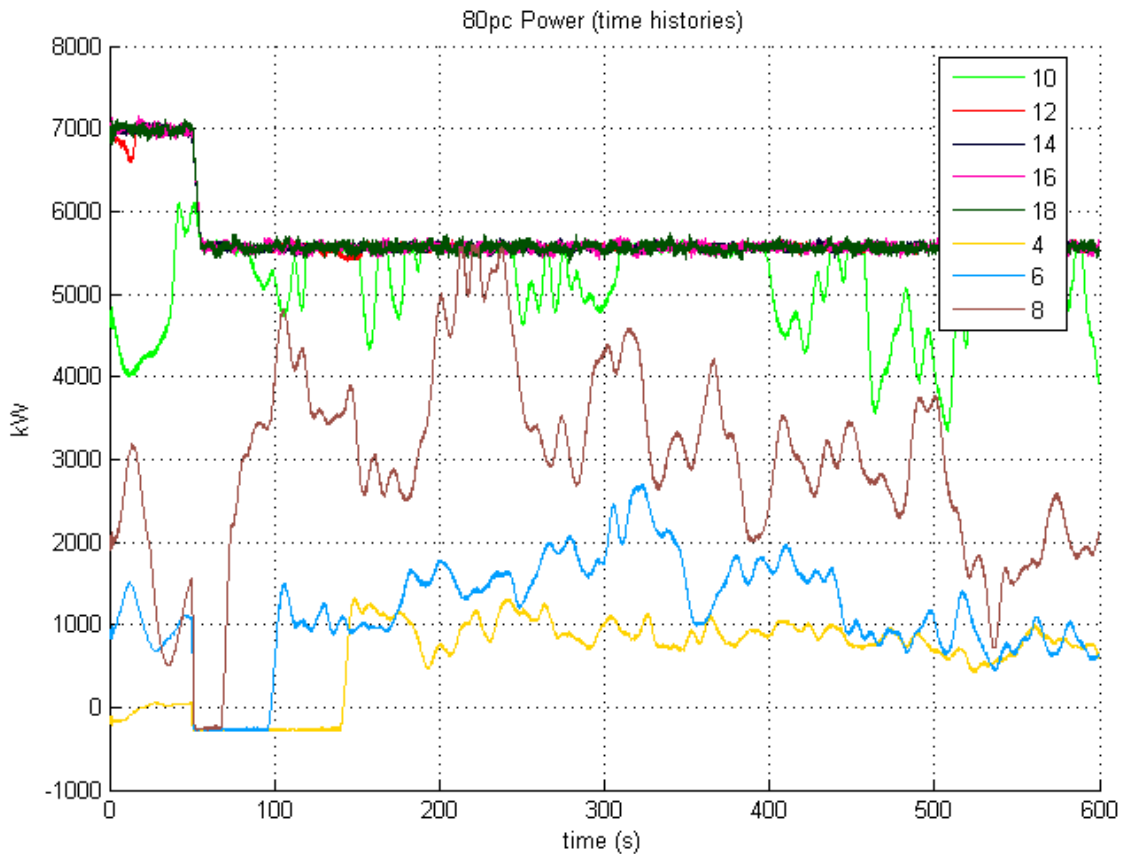
FIGURE 29: ELECTRICAL POWER TIME HISTORIES FOR 80% DERATING (MAX ROTATION)
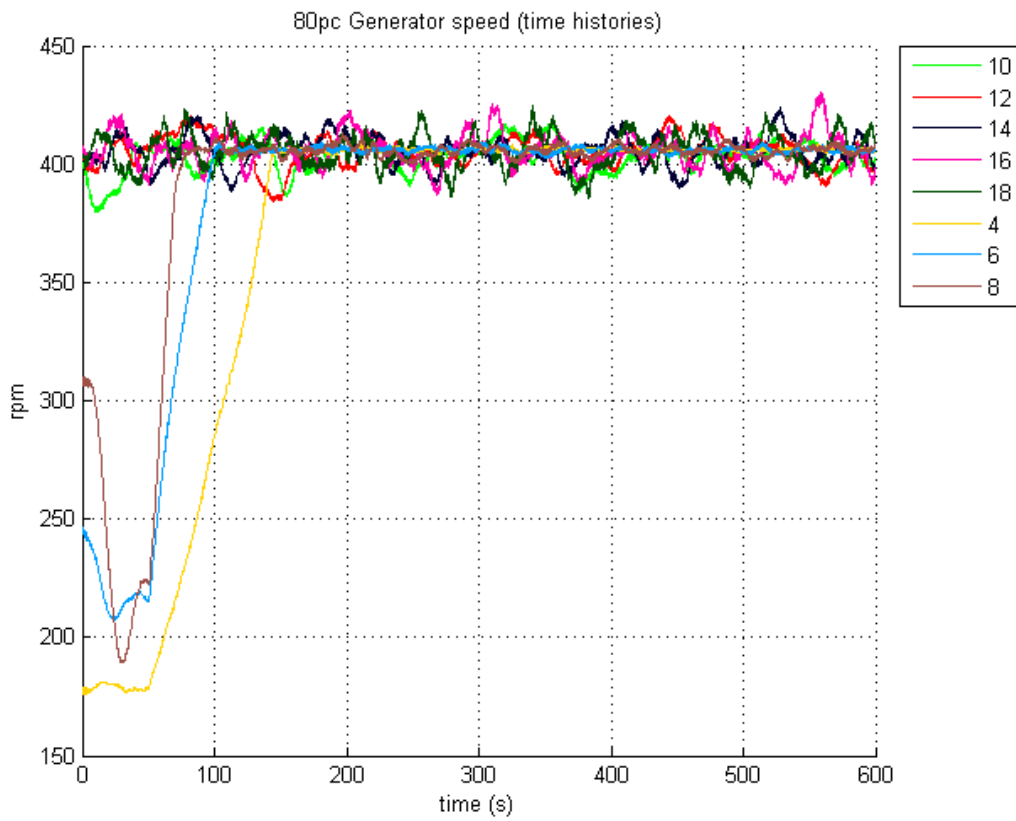
FIGURE 30: GENERATOR SPEED TIME HISTORIES FOR 80% DERATING (MAX ROTATION)
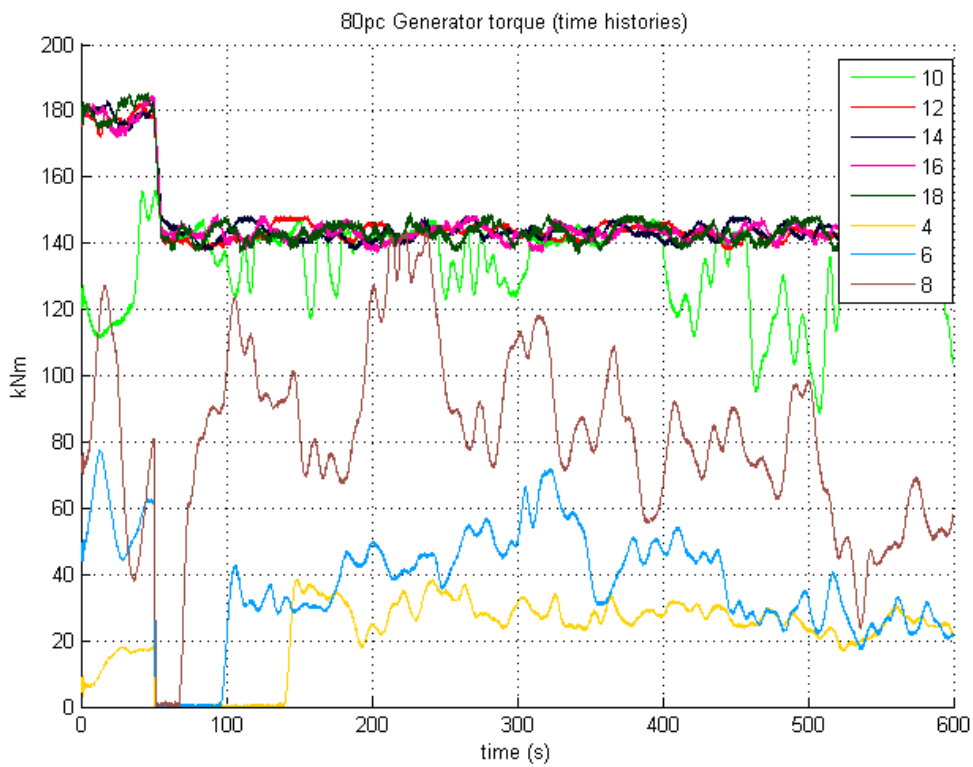
FIGURE 31: GENERATOR TORQUE TIME HISTORIES FOR 80% DERATING (MAX ROTATION)
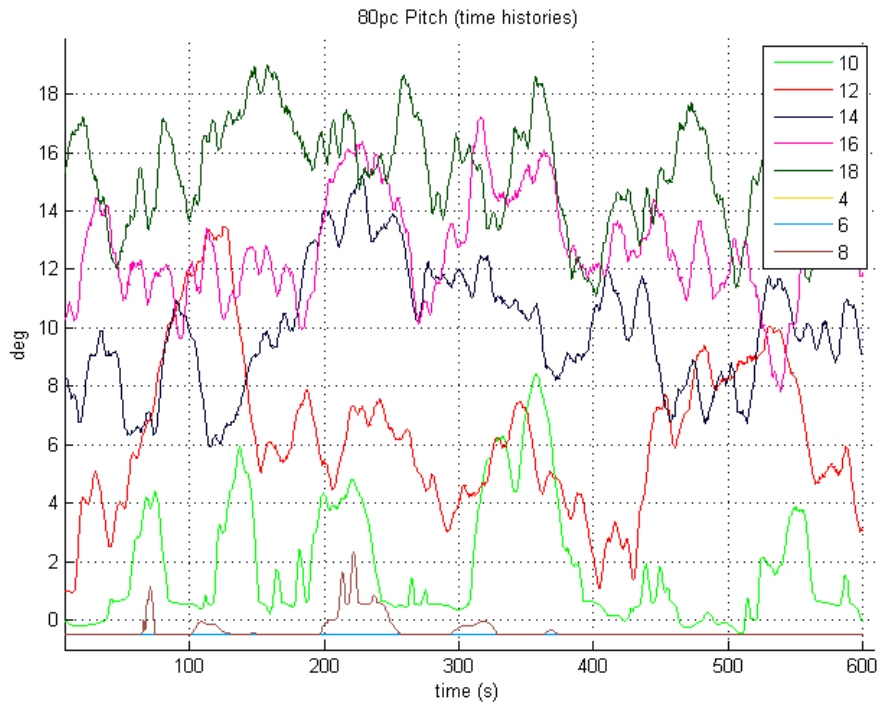
FIGURE 32: PITCH TIME HISTORIES FOR 80% DERATING (MAX ROTATION)
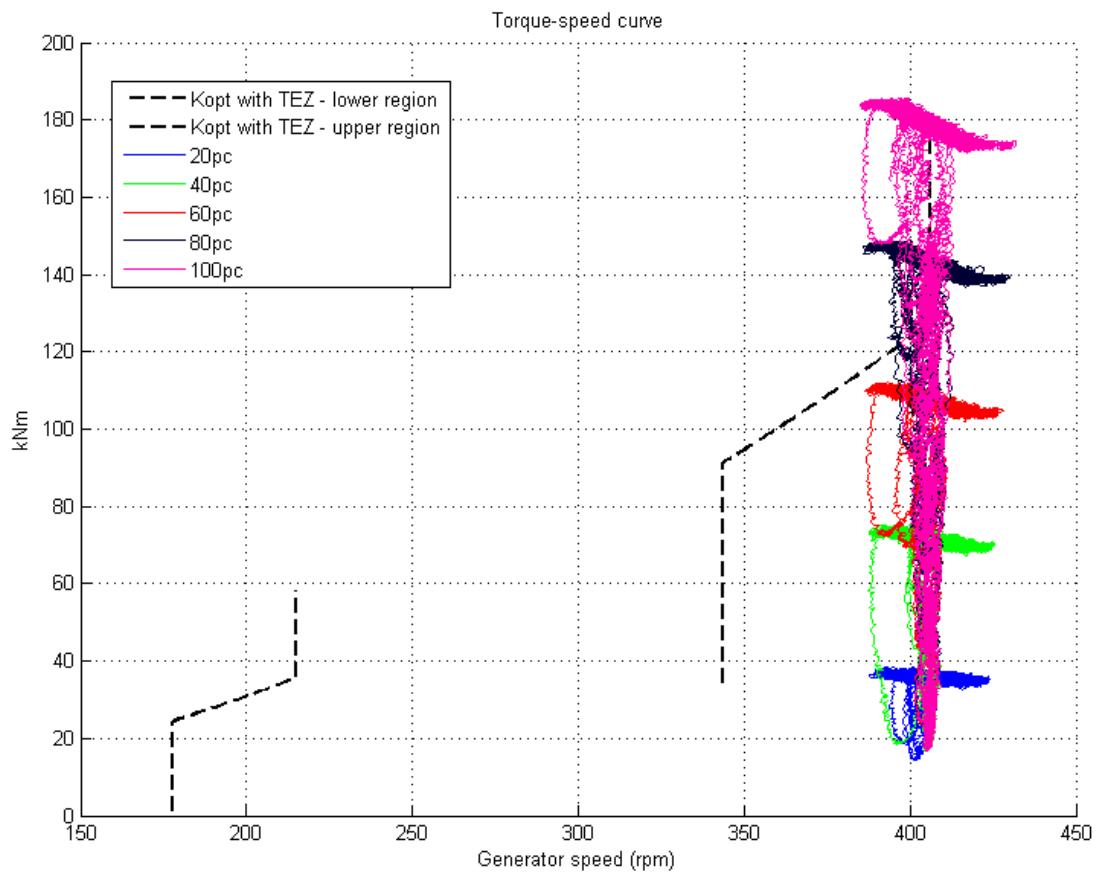
FIGURE 33: TORQUE SPEED CURVE FROM TURBULENT WIND SIMULATIONS (MAX ROTATION)

4.4 Constant Rotation

4.4.1 Steady wind

Steady wind simulations were run from 4m/s to 24 m/s wind speed in 0.5m/s steps.

After 50 seconds the power fraction is decreased from 100% to 80%, 60%, 40% or 20%. The average value of pitch angle, generator speed, generator torque and electrical power is calculated over the last 50 seconds of each 300 second simulations to produce steady state curves.

Figure 34 to Figure 37below show the results for Electrical power, generator speed and torque, and pitch angle.

As the strategy is Constant Rotation, generator speed mean values against generator torque mean values follow the optimal mode gain curve, as shown in Figure 37: STEADY pitch angle TRAJECTORIES FOR CONSTANT ROTATION DERATING STRATEGY
 (with the exclusion of the speed range 215rpm to 344rpm to avoid exciting the tower first mode of vibration)
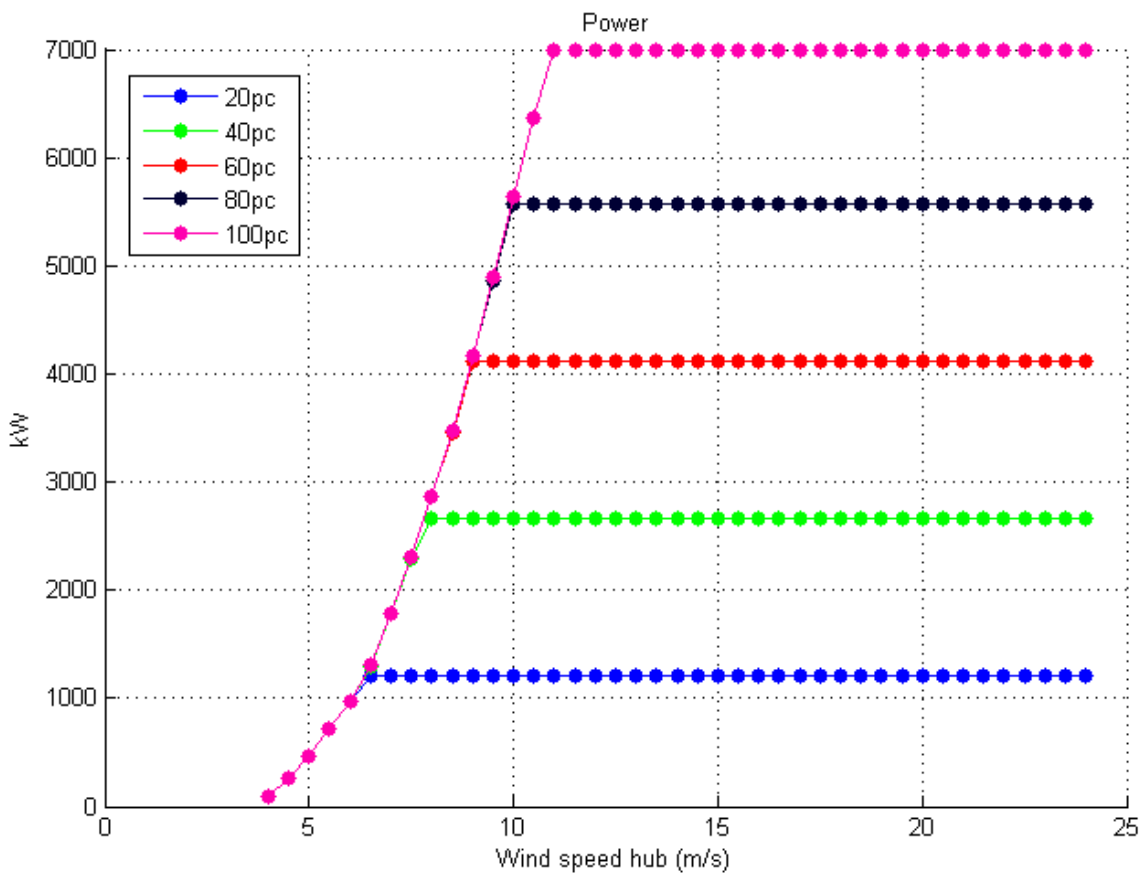
Figure 34: STEADY Power curves FOR CONSTANT ROTATION DERATING STRATEGY
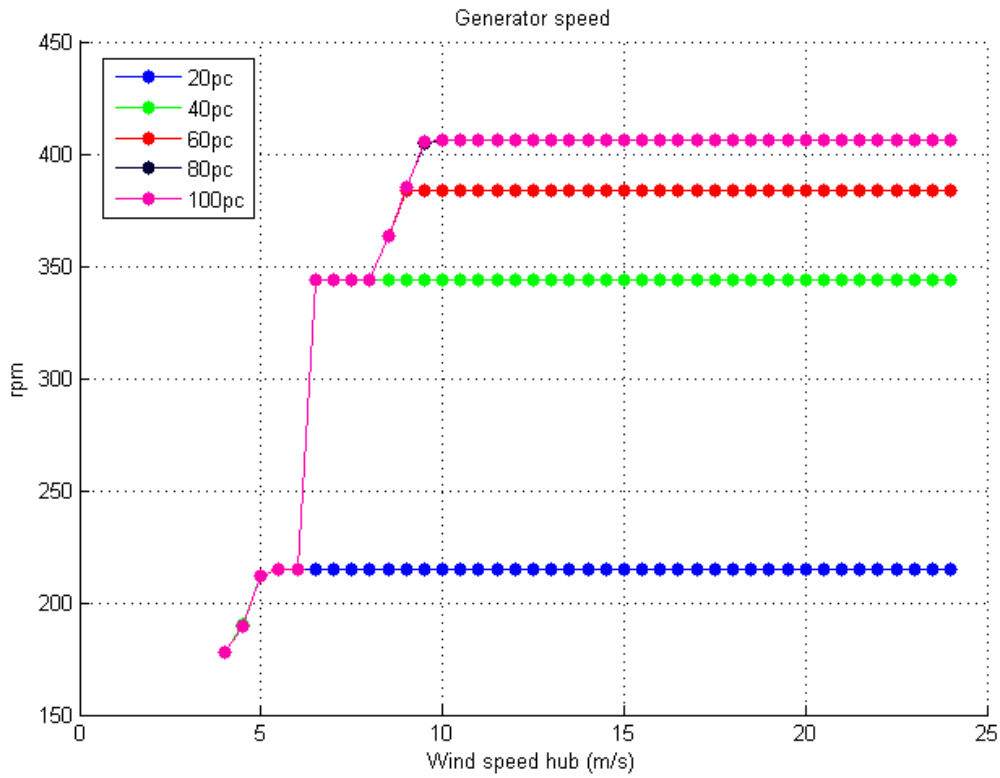
FIGURE 35: STEADY GENERATOR SPEED TRAJECTORIES FOR CONSTANT ROTATION DERATING STRATEGY
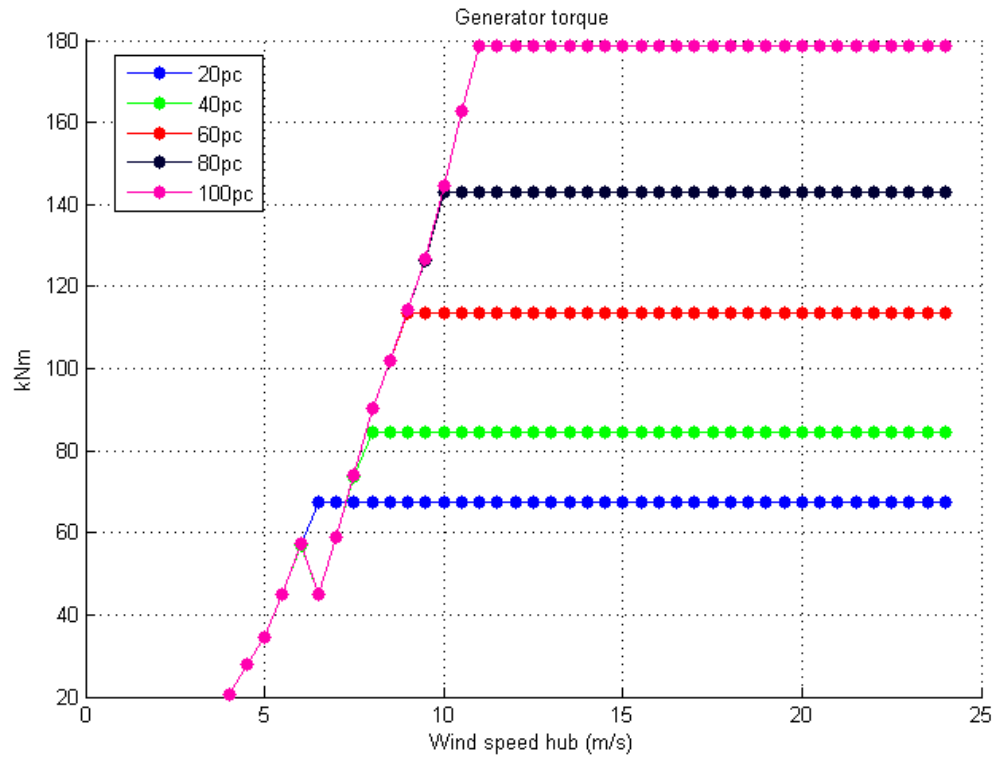
FIGURE 36: STEADY GENERATOR TORQUE TRAJECTORIES FOR CONSTANT ROTATION DERATING STRATEGY
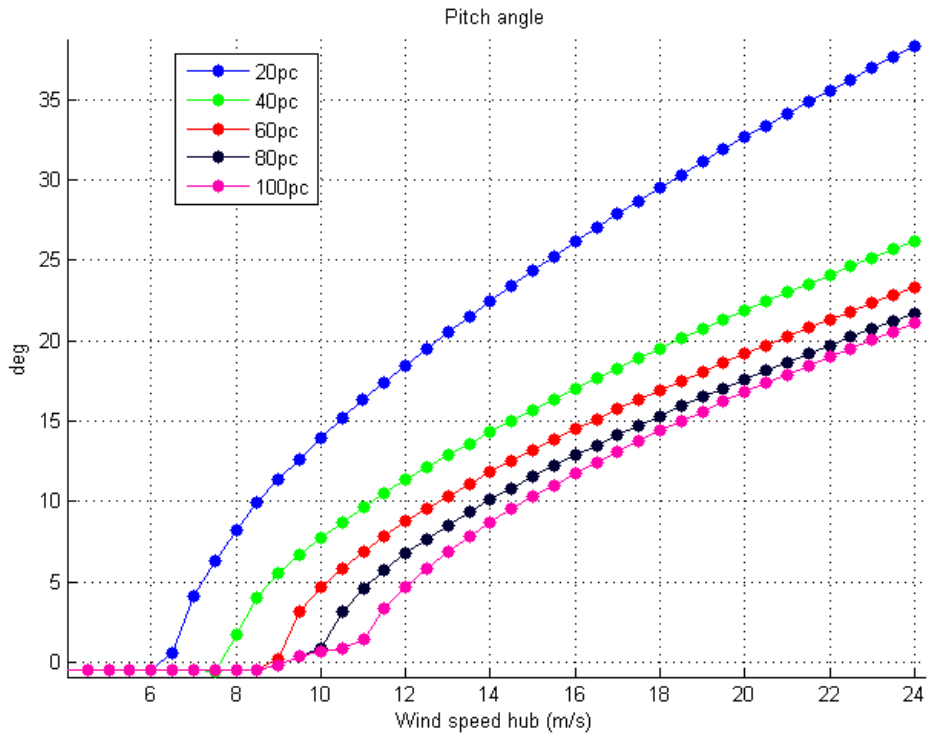
FIGURE 37: STEADY PITCH ANGLE TRAJECTORIES FOR CONSTANT ROTATION DERATING STRATEGY
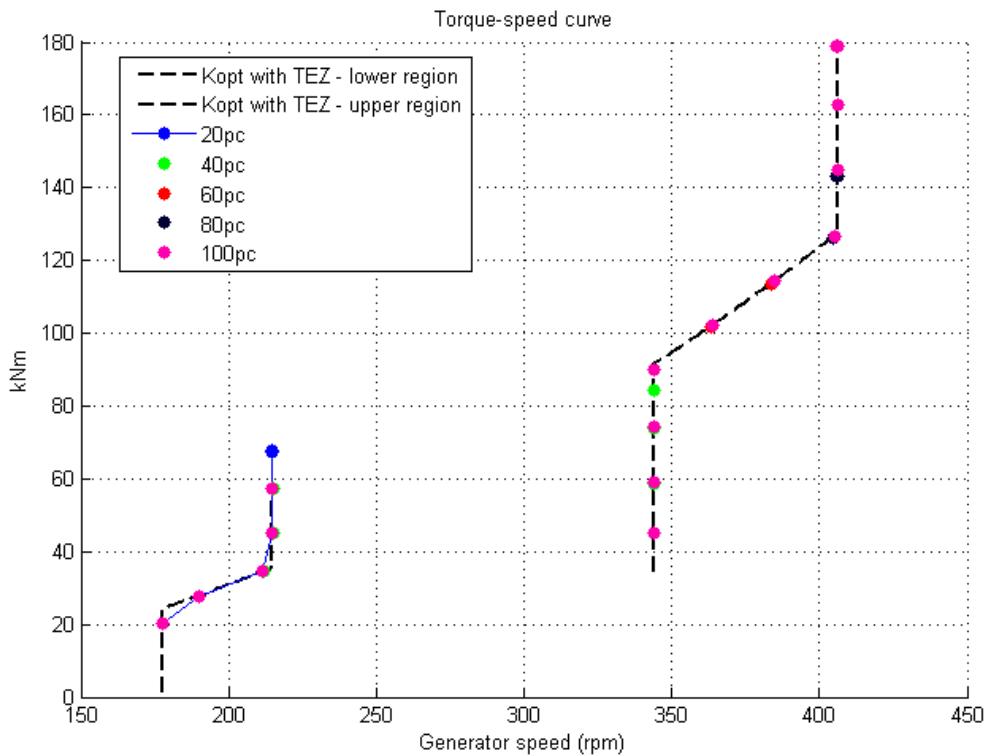
Figure 38: Torque speed curve FOR CONSTANT ROTATION DERATING STRATEGY

4.4.2 TURBULENT WIND

Plots in this section show results when the Constant Rotation derating percentage is 80%.

Time histories of Electrical power, generator speed & torque, and pitch angle are presented in Figure 39 to Figure 42 below.

As in the steady wind case, the derating percentage is changed 50 seconds into the simulation.

Figure 42: Pitch TIME HISTORIES FOR 80% DERATING (CONSTANT ROTATION)
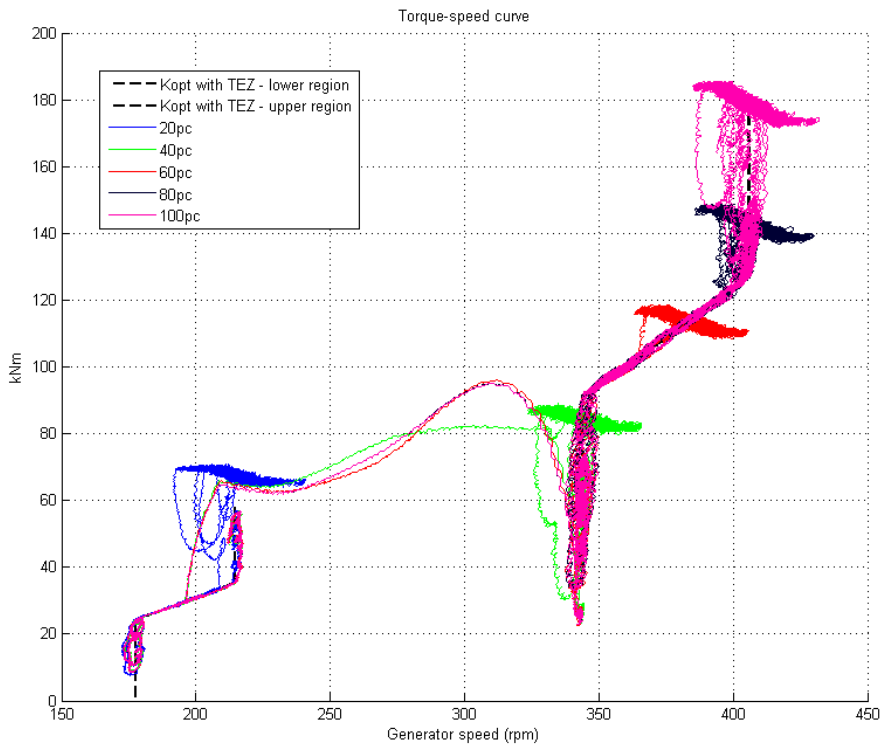
Figure 43 shows the new torque-speed curve derived when instantaneous generator torque is plotted against the generator speed, for all wind conditions and derating percentages. The data shown on that plot is from 250 seconds to the end of simulations, to avoid transients occurring at the beginning of each simulation. As expected, the turbine operates along the optimal mode curve, with the exception of the speed exclusion zone from 215rpm to 344rpm.
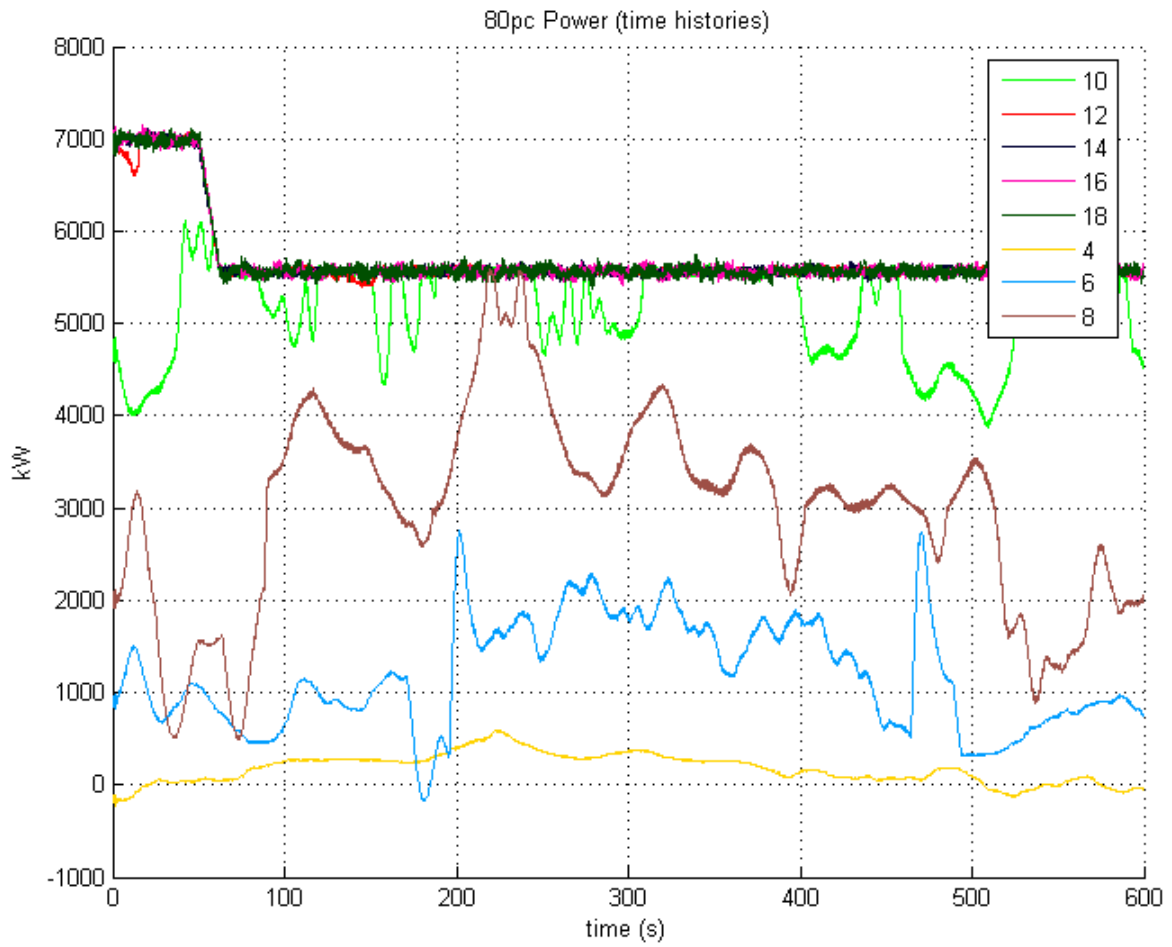
FIGURE 39: ELECTRICAL POWER TIME HISTORIES FOR 80% DERATING (CONSTANT ROTATION
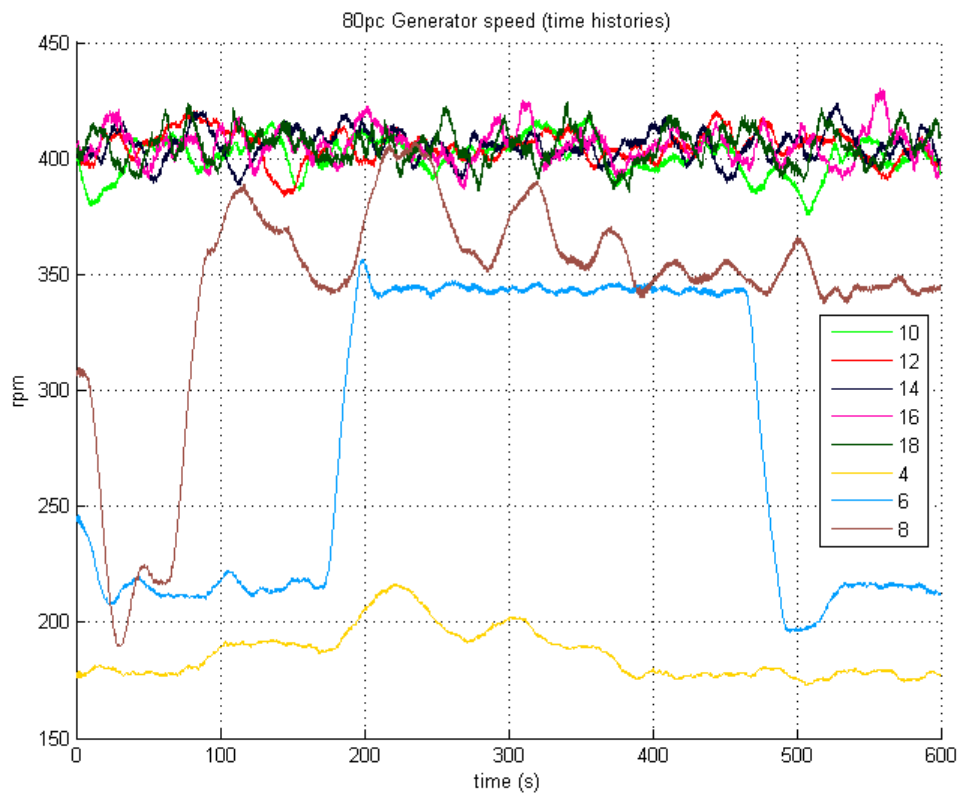
FIGURE 40: GENERATOR SPEED TIME HISTORIES FOR 80% DERATING (CONSTANT ROTATION)
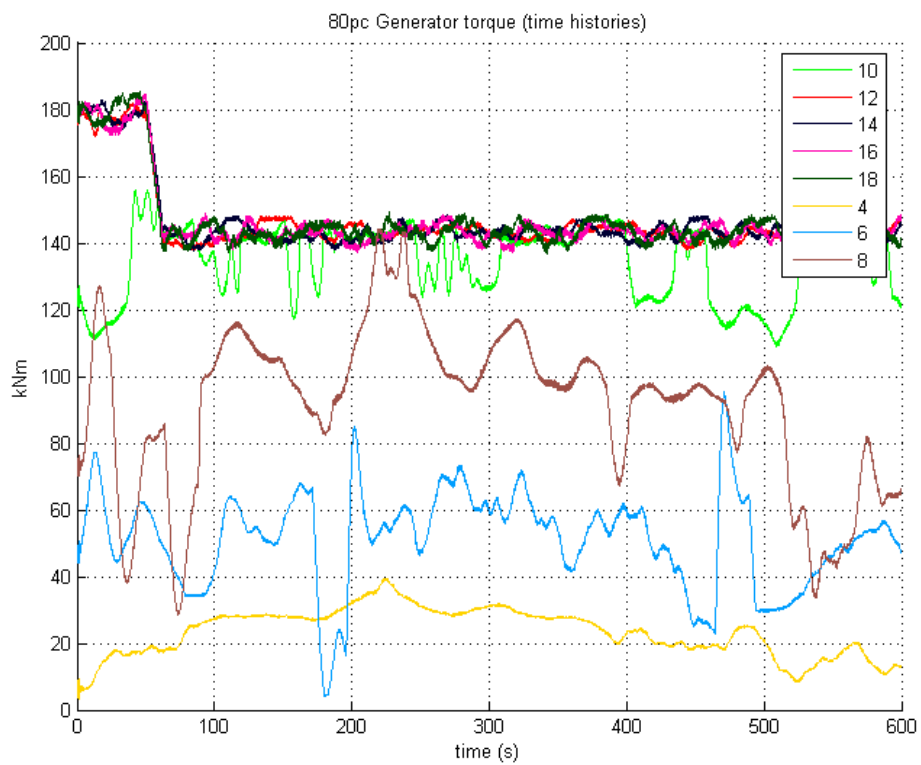
FIGURE 41: GENERATOR TORQUE TIME HISTORIES FOR 80% DERATING (CONSTANT ROTATION)
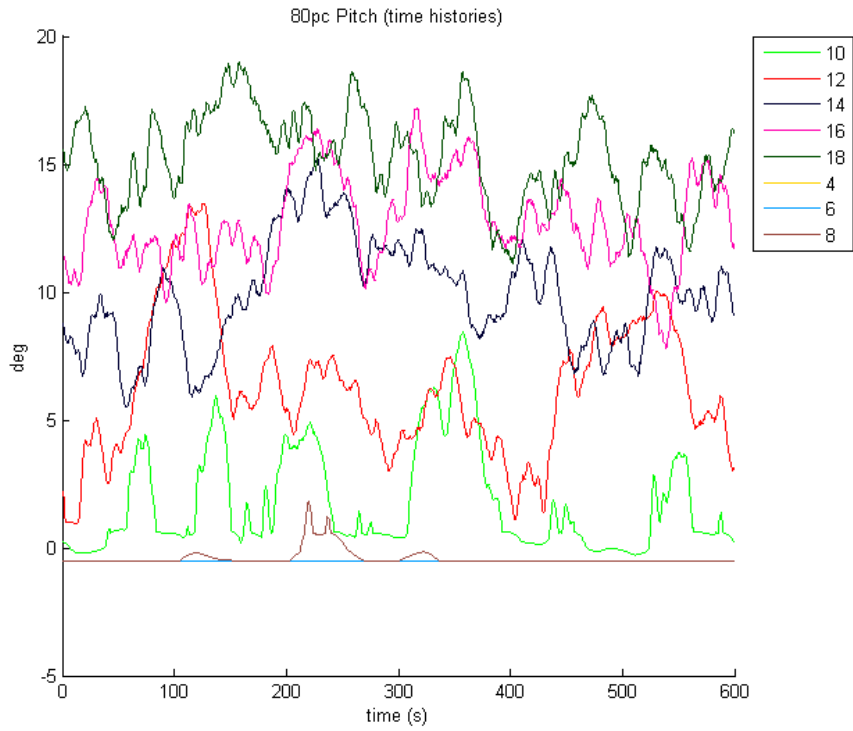
FIGURE 42: PITCH TIME HISTORIES FOR 80% DERATING (CONSTANT ROTATION)
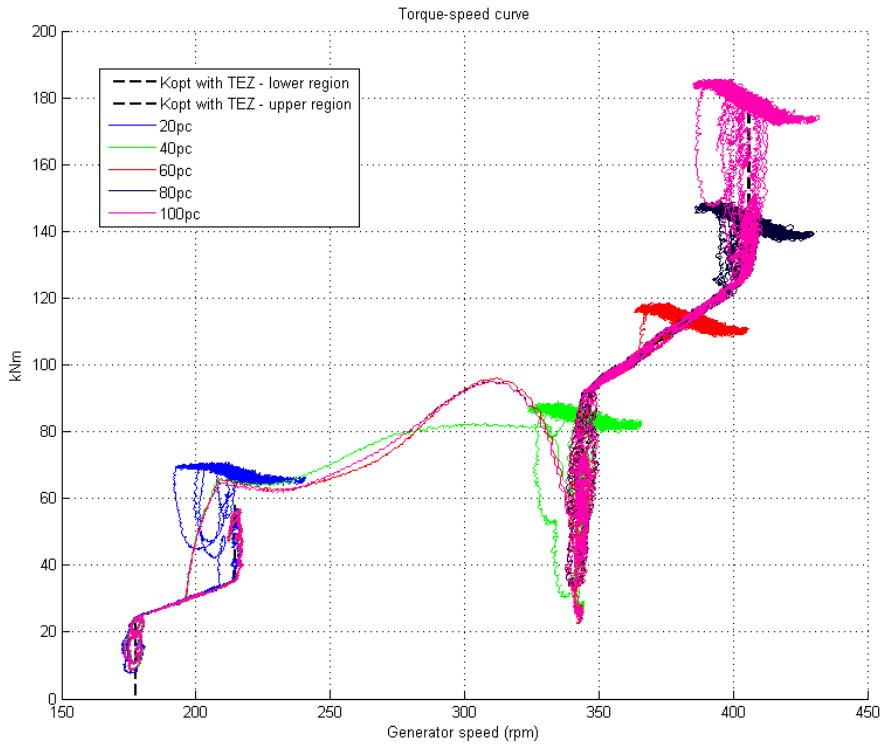
FIGURE 43: TORQUE SPEED CURVE FROM TURBULENT WIND SIMULATIONS (CONSTANT ROTATION)

4.5   CONCLUSION

Both DTU derating strategies have been successfully incorporated into the existing turbine controller software. Simulations have demonstrated that they operate as expected. Both strategies can now be incorporated into the schedule of field tests which are intended to be carried out on the 7MW turbine in the coming year.

5   APPLICATION OF VIRTUAL SYNCHRONOUS MACHINES FOR WIND GENERATION

The concept of virtual synchronous machine (VSM) emerged as an approach for controlling converters in order to replicate the behaviour of standard synchronous machines. This control approach can ensure the operation of multiple converter units in parallel without relying on any master-slave structure, thus offering inherently better reliability and power sharing during transient operations. In the context of wind power plants, VSM is an advanced implementation of synthetic inertia where the active power references are not calculated depending on the rate of change of the frequency (df/dt) of the grid, but by an internal inertia model. Apart from providing virtual inertia, VSM control may enable operation in both grid-connected and islanded system configurations without any change of control structure and parameters. To obtain the functionality required for fulfilling both these purposes, VSMs must rely on a similar power-balance-based synchronization mechanism as synchronous machines (SMs). Thus, VSMs do not depend on conventional phase-locked loops (PLLs) for grid synchronization.

All VSM implementations include a representation of a SM, executed in real time to generate internal control references. The internal model can represent the SM behaviour with different degrees of fidelity, while it must be formulated according to the interfaces with the other control loops of the power converter.

In general, there are two dominating architectures, depending on whether the machine model provides a current reference or a voltage reference for controlling the converter operation.o
In this project, the VSM concept has been adapted to be compatible for implementation within a wind turbine converter. Some work in this direction is already reported in the literature. VSM control concepts for doubly fed induction generator (DFIG) type wind turbines have been discussed by Wang et al.[2] and Zhao et al.[3] For full converter wind turbines, one possibility studied e.g. by Ma et al.[4] is to include a dc link energy storage (battery) which controls dc link voltage and can provide energy very fast when needed. However, the battery also adds costs. Zhong et al.[5] discuss a VSM scheme referred as synchronverter [6] applied to wind turbines with back-to-back converters. In this setup, the dc link voltage is controlled by the rotor-side converter and the maximum power point tracking (MPPT) is achieved by the grid-side converter, opposite of the typical setup. Both converters are controlled according to the synchronverter concept. The real power control of the rotor-side converter has three cascaded control loops: The inner loop is the frequency regulation loop, the middle loop is a torque loop, and the outer loop is the dc link voltage loop. The first two loops are part of the model of a virtual synchronous motor. Another

approach, where the VSM-type control is implemented on the grid-side converter is described by Huang et al.[7] In this scheme, the grid-side converter controls dc voltage and reactive power output (dcVQ control) and utilises the dynamics of the dc-link capacitor to realize self-synchronization and emulate inertia.

5.1 Overview of VSM control structures

This section describes VSM control schemes previously implemented and taken as starting points for adaptations in the present study. The actual adaptations are described in Section 5.2.

In general, VSM control includes an internal *inertia model* that emulates the rotating inertia of a synchronous machine and the power-balance based synchronization mechanism. This is usually based on the swing equation of traditional machines and is the main difference between VSM control and conventional control systems for voltage-source converters (VSCs) based on grid synchronization by PLL or FLL. In addition to the inertia model, an internal *electrical model* (or *virtual impedance*) emulating the electrical dynamics of the synchronous machine is also present. This electrical model can be formulated with the full dynamics of a real synchronous machine, or it can be a simplified model. The VSM implementation applied in this study includes both a dynamic model and a quasi-stationary model for the armature reactance of the machine. An important point to bear in mind regarding VSMs is that they are indeed *virtual* synchronous machines, emulating real synchronous machines through *controls;* it is not necessarily beneficial to emulate *all* dynamic behaviour.

Two basic VSM control structures are implemented in the models and presented in the following sections. The first, referred to as *Voltage Control VSM (VCVSM)*, has a cascaded control structure where the internal electrical model outputs voltage references that are fed through a voltage regulator to provide current references to the inner current control loop. The other, referred to as *Current Control VSM (CCVSM)*, has an internal electrical model that generates current references directly.

Detailed descriptions of the Voltage Control VSM and Current Control VSM modes are provided in papers by D'Arco et al.[8] and Mo et al.[9] respectively. The latter includes a comparison of VSM control with quasi-steady vs. dynamic electrical model. Brief summaries of these control structures are provided in the following.

Voltage Control VSM (VCVSM): The simulated synchronous machine (SM) model provides frequency and phase angle references to the internal control loops for operating the VSC, while a reactive power controller provides the voltage amplitude reference. Thus, the VSM inertia emulation and the reactive power controller appear as outer loops providing the references for the cascaded voltage and current controllers. A PLL detects the actual grid frequency, but this frequency is only used for implementing the damping term in the swing equation. Thus, the operation of the inner loop controllers does not rely on the PLL as in conventional VSC control systems,

but only on the power-balance-based synchronization mechanism of the VSM inertia. A schematic of the control structure is shown in Figure 44. Alternatively the damping term could be obtained by low pass filtering the virtual inertia speed.

Current Control VSM (CCVSM): The simulated synchronous machine (SM) model provides current references for a conventional set of decoupled PI current controllers in a synchronous reference frame established by the VSM swing equation. A quasi-stationary equation is used to represent the impedance of the simulated synchronous machine. Thus, this scheme is referred to as CCVSM with Quasi-Stationary Electrical Model (QSEM). A schematic of the control structure is shown in Figure 45.
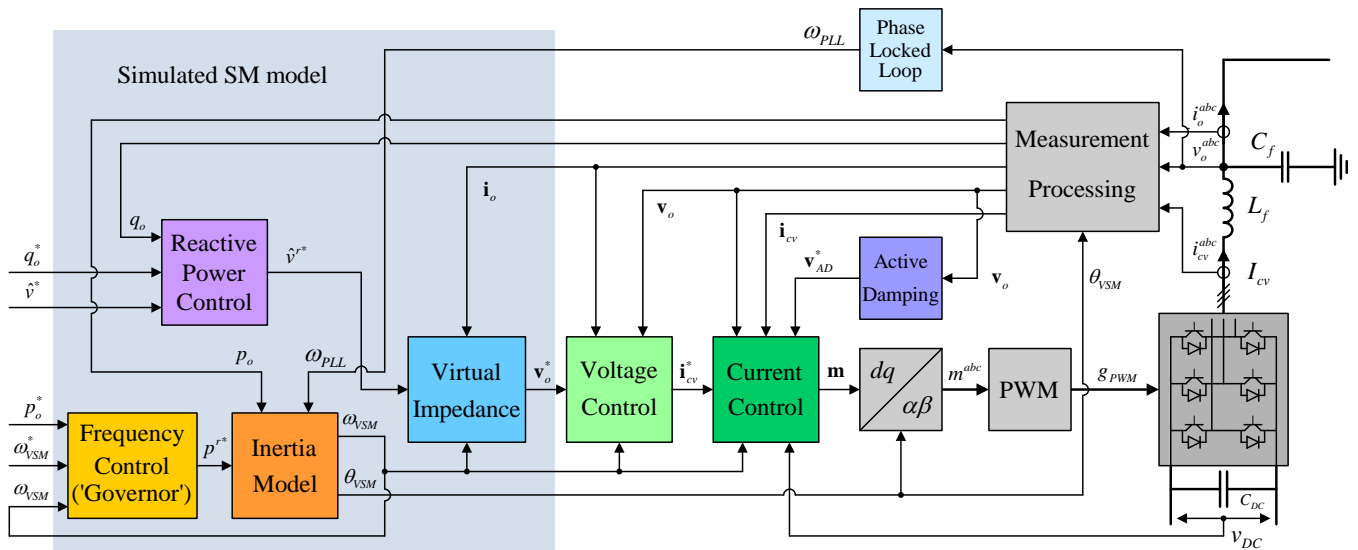
FIGURE 44: VOLTAGE CONTROL VSM (VCVSM) CONTROL STRUCTURE [8]
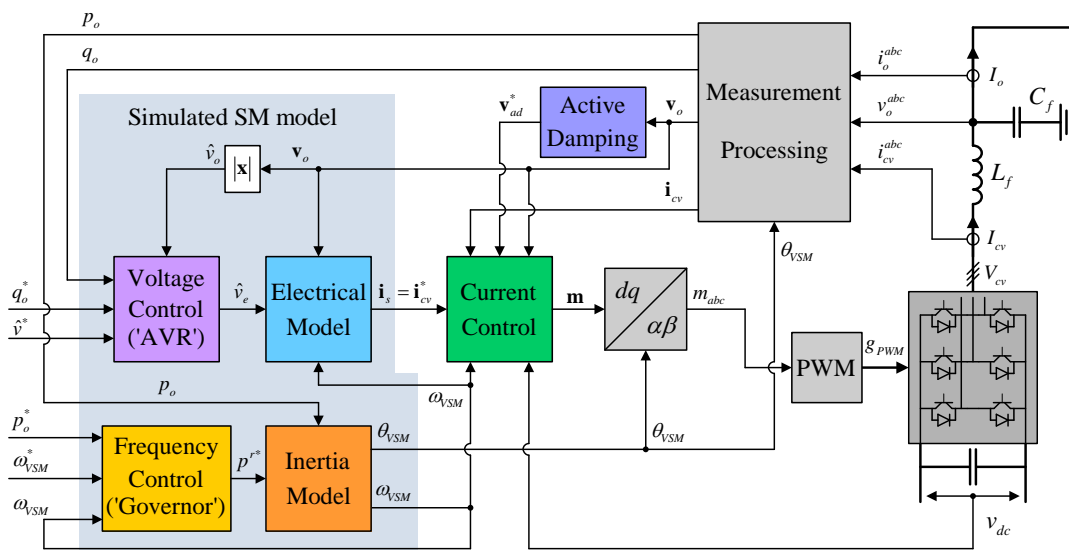
FIGURE 45: CURRENT CONTROL VSM (CCVSM) CONTROL STRUCTURE [9]

5.2 CONVERTER CONTROL ADAPTATIONS FOR IMPLEMENTATION ON WIND TURBINES

This section describes adaptations of the above converter control schemes to facilitate the implementation of VSM control on individual wind turbines.

Figure 46 illustrates the typical control structure of a full-converter wind turbine system, where the generator side converter aims to achieve maximum power extraction, and the grid-side converter controls the internal dc bus voltage and reactive power to the grid. Keeping the dc voltage stable ensures that power generated by the wind turbine is fed directly to the grid.
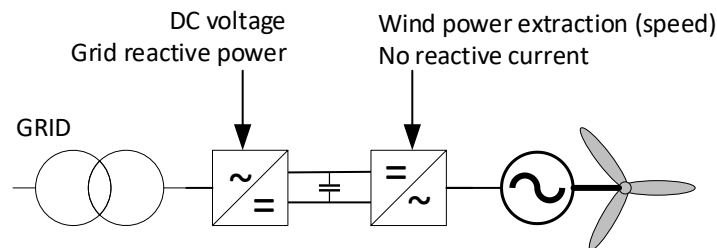
FIGURE 46: TYPICAL CONTROL OF FULL CONVERTER WIND TURBINE

The aim here is to apply the VSM concept to provide fast frequency support to the grid. Hence the VSM should be implemented on the grid-side converter. There are then two main options for how to realise this: 1) The VSM converter controls the dc bus voltage and the generator-side converter controls the active power; 2) The VSM converter controls the active power and the generator-side converter controls the dc bus voltage. The first option resembles the standard setup (Figure 46) and implies a change only on the grid-side converter. However, the second option has some advantages as we will see below. These two options are discussed further in the following.

5.2.1 VSM CONTROLLING DC BUS VOLTAGE

This scheme considers the dc voltage control implemented with the VSM control of the grid-side converter, with active power output controlled by the generator-side converter as in the standard setup.

Two options for implementing the dc voltage control with the VSM controller have been considered:
  A. Add the dc voltage control as an outer loop that sets the power setpoint input to the standard VSM control. This is illustrated in Figure 47.
  B. Modify the inertia model to control the dc voltage directly [7]. This is a variation of the above option that will not be discussed further here. Indeed, performance could be slightly improved by a higher control bandwidth without cascaded controls but the inherent limitations would still remain.

A general challenge with this scheme is that the dc voltage control will be relatively slow, potentially leading to unwanted, large oscillations.

Because the current controller in the generator-side converter aims to follow a reference value given by the wind turbine speed control, it compensates for changes in the voltage. This means that the need for inertia support is not communicated across to the wind turbine side, and the turbine rotor and generator will thus not contribute with their inertia. Unless the generator-side current controller is modified to respond to what happens on the grid side, this scheme will only draw energy from the dc link capacitor for inertial support. Such modifications to the generator-side control are possible and should be explored. An illustration of how this could be included is shown in Figure 48. Due to the limited scope of this study, however, this has not been included in the model. Instead, as described in the next sub-section, a scheme with dc control on the generator-side has been pursued.
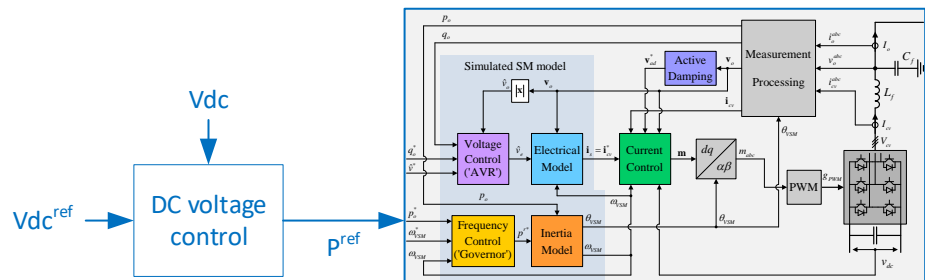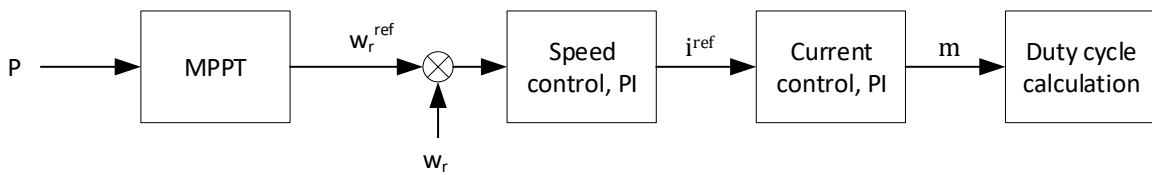
FIGURE 47: VSM SCHEME WITH DC BUS VOLTAGE CONTROL AS AN OUTER LOOP
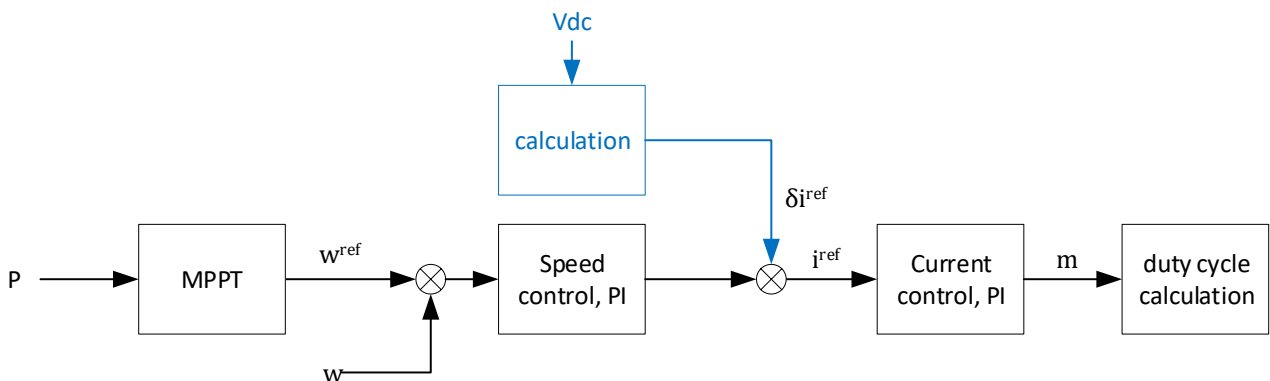
FIGURE 48: SCHEMATIC OF CONTROL ADAPTATION TO ENABLE WIND TURBINE ROTOR TO PROVIDE INERTIA

5.2.2 VSM CONTROLLING POWER EXTRACTION

This scheme moves the dc voltage control to the generator-side (turbine) converter, see Figure 49. This has the practical advantage that the VSM control of the grid-side converter can be left more or less as in the previously implemented basic configuration (see Section 5.1). Additionally, it has the advantage that the need for inertia support is automatically communicated to the generator side via a change in the dc voltage, thus enabling energy to be drawn from the rotational kinetic energy of the rotor.

On the other hand, the active power control must be controlled by the grid-side converter, according to measured generator speed and the maximum power point tracking (MPPT). This coupling between the generator and the grid-side converter may result in undesired control interactions.
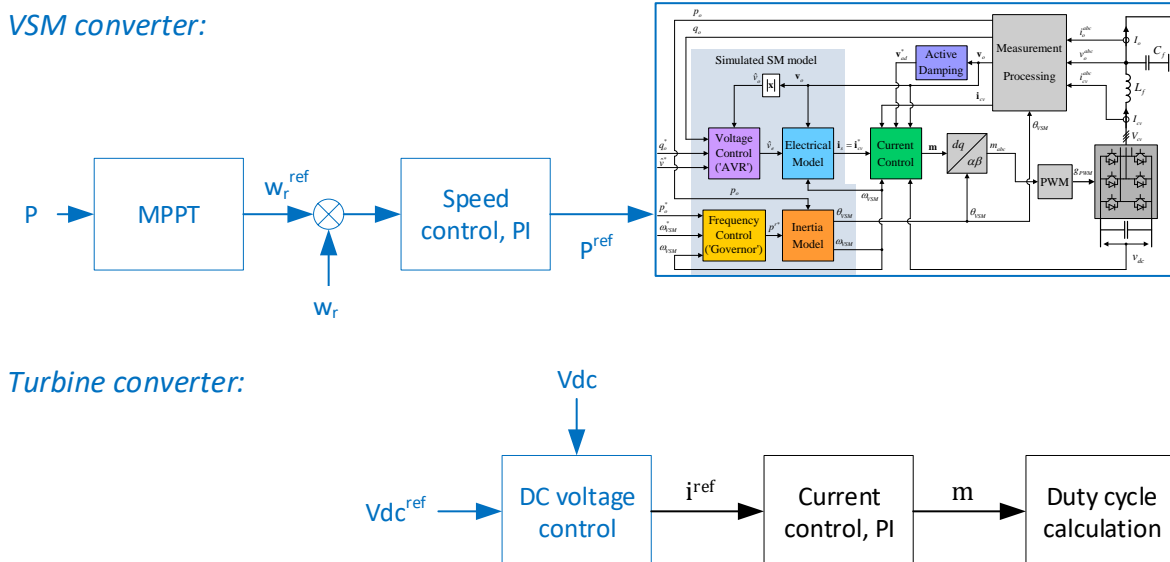
FIGURE 49: VSM SCHEME WITH ACTIVE POWER CONTROL BY VSM CONVERTER AND DC BUS VOLTAGE CONTROL BY TURBINE CONVERTER. SCHEME 2: DC CONTROL ON THE GENERATOR-SIDE AND ACTIVE POWER REFERENCE FED TO GRID-SIDE CONVERTER

6 REFERENCE MODEL FOR ASSESSING FAST FREQUENCY SUPPORT

For the development and testing of the VSM and overpowering control schemes, a simulation model representing an offshore wind power plant with high voltage ac transmission to the onshore grid has been created (see Figure 50). This model has been aligned with the specifications for the TotalControl Reference Wind Power Plant as described in project reports D1.3 [10] and D1.5 [11]. The reference wind power plant has five collection grid feeders at 66 kV, with 7 turbines on two strings and 6 turbines on three strings. Total wind power capacity is 32×10MW = 320 MW. To limit the simulation time, and since it will not significantly affect the results, the present simulation model includes a single feeder, where wind turbines have been aggregated to a single 50

MW turbine. The transmission to shore is via 220 kV ac cables with a total length of 60 km. The onshore grid is represented as a simple equivalent grid model consisting of a synchronous machine and a load. Since only a part of the reference wind farm is included in our model, only one of the two 66/220 kV and the two 220/400 kV transformers are included.

The following sections give a detailed description of the electrical system modelling, with emphasis on the wind turbine grid side converter controls, which is the focus of the investigations. The model has been implemented in MATLAB SimPowerSystems. The biggest part of the model consists of multiple, alternative converter control implementations, both standard non-VSM control and different VSM schemes. These control schemes are the basis for what will be implemented later for laboratory testing as part of WP4.1.
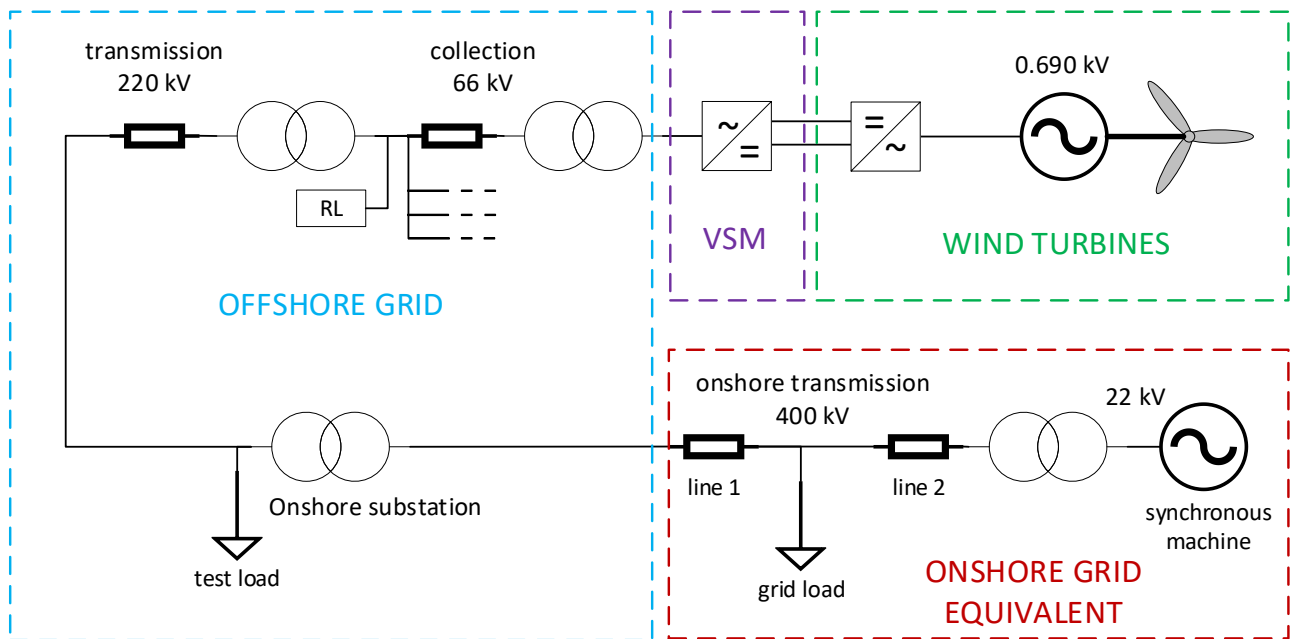
FIGURE 50: OVERVIEW OF SIMULATED ELECTRICAL SYSTEM

6.1 WIND TURBINE

The aggregated model for the wind turbines consists of the turbine, turbine shaft, synchronous generator and a voltage source converter (rectifier) [12]. The grid-side converter (inverter) is considered separately and described below in Section 6.4. The schematic that describes the turbine is shown in Figure 51.
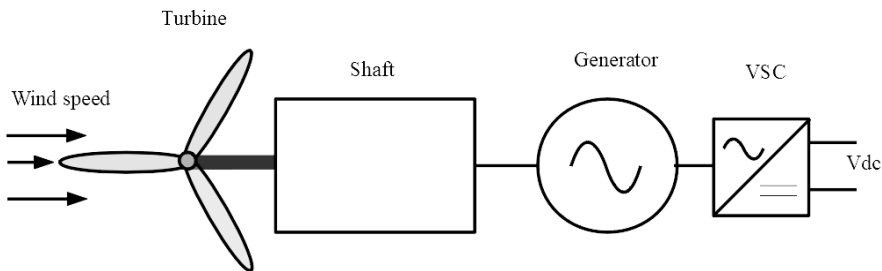
FIGURE 51 WIND TURBINE SCHEMATIC.

48

The wind on the turbine blades generate a mechanical torque that drives the shaft. The shaft, modelled as a spring-damper system drives the generator rotor, which in turn sets up a magnetic field that induces currents in the stator windings and, via the rectifier, dc current in the dc link. The converter control determines stator voltages such as to provide an electric torque that balances the mechanical torque and keeps the rotor speed at the desired value. The wind turbine also has blade pitch control, primarily to limit power above rated wind speeds. However, the pitch control is not relevant for the present study. Model parameter for the aggregated turbines are given in Table 2.

An outline of the default wind turbine controller was already given in Figure 47 (bottom). The main goal of the turbine controller is to extract maximum power from the wind, within certain constraints. Measured power is fed through a maximum power point tracking (MPPT) block to give reference rotational speed. Together with measured speed, this is fed through a PI speed controller to give the current reference for the converter (rectifier) control. Rectifier parameters are given in Table 3.

TABLE 2: WIND TURBINE MODEL PARAMETERS

Parameter	Value	Parameter	Value
Wind turbine:		*Generator:*	
Nominal power	2 MW	Number of turbines	25
Number of turbines	25	Nominal power	2.2 MVA
Nominal wind speed	11 m/s	Nominal voltage	0.69 kV
Shaft:		Nominal frequency	50 Hz
Inertia constant, H	4.32 s	Inertia constant, H	0.62 s
Spring constant, K	0.3 pu/rad	Friction factor	0.01
Mutual damping, D	1.5 pu	Stator resistance, r_{st}	0.006 pu
Speed PI regulator:		Synchronous reactance d-frame, x_d	1.305 pu
Proportional gain	5	Transient reactance d-frame, x_d'	0.296 pu
Integral gain	1	Sub-transient reactance d-frame, x_d''	0.252 pu
Field excitation controller:		Synchronous reactance q-frame, x_q	0.474 pu
Proportional gain	10	Sub-transient reactance q-frame, x_q''	0.243 pu
Integral gain	20	Leakage reactance, x_l	0.18 pu
Pitch controller:		Transient time constant, T_{do}'	4.49 s
Proportional gain	15	Sub-transient time constant, T_{do}''	0.0681 s
Pitch compensation, proportional gain	1.5	Sub-transient time constant, T_q''	0.0513 s
Pitch compensation, integral gain	6		

TABLE 3: WIND TURBINE RECTIFIER PARAMETERS

Parameter	Value	Parameter	Value
Nominal power	55.5 MVA	Filter ac, resistance, R	0.003 pu
Nominal voltage	0.69 kV	Filter ac, inductance, L	0.15 pu
Nominal frequency	50 Hz	Current controller, proportional gain	1.5915
Nominal dc voltage	1.127 kV	Current controller, integral gain	10

6.2 OFFSHORE COLLECTION AND TRANSMISSION GRID

This part of the model consists of the collection grid (including the 0.69/66 kV wind turbine transformers) and the transmission cable to shore. There are three 66 kV collection grid feeders, a 60 km 220 kV transmission cable to the onshore connection point, and a 66/220 kV transformer and reactive compensation at the offshore substation and a 220/400 kV transformer at the onshore substation. The collection grid and transmission system has been modelled as described in Total-Control report D1.5. Parameters of the transformer, line and reactive compensation models are given in Table 4. The test load is a load connected at the onshore connection point and used in the simulations to create a need for frequency support from the wind farm, via a sudden increase in its power demand.

TABLE 4: OFFSHORE GRID MODEL PARAMETERS

Parameter	Value	Parameter	Value
Wind turbine transformer:		***Onshore transformer:***	
Nominal power	55.6 MVA	Nominal power	180 MVA
Winding 1 voltage	0.69 kV	Winding 1 voltage	220 kV
Winding 1 resistance, r_1	1e-6 pu	Winding 1 resistance, r_1	0.005 pu
Winding 1 inductance, l_1	0	Winding 1 inductance, l_1	0
Winding 2 voltage	66 kV	Winding 2 voltage	400 kV
Winding 2 resistance, r_2	1e-6 pu	Winding 2 resistance, r_2	0.005 pu
Winding 2 inductance, l_2	0.15 pu	Winding 2 inductance, l_2	1.59e-4 pu
Magnetization resistance, r_m	1e6 pu	Magnetization resistance, r_m	1e6 pu
Magnetization inductance, l_m	500 pu	Magnetization inductance, l_m	500 pu
Offshore transformer:		***Offshore 220 kV transmission:***	
Nominal power	180 MVA	cable length	60 km
Winding 1 voltage	66 kV	Resistance, positive sequence, r_1	0.0385 Ω/km
Winding 1 resistance, r_1	0.0015 pu	Resistance, zero sequence, r_0	0.172 Ω/km
Winding 1 inductance, l_1	0	Inductance, positive sequence, l_1	3.57e-4 H/km
Winding 2 voltage	220 kV	Inductance, zero sequence, l_0	4.52e-4 H/km
Winding 2 resistance, r_2	0.0015 pu	Capacitance, positive sequence, c_1	1.94e-7 F/km
Winding 2 inductance, l_2	3.5e-4 pu	Capacitance, zero sequence, c_0	1.94e-7 F/km
Magnetization resistance, r_m	1e3 pu	***Collection grid 66 kV feeders:***	
Magnetization inductance, l_m	1.14 pu	cable length	5 km
Offshore reactive compensation:		Resistance, positive sequence, r_1	0.0473 Ω/km
RL load, active power	2.5 MW	Resistance, zero sequence, r_0	0.181 Ω/km
RL load, inductive reactive power	100 MVA	Inductance, positive sequence, l_1	3.24e-4 H/km
Onshore test load:		Inductance, zero sequence, l_0	4.49e-4 H/km
R load, active power	25 MW	Capacitance, positive sequence, c_1	3.20e-7 F/km
		Capacitance, zero sequence, c_0	3.20e-7 F/km

6.3 ONSHORE AC GRID EQUIVALENT

The onshore ac grid is modelled to give reasonable frequency and voltage behaviour at the wind farm connection grid. Since the emphasis in this study is on the wind turbine converter control, a simple representation of the onshore grid is chosen where it is modelled as a synchronous machine with standard exciter and governor controls. The synchronous machine power capacity and inertia represents the regional grid where the wind power plant is connected. The choice to model

the *regional* grid, with its lower inertia, instead of the *entire* onshore grid is because frequency variations take some time to propagate throughout the grid and will first be detected in the local area. Since the focus in on fast frequency response and support at the connection point of the wind farm, the regional grid properties are therefore more relevant.

In addition to the synchronous machine, the grid equivalent includes onshore transmission lines, modelled as pi-section equivalents, as well as a parallel RLC load.

Parameters for the generator, transformer, lines and load that constitute the onshore grid equivalent are provided in Table 5.

TABLE 5: ONSHORE GRID EQUIVALENT PARAMETERS

Parameter	Value	Parameter	Value
Generator:		*Transformer:*	
Nominal power	250 MVA	Nominal power	250 MVA
Nominal voltage	22 kV	Winding 1 voltage	22 kV
Nominal frequency	50 Hz	Winding 1 resistance, r_1	0.0025 pu
Inertia coefficient, H	1 s	Winding 1 inductance, l_1	0
Friction factor	0	Winding 2 voltage	400 kV
Number of pole pairs, p	20	Winding 2 resistance, r_2	0.0025 pu
Stator resistance, r_{st}	0.001 pu	Winding 2 inductance, l_2	4.77e-4 pu
Synchronous reactance d-frame, x_d	1.2 pu	Magnetization resistance, r_m	1.66e3 pu
Transient reactances d-frame, x_d'	0.3 pu	Magnetization inductance, l_m	412 pu
Sub-transient reactances d-frame x_d''	0.25 pu	***Onshore 400 kV transmission:***	
Synchronous reactance q-frame, x_q	0.25 pu	line 1 length	20 km
Sub-transient reactances q-frame, x_q''	0.8 pu	line 2 length	10 km
Leakage reactance, x_l	0.14 pu	Positive sequence resistance, r_1	0.0166 Ω/km
Transient time constant, T_{do}'	1 s	Zero sequence resistance, r_0	0.109 Ω/km
Sub-transient time constant, T_{do}'', T_{qo}''	0.05 s	Positive sequence inductance, l_1	7.94e-4 H/km
Grid load:		Zero sequence inductance, l_0	2.07e-4 H/km
Active power	125 MW	Zero sequence capacitance, c_0	2.20e-7 F/km
Inductive reactive power	20 MVA	Positive sequence capacitance, c_1	2.20e-7 F/km
Capacitive reactive power	9 MVA		

6.4 Converter circuit and control schemes

The converter model described in this section is the grid-side wind turbine converter, i.e. the inverter. The generator-side converter was described together with the wind turbine model in Section 6.1.

The inverter and filter circuit are illustrated in Figure 52. The converter is modelled as a three-phase, two-level average-model based voltage source converter (VSC). An LCL filter is included on the ac side, and a capacitor and resistor on the dc side as indicated in the illustration. Parameter values are given in Table 6. The dc-side is connected to the dc-terminals of the wind turbine model (see Section 6.1), and the ac-side is connected to the offshore grid (see Section 6.2).
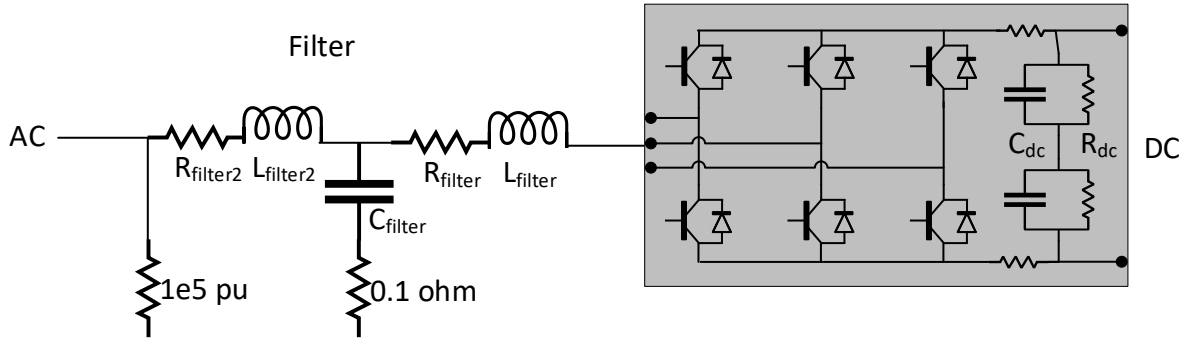
FIGURE 52: WIND TURBINE GRID-SIDE CONVERTER AND FILTER CIRCUIT

TABLE 6: CONVERTER CIRCUIT PARAMETERS

Parameter	Value	Parameter	Value
Filter, R_{filter}	0.01 pu	dc-link capacitance, C_{dc}	4 pu
Filter, L_{filter}	0.05 pu	dc-link resistance, R_{dc}	800 pu
Filter, C_{filter}	0.05 pu	dc series resistance, $R_{series,dc}$	2e-9 pu
Filter, $R_{filter2}$	0.01 pu		
Filter, $L_{filter2}$	0.2 pu		

6.4.1 STANDARD CONVERTER CONTROL

A conventional converter control based on PI regulators in the synchronous reference frame is implemented in the model with a structure as illustrated in Figure 53. This control structure relies on a phase-lock loop (PLL) to obtain the ac grid frequency (w). The output is the duty cycle, which determines converter switching. The controller may include active damping based on ac voltage measurements. For full converter wind turbines, the principle is the same for grid-side and turbine-side converters, with the difference being which variables are being controlled. As indicated in Figure 46, the typical setup is that the grid-side converter controls dc bus voltage and reactive power, whilst the turbine-side converter controls active power (by regulating the rotor speed) and reactive power (keeping it minimal).
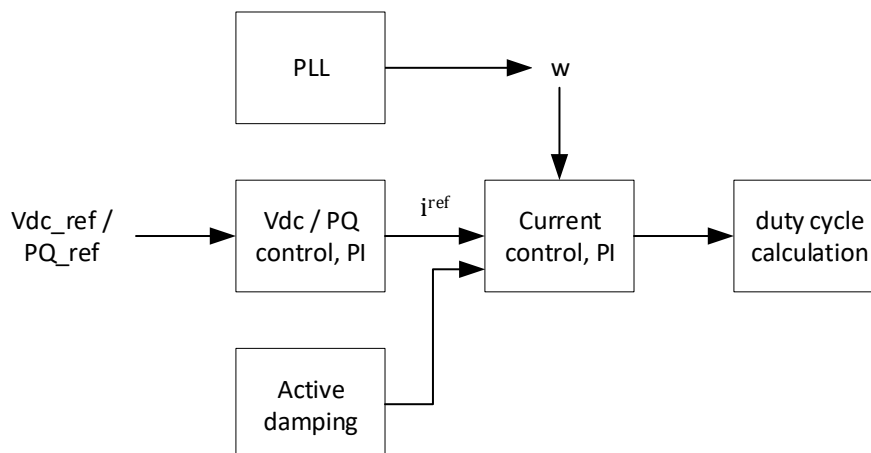
FIGURE 53: STANDARD CONVERTER CONTROL STRUCTURE WITH AN INNER CURRENT CONTROL AND OUTER DC VOLTAGE (VDC) OR ACTIVE/REACTIVE (PQ) POWER CONTROL

6.4.2 VSM CONVERTER CONTROL

VSM control schemes were presented in Sections 5.1 and 5.2. These have been implemented with key parameters as given in Table 7. The virtual inertia is an important parameter that is specified for each simulation case. Other parameters depend on the type of VSM implementation (VCVSM or CCVSM) and dc voltage control parameters apply only for the scheme where the VSM converter controls dc bus voltage. The inertia model damping torque coefficient and current controller parameters are the same in all simulation cases.

TABLE 7: VSM KEY CONTROL PARAMETERS

Parameter	Value	Parameter	Value
Inertia model:		*VCVSM:*	
Virtual inertia, $\tau_{vsm} =2H$	2 s	Voltage controller PI proportional gain	1
damping torque coefficient, k_D	40	Voltage controller PI integral gain	100
Power droop control:		Virtual inductance	0.20 pu
Reactive power droop gain	0	Virtual resistance	0.01 pu
Active power droop gain	5	*CCVSM:*	
Current controller:		Virtual inductance	0.25 pu
Current controller PI proportional gain	0.5	Virtual resistance	0.01 pu
Current controller PI integral gain	65	*dc voltage control (scheme 1):*	
Feed-forward term	true	dc voltage PI controller proportional gain	0.1
Active damping term	true	dc voltage PI controller integral gain	0.2399

7 NUMERICAL RESULTS FOR VSM-BASED FREQUENCY SUPPORT

This section provides results from numerical simulations demonstrating the capabilities offered by a VSM implementation in a wind farm for inertia emulation and fast frequency support. The electrical model simulated consists of an offshore wind farm, represented by a single feeder and an aggregated turbine with a full converter, an offshore transmission grid and connection to an onshore grid equivalent as presented in Figure 50 and described in Section 6. Sudden load changes in a load connected at the onshore connection point are used to create a frequency disturbance that could be mitigated with support from the wind farm. All simulation results presented here are all based on a situation with 6 m/s wind speed, where the wind turbines produce about 12 % of rated power. A 25 MW sudden increase in active power load is assumed 30 s after simulation start.

In the following, simulation results from different VSM control schemes are presented, compared and discussed. In a first batch of simulations (Section 7.1) a simplified wind turbine model has been applied to highlight the impact of inertia support on the grid. This model represents an ideal wind turbine operating at optimal speed (maximum power) without any speed regulation included. A second batch of simulations (Section 7.2) with a complete wind turbine model indicates limitations and risks for implementation of VSM schemes, especially concerning control interactions. These results illustrate that to increase the inertia support the tuning of controllers is

essential to avoid instabilities. However, a thorough analysis of the tuning aspects and potential solutions to avoid control interactions is beyond the scope of this report and should be assessed in more detail when attempting a real implementation.

7.1 SIMPLIFIED WIND TURBINE MODEL

The aim of this section is to validate the capability of the VSM to support the grid assuming a simplified wind turbine (WT) model. With this test the VSM can operate with lower practical restrictions than under a full dynamic model test. Therefore, a static power model of the WT is connected to the VSM.

The static wind turbine represents a model for power extraction assuming the turbine operates at optimal tip speed ratio and the power coefficient C_p is at the maximum value, the output is the power available. Besides, the pitch angle is assumed zero. The power losses of the machine-rectifier converter have been neglected. This model produces an approximation of the maximum power that can be extracted with the full model WT based on the wind speed input v_{wind}.

$$P_{WT} = \frac{1}{P_{baseWT}}(K v_{wind}^3 C_p),$$ (1)

where, P_{baseWT} is the base power of the WT and the gain K is calculated as follows:

$$K = \frac{P_{rated\omega_r\theta 0}P_{nom,mec}}{v_{wind,nom}^3 C_{p,max}}$$ (2)

the nominal wind speed for the WT is $v_{wind,nom}$, $P_{rated\omega_r\theta 0}$ is the power rated at the rated rotational speed in pu in this test this value is assumed 0.75 pu, $C_{p,max}$ is the maximum value of the power coefficient and $P_{nom,mec}$ is the nominal mechanical power for the WT. The power is thus calculated from the wind speed, and by dividing the power by the dc voltage, the dc current is found. In the model, this is applied to the VSM with an ideal current source, see Figure 54.
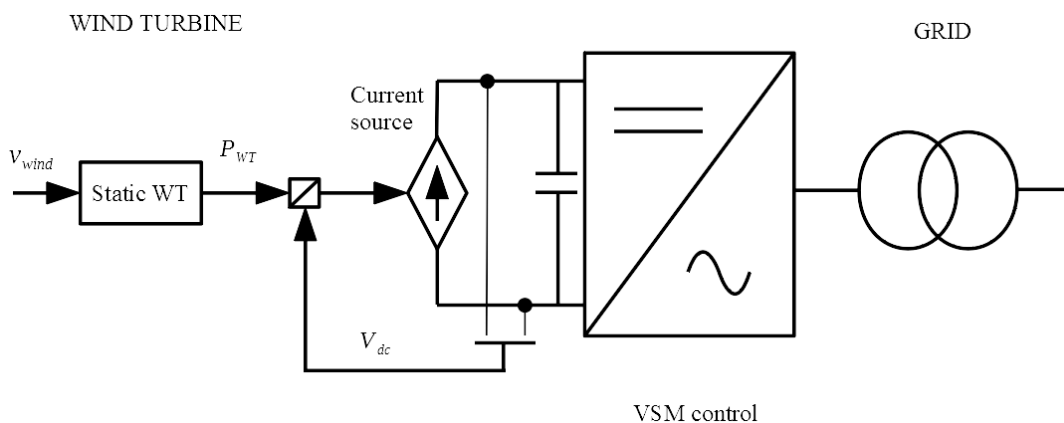
FIGURE 54: SIMPLIFIED WIND TURBINE MODEL

This simplified model has been used to assess the two VSM control schemes presented in Section 5.2: 1) VSM controlling dc bus voltage and 2) VSM controlling power extraction. For each case, three different VSM algorithms as outlined in Section 5.1 have been tested: i) Voltage control

VSM (VCVSM), ii) Current control VSM with quasi-stationary electrical model (CCVSM QSEM) and iii) Current control VSM with dynamic electrical model (CCVSM DEM). In order to standardize the test, the droop gain of the VSM has been removed for all the schemes and the damping coefficient is kept constant. Finally, multiple simulations have been performed with values of the virtual inertia time constant varied from a low value (τ_{vsm}=0.5s) to a high value (τ_{vsm}=8 s).

The performance of the VSM algorithms under the different schemes shows some static and dynamic basic limitations. Those limitations are reference restrictions to consider in the next step where the full model of the WT and the VSM are coupled. Detailed results are provided in the following.

7.1.1 VSM CONTROLLING DC BUS VOLTAGE

The three types of VSMs have been tested with multiple values of the virtual inertia time constants τ_{vsm}. The dc voltage operating points that have been considered correspond to 1.06 pu which is 1200 V (the base case) and 2.22 pu that is 2500 V.

CCVSM-QSEM: Results from this test are given in Figure 55 for dc reference voltage of 1.06 pu. For the cases with a low value of the VSM inertia ($\tau_{vsm} \leq 2$ s), the frequency response is stable, whereas for higher values, deteriorating response is observed with oscillations due to overmodulation occurring after the load step at 30 s.

The performance can be improved and the overmodulation issue avoided by choosing a higher dc bus voltage. This is shown in Figure 56 which are the results of simulations with dc voltage reference to 2.22 pu. The increased voltage means there is more energy stored in the dc link capacitor that the VSM can inject to support the ac power transient. The results show clearly that the overmodulation issue is absent for all values of the VSM inertia.

CCVSM-DEM: This VSM type is the same as CCVSM-QSEM, except the internal electrical model of the VSM includes dynamic equations and as such is a more accurate emulation of a real synchronous machine armature reactance. Simulation results for different values of the VSM inertia time constants and with dc voltage reference set to 1.06 pu are given in Figure 57. The curves are similar to those for CCVSM-QSEM, but they are not identical. There are more spikes in QSEM and the oscillations in the DEM case are smoother for the case τ_{VSM}=8. Moreover, for DEM, a ripple is observed already for τ_{VSM} =0.5 s, which indicates that this VSM type cold have poorer stability compared to the CCVSM-QSEM type when coupled to the complete model of the WT.

VCVSM: Results from tests with this VSM type are shown in Figure 58. Again, the test has been performed with dc voltage reference of 1.06 pu, and a range of VSM inertia time constants. The performance of this VSM is similar to CCVSM-QSEM. The lowest value of the time constant produces a smooth transient. However, the next time constant (τ_{VSM} =2 s) shows an oscillation at the beginning of transient response. Again, for the largest values of the VSM inertia time constant, there are oscillations for the initial part of the transient.
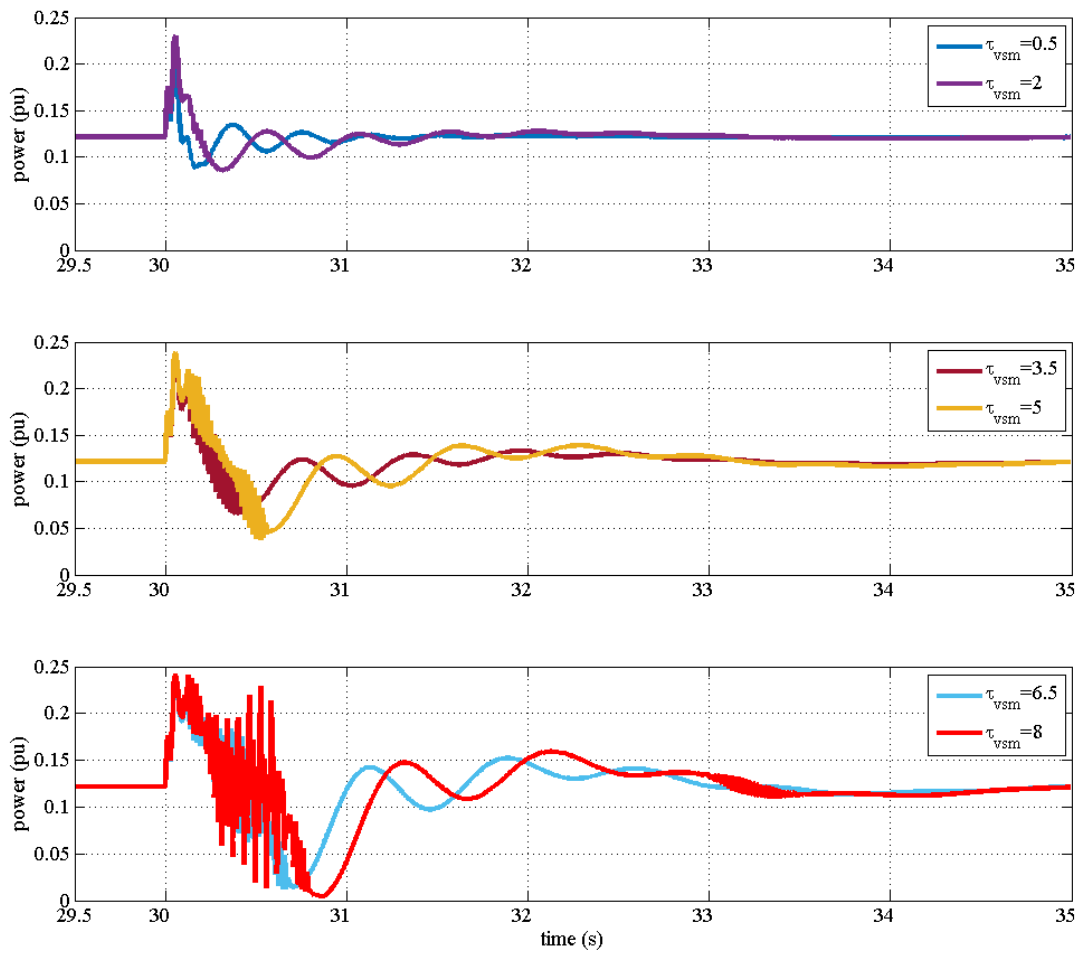
FIGURE 55 CCVSM-QSEM: POWER OUTPUT OF THE VSM WITH DC VOLTAGE CONTROL FOR (VDC=1.06 PU, BASE POWER=50 MVA)
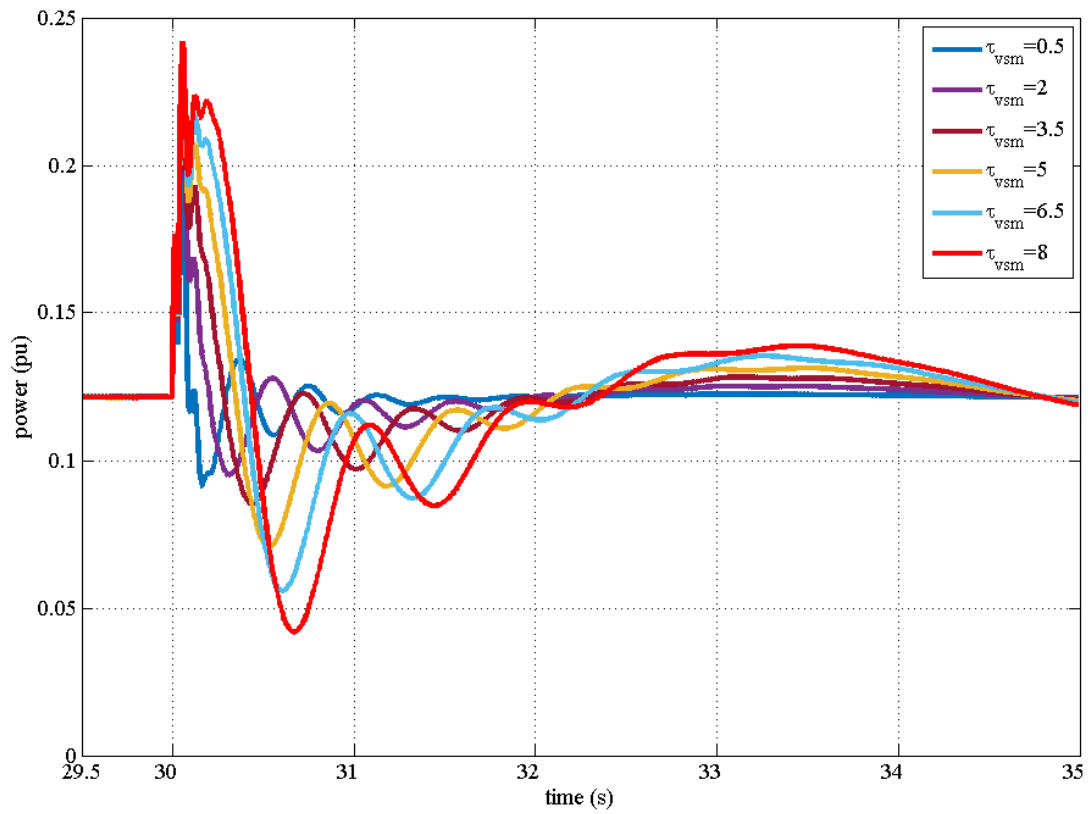
FIGURE 56 CCVSM-QSEM: POWER OUTPUT OF THE VSM WITH DC VOLTAGE CONTROL FOR (VDC=2.22 PU, BASE POWER=50 MVA)
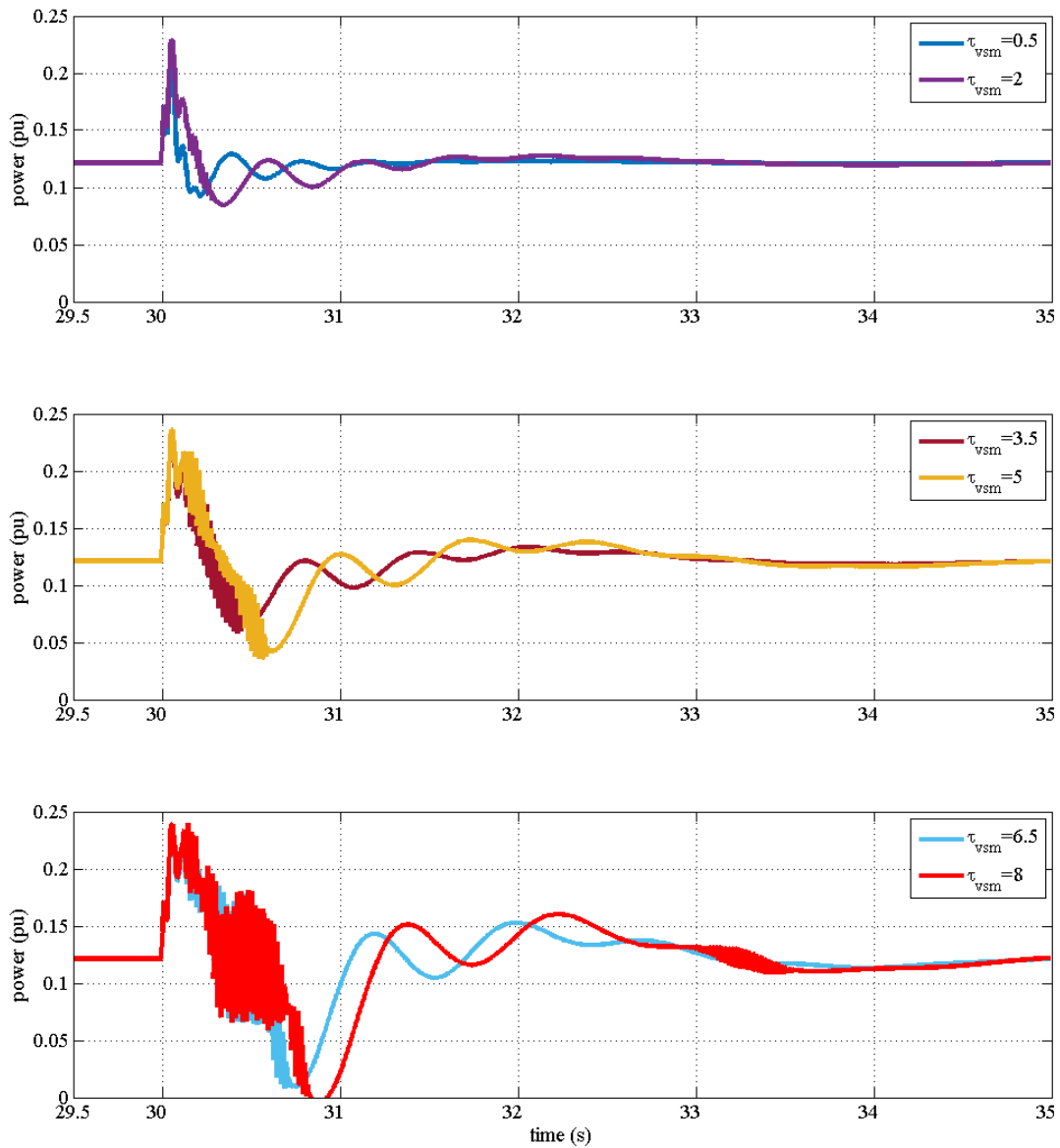
FIGURE 57 CCVSM-DEM: POWER OUTPUT OF THE VSM WITH DC VOLTAGE CONTROL (VDC=1.06 PU, BASE POWER=50 MVA)
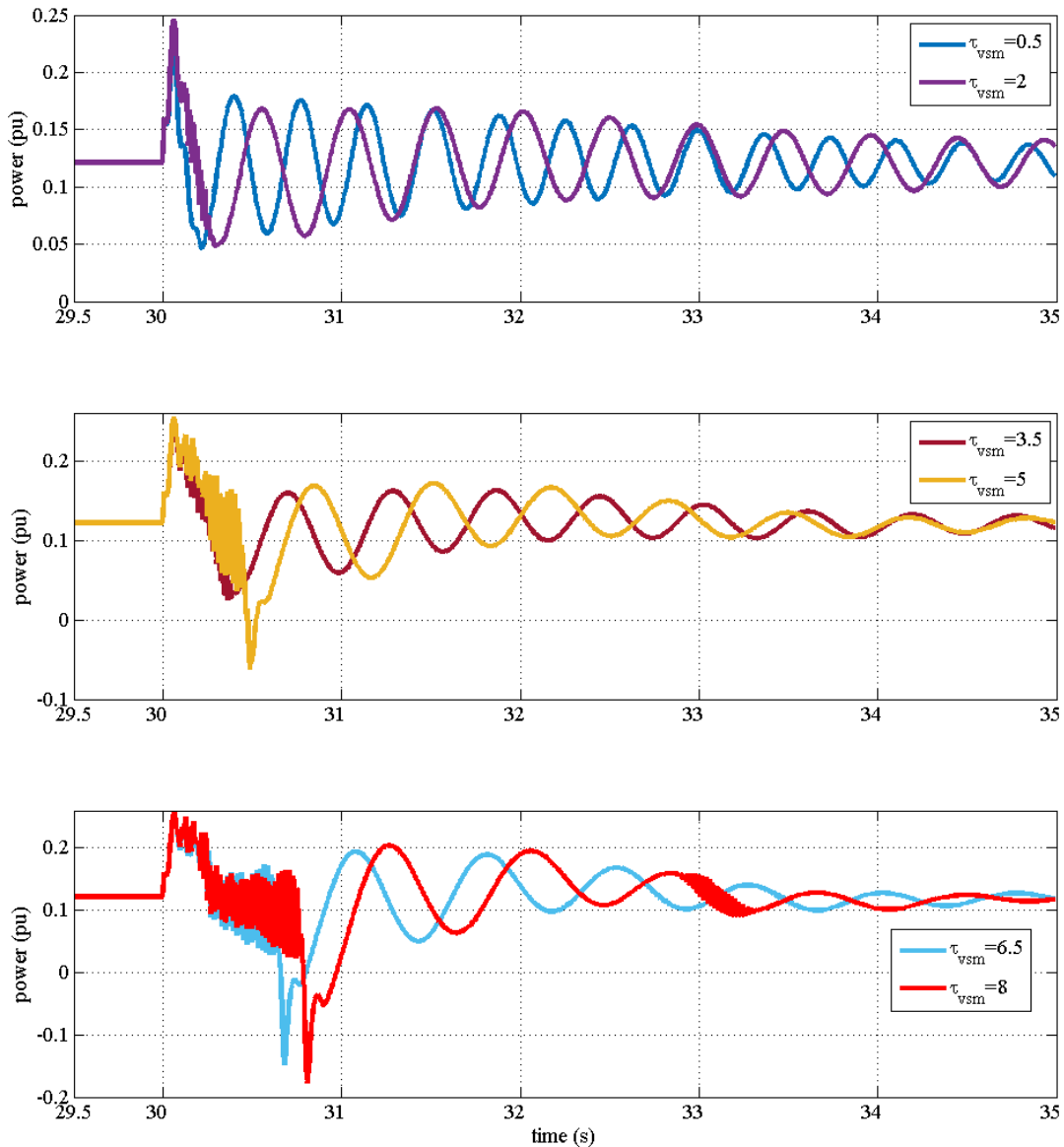
FIGURE 58 VCVSM: POWER OUTPUT OF THE VSM WITH DC VOLTAGE CONTROL (VDC=1.06 PU, BASE POWER=50 MVA)

IN GENERAL, THESE RESULTS SHOW THAT THE VSM IS STABLE WITH A DC VOLTAGE CLOSE TO 1 PU FOR SMALL VALUES OF THE VSM INERTIA. HOWEVER, THESE SMALL VSM INERTIA VALUES MEANS THAT THE VSM WILL PROVIDE LIMITED FREQUENCY SUPPORT TO THE GRID.

The above results indicate that the CCVSM-DEM is more prone to power oscillations than the other types of VSM since the small ripples are present for VSM inertia value of 0.5 s (see Figure 57).

As evident from Figure 56, a possible way to avoid the use of a low VSM inertia time constant is to increase the dc voltage. Then we could alleviate the oscillation cases while operating the VSM with a dc voltage close to 1 pu.

7.1.2 VSM CONTROLLING POWER EXTRACTION

The configuration for this test is the same as above, but now with a control scheme where the dc voltage is controlled by the turbine-side converter, as presented in Section 5.2.2. In the simplified wind turbine model, this is implemented by letting the ideal current source control the dc voltage while the power from the static wind turbine is used as the reference for the active power of the VSM. The same simulation cases as previously have been performed with this setup. In all tests, the dc voltage reference has been 1.06 pu.

CCVSM-QSEM: Results from this test are shown in in Figure 59. The performance is stable for all values of the VSM inertia time constant. It is clear from the figure that the higher the VSM inertia the larger the energy compensation.

CCVSM-DEM: Results from this test are shown in Figure 60. The results are almost the same as the previous case.

VCVSM: Results from this test are shown in Figure 61. As in the previous scheme (see Figure 58), the power oscillations are less damped than for CCVSM, and the dependence on the VSM inertia seems to be smaller.
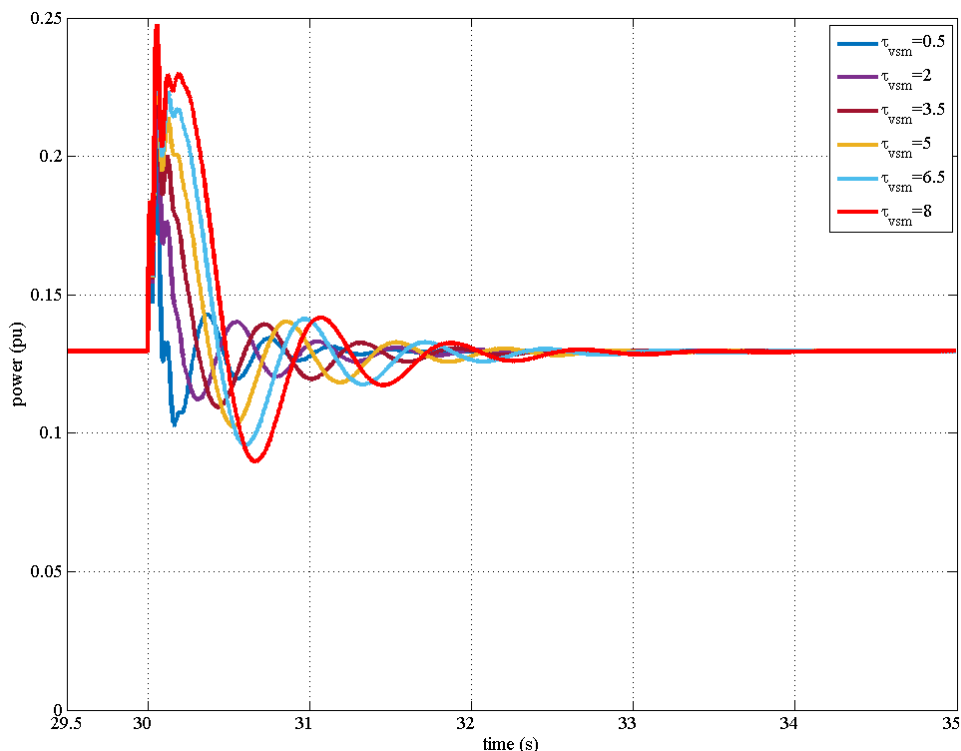
FIGURE 59 CCVSM-QSEM: POWER OUTPUT OF THE VSM WITH REFERENCE POWER (BASE POWER=50 MVA).
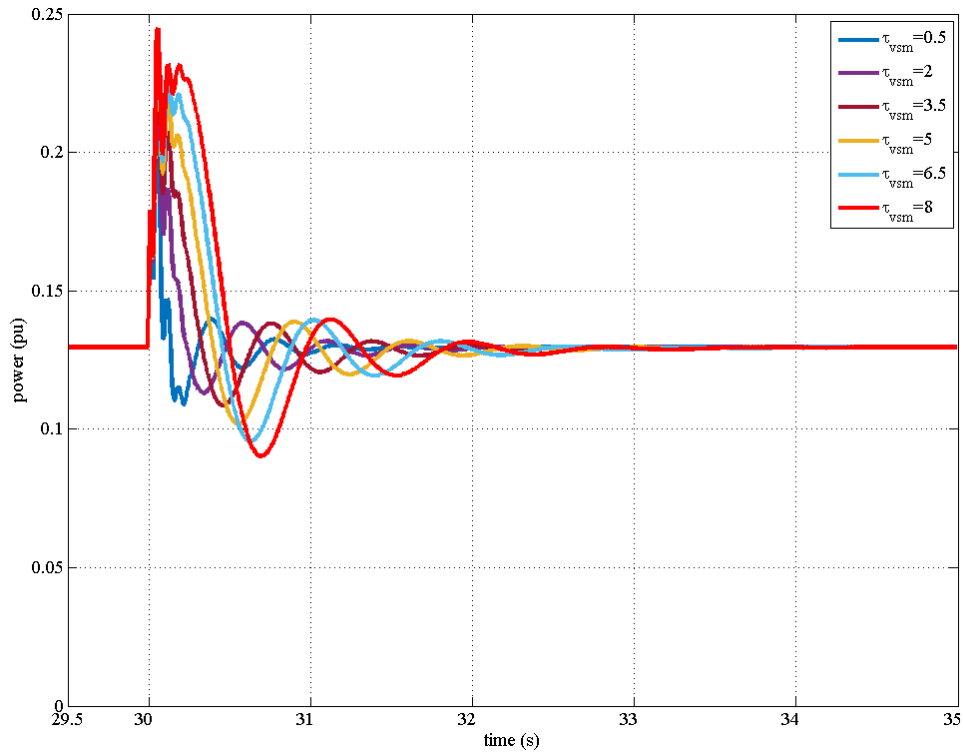
FIGURE 60 CCVSM-DEM: POWER OUTPUT OF THE VSM WITH REFERENCE POWER (BASE POWER=50 MVA).
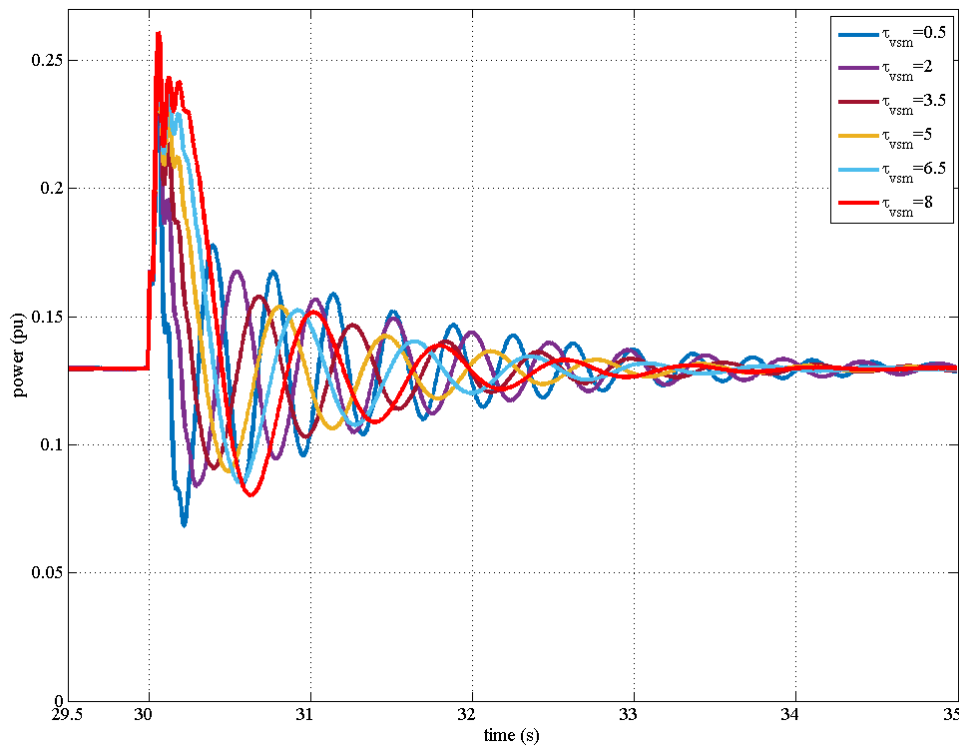
FIGURE 61 VCVSM: POWER OUTPUT OF THE VSM WITH REFERENCE POWER (BASE POWER=50 MVA).

7.1.3 COMPARISON OF VSM CONTROL SCHEMES

A measure of the frequency support provided by the converter is the overall energy output during the transient. The disturbance being studied is an increase in the load, so additional energy is required. Thus, the more energy provided, the more frequency support. Energy can be computed as the integral of the active power output over the relevant time period. This integral has been calculated for the interval from 30 s to 35 s using discrete steps of 4 ms. Computed values for the different control schemes for the CCVSM-QSEM type control is provided in Table 8. The scheme with the VSM controlling active power is found to give the largest energy injected into the ac grid, and we may therefore conclude that this scheme delivers better power support to the ac grid. Moreover, this VSM scheme does not require any modifications of the dc bus voltage.

TABLE 8 ENERGY INJECTION FOR THE TWO VSM SCHEMES FOR CCVSM-QSEM TYPE. VALUES IN MJ.

VSM scheme \ Inertia (τ_{vsm})	0.5 s	2.0 s	3.5 s	5.0 s	6.5 s	8.0 s
dc voltage control (Vdc=1.06 pu)	0.6671	0.6668	0.6664	0.6659	0.6652	0.6645
dc voltage control (Vdc=2.22 pu)	0.6681	0.6696	0.6712	0.6729	0.6749	0.6769
active power control	0.7137	0.7175	0.7213	0.7251	0.7289	0.7326

7.2 FULL DYNAMIC MODEL OF THE WIND TURBINE

This section presents simulation results with the full wind turbine model as described in Section 6.1, including the speed controller, rectifier, generator and the shaft dynamics. Simulations have been performed for the same two VSM control schemes as above. Since the above results have shown the differences between the three different VSM types to be small, we henceforth concentrate on the one that gave the marginally best performance, namely current control VSM with quasi-steady electrical model (CCVSM-QSEM).

7.2.1 VSM CONTROLLING DC BUS VOLTAGE

This test is a repetition of what was described in Section 7.1.1, but now with the full wind turbine model. In the previous simulation it was found that the overmodulation-induced oscillations with 1 pu dc voltage reference were avoided with a higher dc voltage. Hence, dc voltage reference of 2.22 pu was chosen for these simulations. The virtual inertia used in this test is $\tau_{VSM} = 2$ s. To get enough energy storage in the dc link to enable stable performance, the capacitance was increased to $C_{dc} = 9$ pu.

The performance achieved with this configuration is presented below. Figure 62 shows transient power and frequency response after the load step. The top plot gives the output from the 250 MW synchronous generator (onshore grid equivalent). The middle plot presents the power generated from the wind turbine, and the active and reactive power injected by the VSM into the ac grid. As expected, the frequency support in this case is taken from the energy stored in the dc link capacitor. The wind turbine itself is isolated from the disturbance and provides constant output. The bottom plot shows the measured frequency at the generator (w_{grid}), the frequency of the VSM ($w_{VSM-cntrl}$) and the frequency measured at the VSM with a PLL ($w_{pll-vsm}$).

Finally, the dc voltage control response is shown in Figure 63. During the load step transient, the dc voltage recovers to the steady state. The dc voltage response shows that clearly overmodulation issues are avoided.
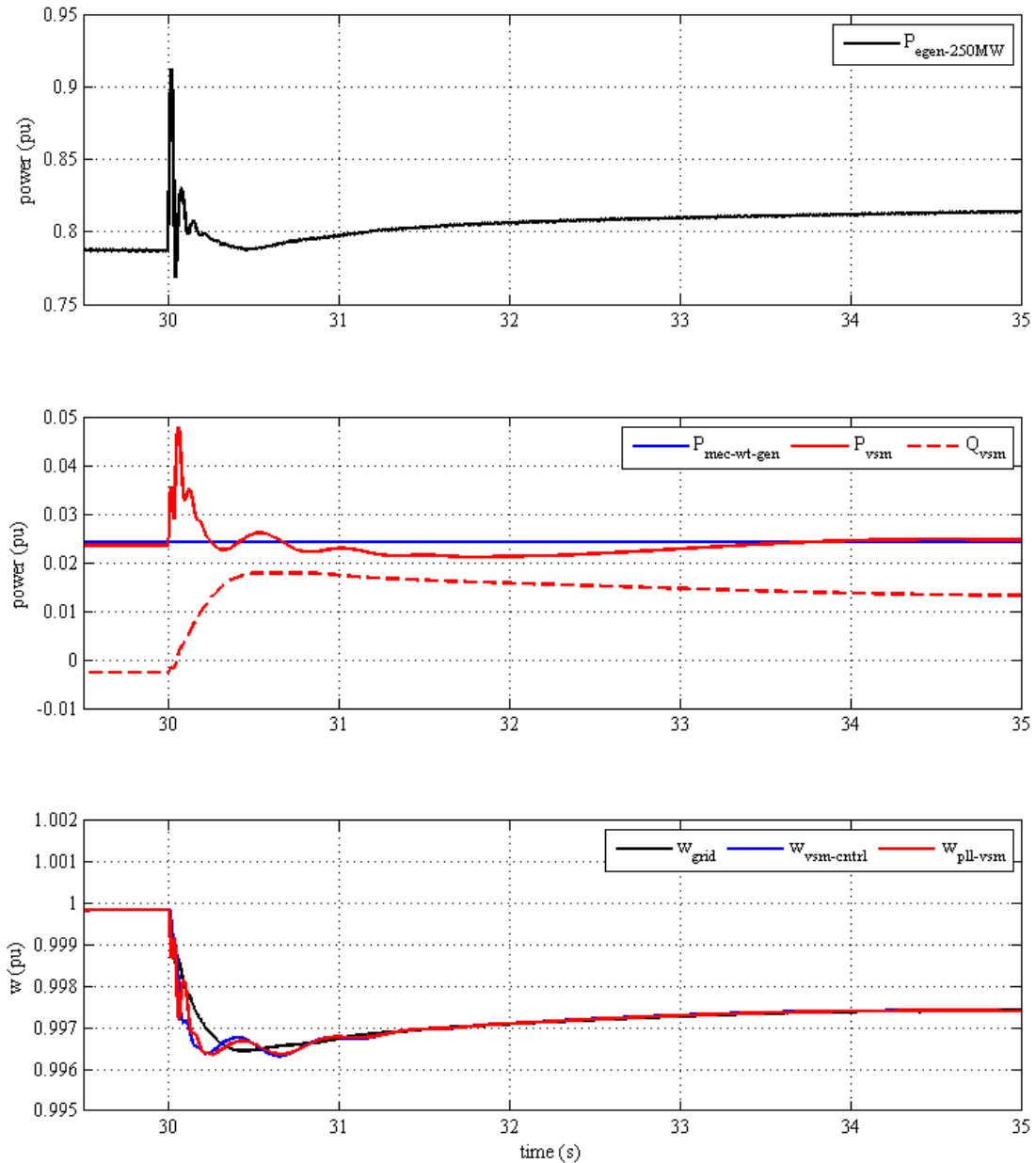
FIGURE 62 POWER AND FREQUENCY RESPONSE FOR CASE OF LOAD STEP AND CONSTANT WIND (BASE POWER 250 MVA).
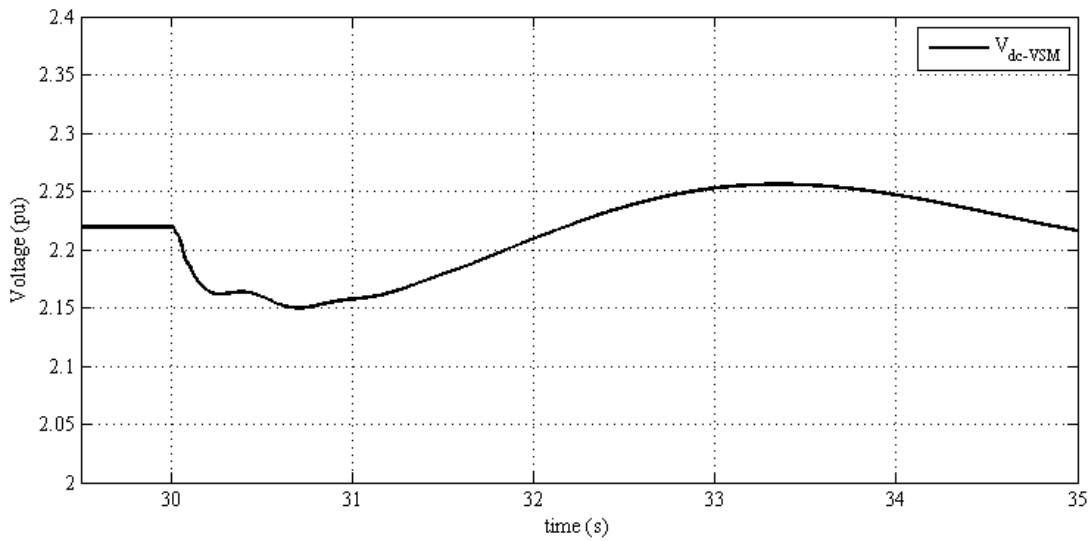
FIGURE 63 DC VOLTAGE RESPONSE FOR CASE OF LOAD STEP AND CONSTANT WIND.

7.2.2 VSM CONTROLLING POWER EXTRACTION

This test again considers the CCVSM-QSEM type control. Recall that in this scheme, the dc voltage is controlled by the turbine-side converter and the VSM converter controls power extraction via a power reference provided by the wind turbine speed regulator. In this case there is therefore a coupling between the grid side and the wind turbine. The load step gives rise to power deficiency that translates to a reduction in dc voltage. The turbine-side converter will then try to compensate this, resulting in increased power extracted from the wind turbine.

Some tuning of parameters was necessary to get stable results. Firstly, the VSM control droop gain was activated. Secondly, to match the dynamic of the wind turbine and the converter, a low virtual inertia was required for the VSM. The chosen value was $\tau_{VSM} = 0.64$ s. Thirdly, a smaller dc link capacitance was used in order for the dc control to be fast enough, C_{dc} = 0.88 pu.

Results are shown below. Figure 64 shows transient power and frequency response after the load step. The top plot gives the output from the 250 MW synchronous generator (onshore grid equivalent). The middle plot presents the power generated from the wind turbine, and the active and reactive power injected by the VSM into the ac grid. In this case, also the wind turbine power output responds to the load step, in line with the comments above. The bottom plot shows the measured frequency at the generator (w$_{grid}$), the frequency of the VSM (w$_{VSM-cntrl}$) and the frequency measured at the VSM with a PLL (w$_{pll-vsm}$). The voltage response is given in Figure 65.
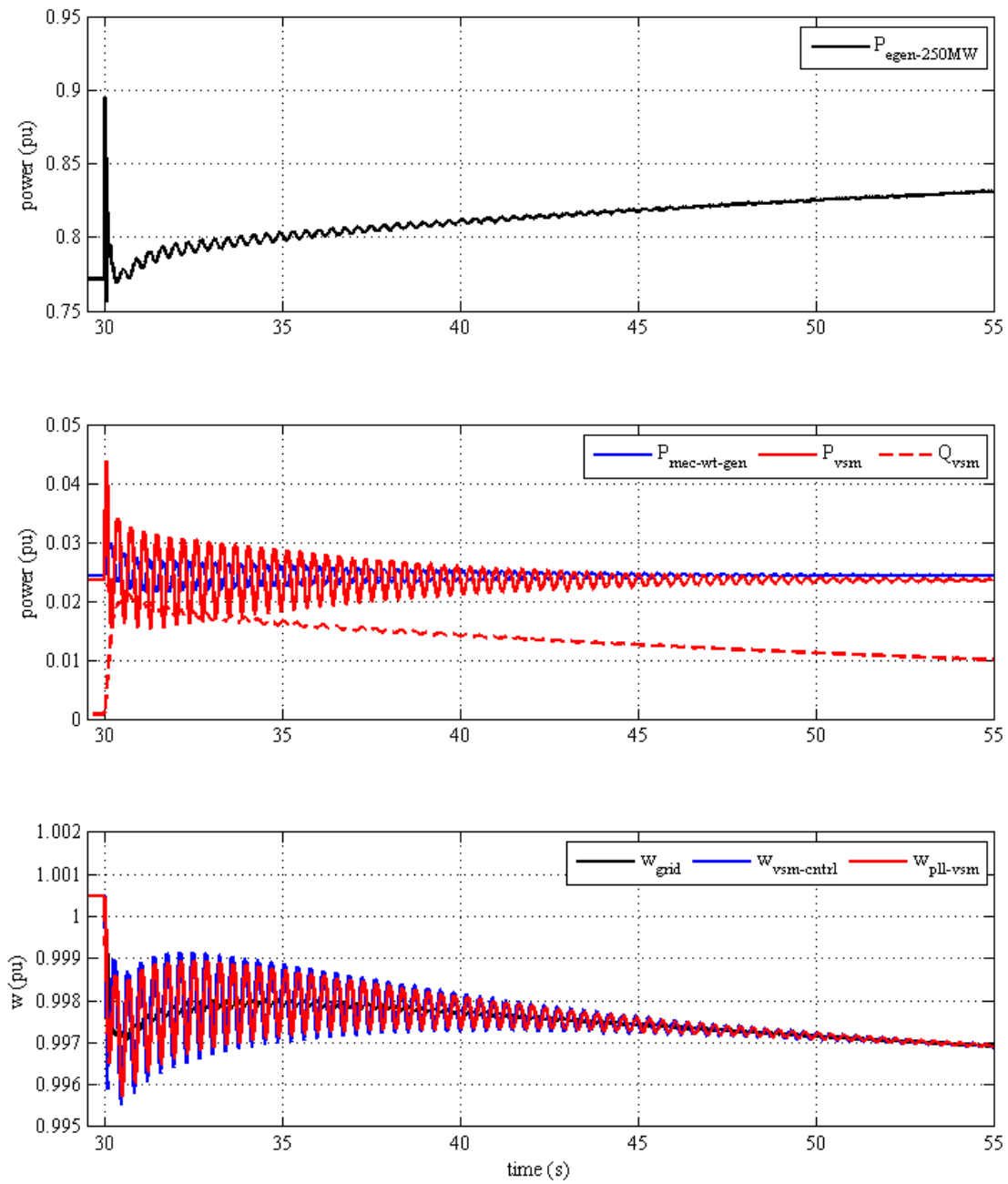
FIGURE 64 POWER AND FREQUENCY RESPONSE FOR CASE OF LOAD STEP AND CONSTANT WIND (BASE POWER 250 MVA)
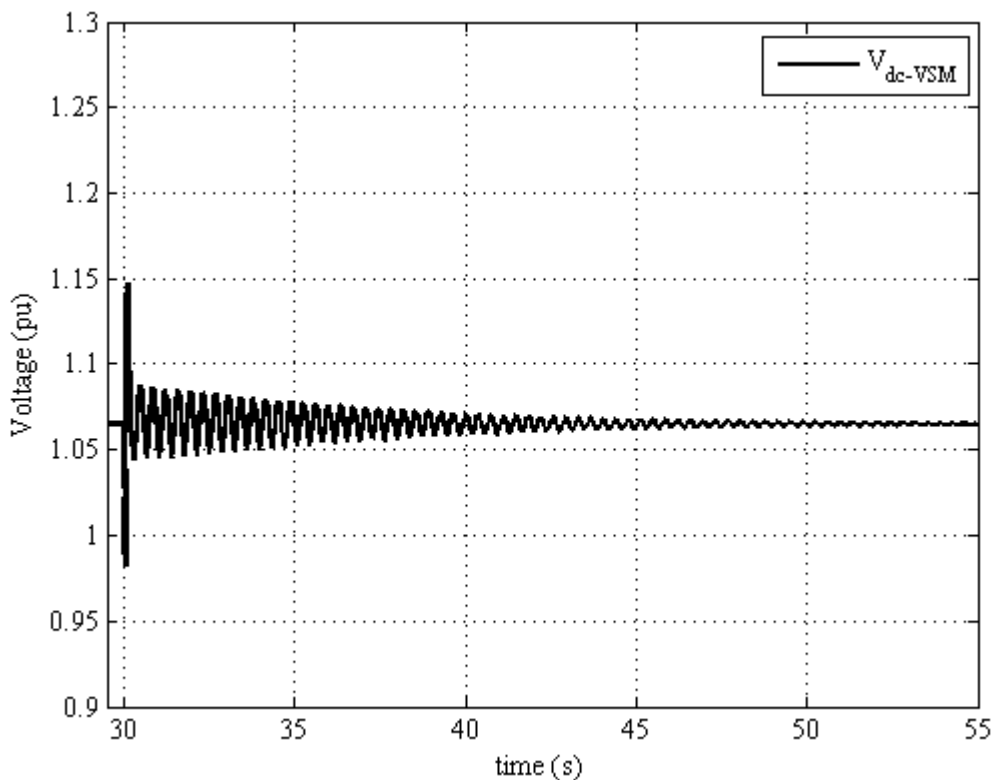
FIGURE 65 DC VOLTAGE RESPONSE FOR CASE OF LOAD STEP AND CONSTANT WIND.

The rapid oscillations shown in all these plots are due to control interactions. A cascade effect occurs: When the load step is triggered, the load suddenly increases, and the frequency starts dropping. The VSM then tries to push more power into the ac grid, which in turn creates a power imbalance in the dc link. Power is extracted from the dc link capacitance and the dc bus voltage drops. The dc voltage controller will compensate for this by consuming more current from the generator side. This in turn increases the electrical torque in the generator, and the imbalance in mechanical and electrical torque makes the rotor speed drop. This reduction in rotor speed is picked up by the turbine speed controller, giving a reduced active power reference value which is then fed into the VSM converter active power controller. The VSM converter then tries to push *less* power into the ac grid, creating a new imbalance in the dc link in the *opposite* direction, i.e. dc bus voltage increases. Without properly tuned controller parameters, this loop of interlinked controllers can give power and voltage oscillations as observed. It is an example of a connection of fast and low multi-systems time constants that can present this slow recovery time. The responsible controller interactions are illustrated in Figure 66.
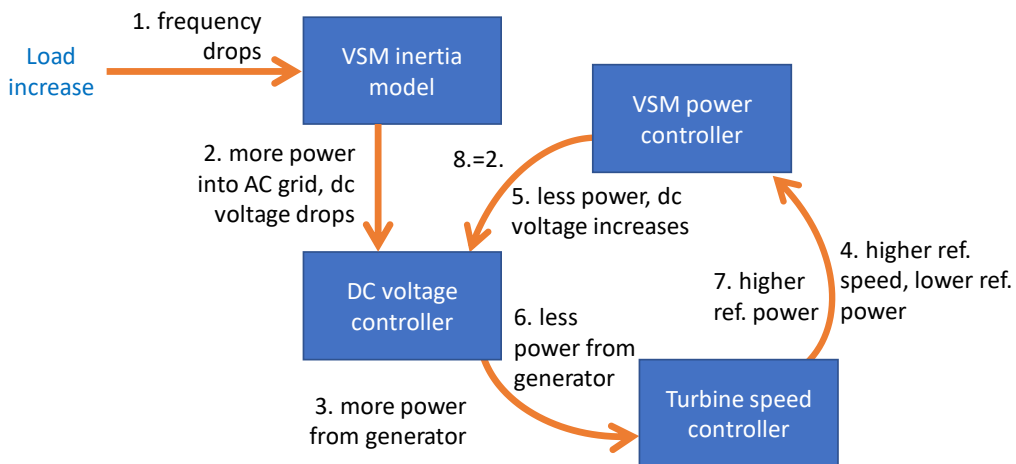
FIGURE 66: SCHEMATIC OF CONTROLLER INTERACTIONS CREATING THE OBSERVED RAPID OSCILLATIONS IN THE NON-TUNED CONTROL SYSTEM.

It is beyond the scope of the present investigation to fine-tune control parameters. However, a potential way to reduce these oscillations is to add a low-pass filter (first-order, T=0.3s) on measured power and measured speed in the turbine speed controller. This produced a slower-varying reference power that is input to the VSM converter power controller. The resulting response is shown in Figure 67 and Figure 68 (to be compared with Figure 64 and Figure 65 respectively). As the results show, the oscillations are greatly reduced, albeit not eliminated. It should be noted, however, that such a modification to the speed controller may have unwanted effects in other operating conditions, for example leading to too slow response in case of a wind gust. Further investigations and parameter tunings are required to establish for certain whether this control concept will work in realistic conditions.
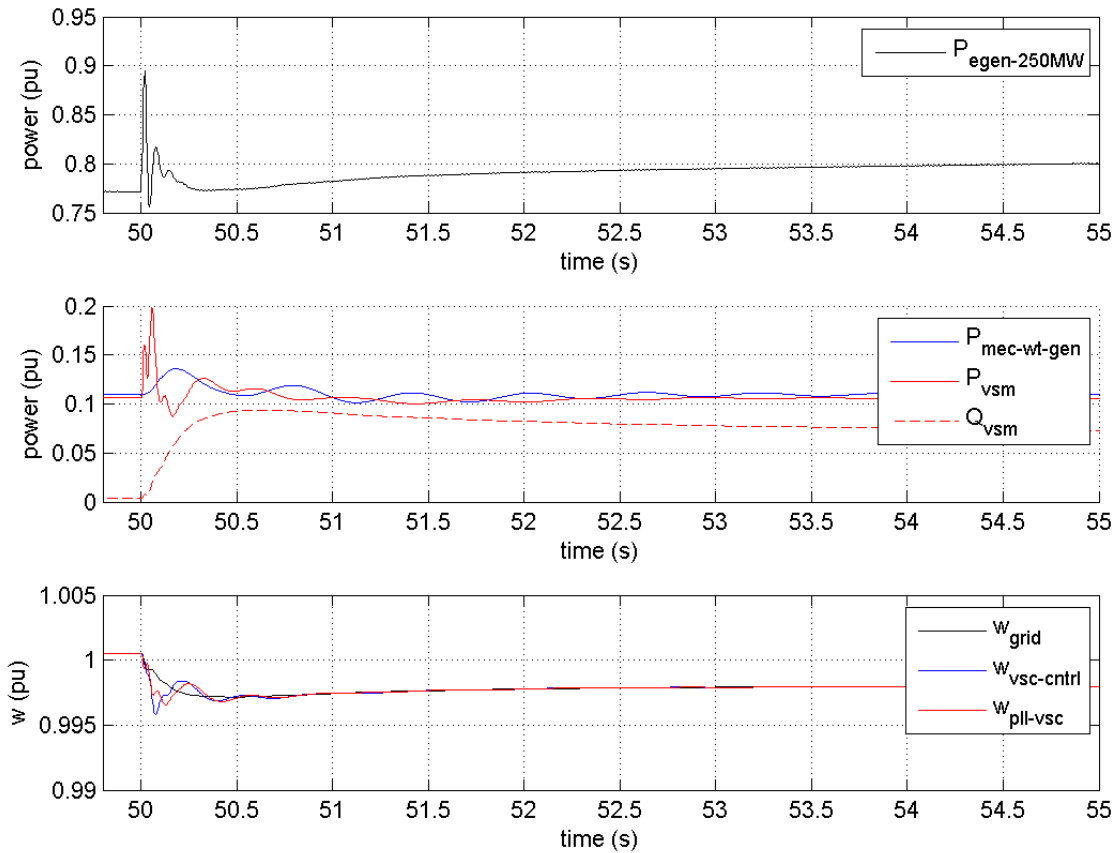
FIGURE 67: POWER AND SPEED RESPONSE WITH FIRST-ORDER FILTER (TIME CONSTANT 0.3 SEC) ON THE TURBINE SPEED CONTROLLER MEASURED POWER AND MEASURED SPEED.
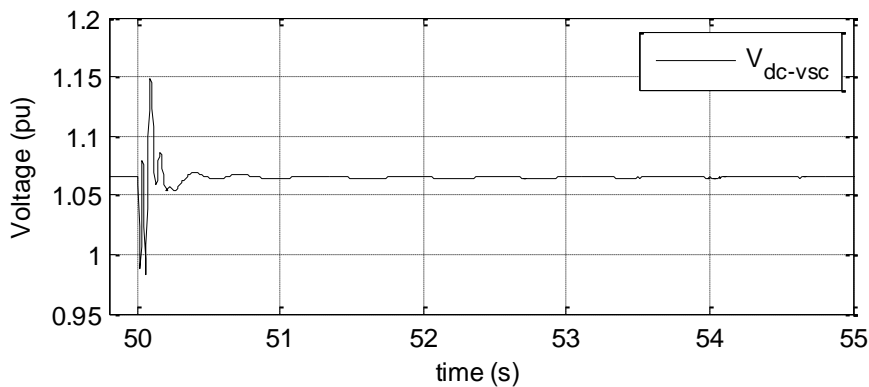
FIGURE 68: VOLTAGE RESPONSE WITH FIRST-ORDER FILTER (TIME CONSTANT 0.3 SEC) ON THE TURBINE SPEED CONTROLLER MEASURED POWER AND MEASURED SPEED.

7.3 DISCUSSION

This chapter has presented numerical results exploring different converter control strategies utilising the virtual synchronous machine (VSM) concept on the grid-side converter. Two main approaches have been investigated: One where the grid-side VSM converter controls the dc

voltage and the generator-side converter controls active power, and another where the VSM converter controls the active power and the generator-side converter controls the dc voltage. The first approach resembles the typical setup for converter-interfaced wind turbines connected to the grid.

Inertia support from the VSM is an inherent characteristic but depends on there being an energy storage to inject or extract power from. The wind turbine dc-link capacitor serves this purpose. For the inertia (i.e. the rotational energy) of the wind turbine rotor to also participate in grid support, the need for inertia support must be communicated across the dc-link. This is not automatic if the dc voltage is controlled by the grid-side VSM converter, isolating it from the generator side. On the other hand, if the dc voltage is controlled on the generator side, the wind turbine will automatically participate in inertia support since the generator-side converter control will respond to the drop in dc voltage arising because the grid-side VSM converter injects extra power into the grid.

For the first approach, where the VSM controls dc voltage, simulation results demonstrated the need for a large dc-link capacitance or increased dc voltage level to allow significant inertia support by the VSM. Converter overmodulation issues occurred in the simulations due to the dc voltage dropping too low, giving poor performance. Increasing the voltage level may not be straightforward as it has consequences for insulation design, protection equipment and possibly turbine maintenance operations.

The second approach where the wind turbine generator-side converter controls the dc voltage seems more promising. This approach allows the VSM to support the frequency deviation with more freedom than the previous strategy. Furthermore, this strategy can use normal design circuit and operating point parameters at the dc link. A drawback is a tighter coupling between controllers, potentially leading to unwanted controller interactions and a need for careful parameter tuning.

8 WIND TURBINE CONVERTER OVERPOWERING FOR FREQUENCY SUPPORT

Ancillary services provision as frequency support and inertia emulation with wind turbines may require temporary increase in the power injection to the receiving grid. If the turbine operates already to the rated power, these ancillary services could arguably not be provided if temporary overpowering of the components is not implemented. In this report, overpowering refers to a situation where active power temporarily exceeds rated power.

The rating of components is normally defined by thermal design considerations since slightly exceeding the rated power leads to higher temperatures compared to design assumptions and possibly early failure. Failure mechanisms may be of different nature depending of the components. Indeed, overtemperatures cause an accelerated aging of the insulation materials and a shorter life span for cables and transformers while power semiconductor devices may suffer from

catastrophic failure (e.g. explosion of components). Moreover, it should be noted that the thermal time constants for the components are linked to their thermal capacity. In this perspective, transformers, generators and cables are characterized by thermal time constants of several minutes to hours while the time constants for the semiconductor devices inside power converters are only fractions of a second. Thus, when overpowering a turbine, the most limiting components with a conventional design are the power electronics converters.

Power semiconductors are specified for continuous operating current but can sustain repetitive bursts of current without physical damage. These overloading capabilities are specified in the components datasheet and could e.g. allow a doubling of the rated current but for a relatively short time (e.g. 1 ms). Exceeding these limits could cause an irreversible damage to the semiconductor and consequently of the entire power converter. However, a converter would be designed with safety measures to absolutely prevent these conditions: A first measure is to introduce a safety margin in the converter ratings so that the rated conditions corresponds to lower currents compared to the ratings of the devices. A second measure is to include overcurrent protections in the converter design that interrupts the operation if the measured currents exceed predefined thresholds. These current protections could act on the instantaneous value and be triggered immediately after the overcurrent is sensed or could account also for the time interval (e.g. low pass filtering or integrating the overcurrent). Converter design could include both these types of protections allowing a temporary overloading of the converter if the overcurrent is relatively small while immediately blocking the converter for more severe overcurrents. The rest of this chapter investigates the impact such temporary converter overloading may have on frequency stability support from wind turbines.

8.1 Numerical example of impact of converter overpowering on the grid

Converter overpowering is possibly feasible but largely depends on the specific protection implementation and this is a specific designer choice. These capabilities should be verified on each turbine model and cannot be generalized. Thus, in this report the system impact of converter overpowering is assessed by simulating how a frequency disturbance can be mitigated with ancillary services requiring the turbine rating to be temporarily exceeded. The overpowering is modelled as a step increase $P \rightarrow P_0 \cdot$ PeakPower of the output power P in the generator side converter for a certain time duration ΔT. Since the frequency disturbance cannot be detected immediately, the overpowering control is assumed to be delayed by a time To. The same system as illustrated in Figure 50 has been simulated, with a simplified representation of the wind turbine (Figure 54).

The left plot of Figure 69 illustrates the frequency transient due to a sudden load increase, and how it should be affected by overpowering support. Immediately after the load step, the frequency drops and then recovers due to generator frequency controls. The intended effect of overpowering is to supply fast-acting frequency support that limits the rate of change and therefore the minimum point of the frequency whilst other frequency control actions are being activated. To assess the performance of overpowering, the focus should be on the section between the load step and the minimum point on the frequency response curve. In the following simulations this corresponds approximately to the first 200 ms after the load step.

The frequency response observed in a simulation of the load step *without any overpowering* is shown in the right-side plot of Figure 69. The load step occurs at 50 s. The response follows the expected curve, but with notable transient oscillations. The question now is if this response can be improved, i.e. whether the frequency drop can be reduced. To assess the impact of overpowering, multiple simulations with varying values of the power step (PeakPower), duration ΔT and delay To have been conducted.

The swing equation gives a way to estimate the change in the generator speed $\Delta\omega$ due to an energy injection ΔE. In the per unit system, this is $\frac{2H}{\omega_s}\frac{d\omega}{dt} = P \Rightarrow \frac{\Delta\omega}{\omega_s} \approx \frac{\Delta E}{2H}$, where H is the inertia constant and ω_s is the base speed corresponding to 50 Hz frequency. Considering that the grid equivalent generator (rating 250 MVA) is the dominant source of inertia ($H = 1$ s), and disregarding other components as well as any control actions, it can be found that a load increase of 25 MW for a duration of 100 ms, i.e. $\Delta E = 25/250 \cdot 100$ ms , gives a relative speed decrease of $\Delta\omega/\omega\_s \approx 0.005$. In absolute terms this corresponds to 0.25 Hz. This is about twice the amount read from the simulation result in Figure 69 at time 50.1 s. The 2x overestimate using the swing is presumably because it only considers the onshore grid equivalent inertia and ignores other parts of the network.
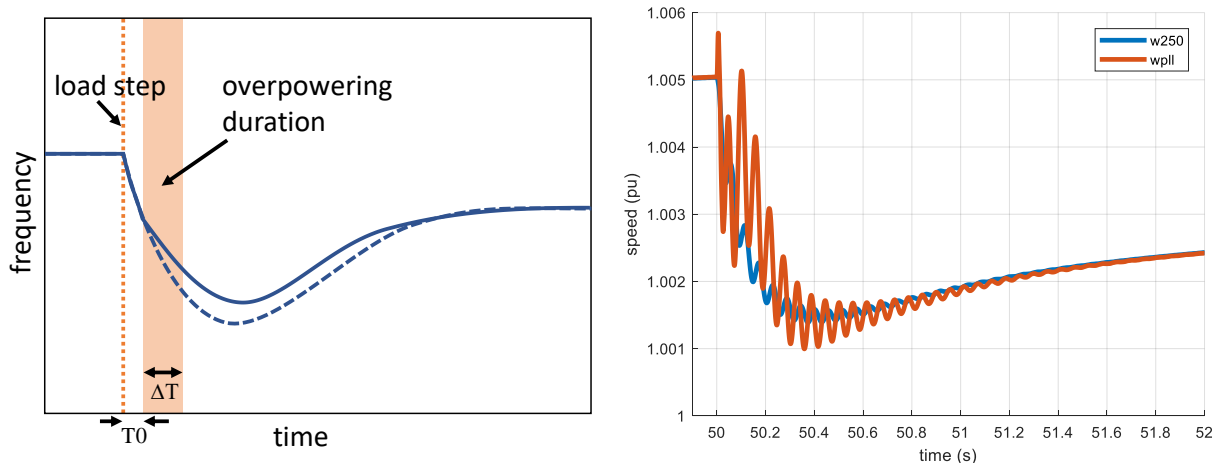
FIGURE 69: FREQUENCY TRANSIENT AFTER LOAD STEP. LEFT: SCHEMATIC SHOWING REPONSE WITHOUT (DOTTED LINE) AND WITH OVERPOWERING SUPPORT (SOLID LINE). RIGHT: SIMULATION RESULT SHOWING SPEED OF ONSHORE GRID EQUIVALENT GENERATOR (W250) AND ESTIMATE BY CONVERTER PLL (WPLL) WITHOUT ANY OVERPOWERING.

8.1.1 WITHOUT CONVERTER CONTROLLER MODIFICATIONS

A first set of tests were done where additional power from the wind turbine is fed through the grid-side voltage-source converter (VSC) without any modifications to the controllers.

Figure 70 shows the first 700 ms after the load step followed by overpowering support with ΔT=20 ms, To=100 ms. The figure shows active power from the wind turbine (WT) in the top plot, active power of the voltage-source converter (VSC) in the next plot, dc-link voltage in the next, and the frequency as given by the onshore grid equivalent generator rotor speed in the bottom plot.

Different curves within each plot correspond to different levels of overpowering, quantified as the peak power in relative units. The amount of extra energy injected into the grid is dependent on both the peak power, and the time duration.

In this overpowering implementation, the extra power from the wind turbine is injected into the dc-link and absorbed by the capacitor as the dc voltage increases. The dc voltage controller tries to maintain the dc voltage by pushing the power through to the grid. This is done by an increase to the current reference. However, the PI block within the dc controller has a saturation parameter that limits the reference current output, which in turn limits the power pushed into the grid. This is why, as we see in Figure 70 (power VSC), the power is the same for all the peak power cases until the dc voltage deviation drops down below a certain limit. So the power from the wind turbine is being buffered by the dc link capacitor, such that the power increase fed through the VSC is limited but extended in time. The more energy being supported, i.e. the higher the peak power, the longer the power injection into the grid lasts. As desired and expected, the effect on the frequency (w_{250MW}) is to decrease the frequency drop, evident by the purple, yellow and red curves lying above the light blue one. The effect is not so clear because the difference between the curves are small compared to the oscillations created by the load step.

To get a more rapid injection of energy, the dc controller saturation parameter could be changed, allowing larger values for the reference current. This may be beneficial for the overpowering situation but can have negative consequences in other circumstances.

8.1.2 WITH FEED-FORWARD TERM ADDED TO CONVERTER CONTROLLER

To provide more support in the crucial first milliseconds of the frequency drop (after the sudden load increase) the converter controller can be modified by adding to the reference current a delta value corresponding to the extra power being fed from the turbine, see Figure 71. In this way, the additional power from the wind turbine is being immediately "pushed through" to the grid. Simulation results in this case are shown in Figure 72.
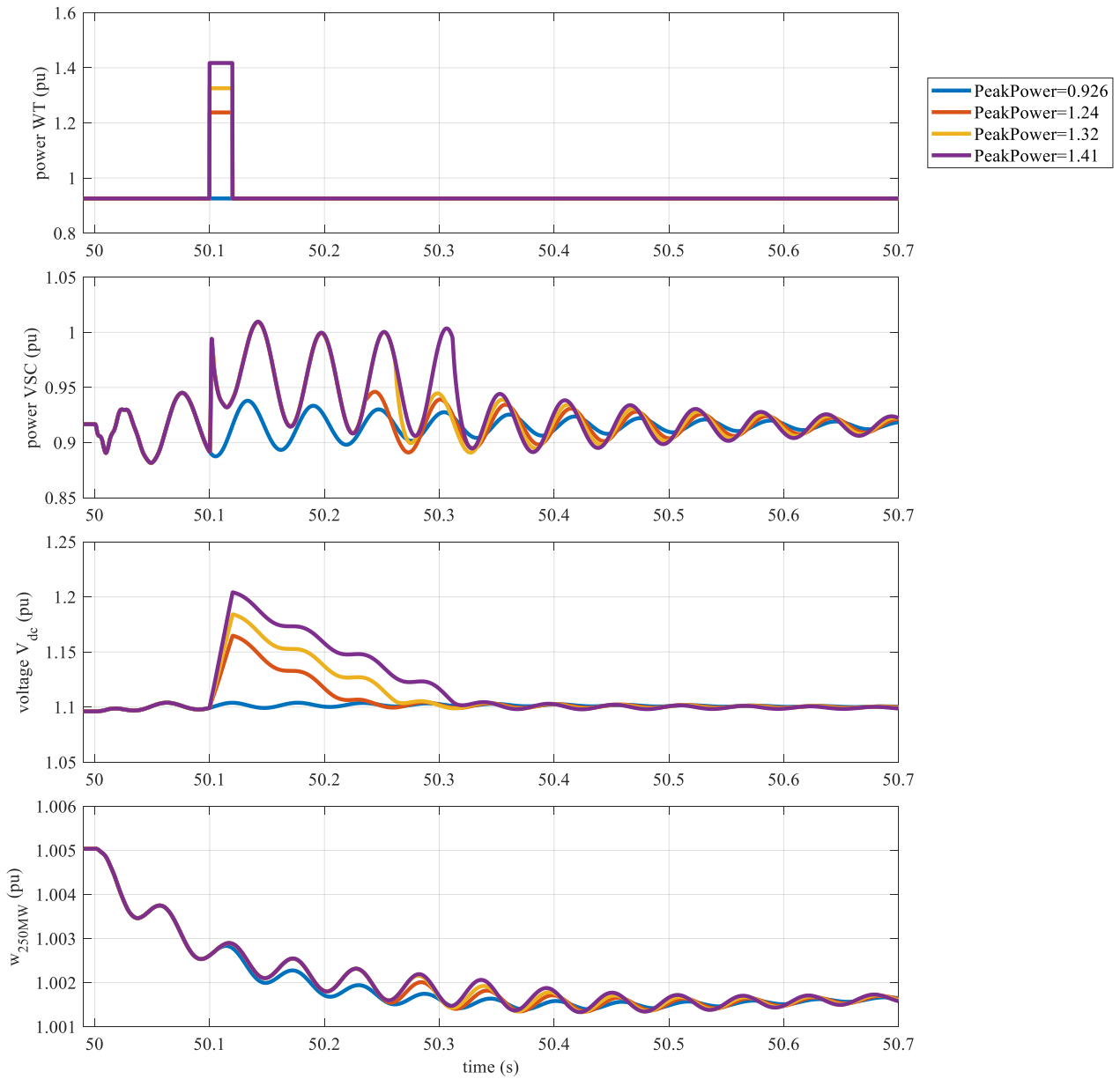
FIGURE 70 OVERPOWERING OF WT AFTER LOAD STEP AT 50 S, FOR ΔT=20 MS WITH T₀=100 MS DELAY
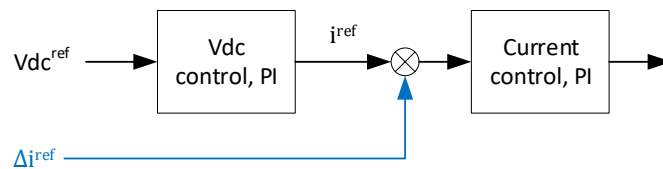
FIGURE 71: MODIFICATION TO THE GRID-SIDE CONVERTER CONTROLLER (SHOWN IN BLUE).
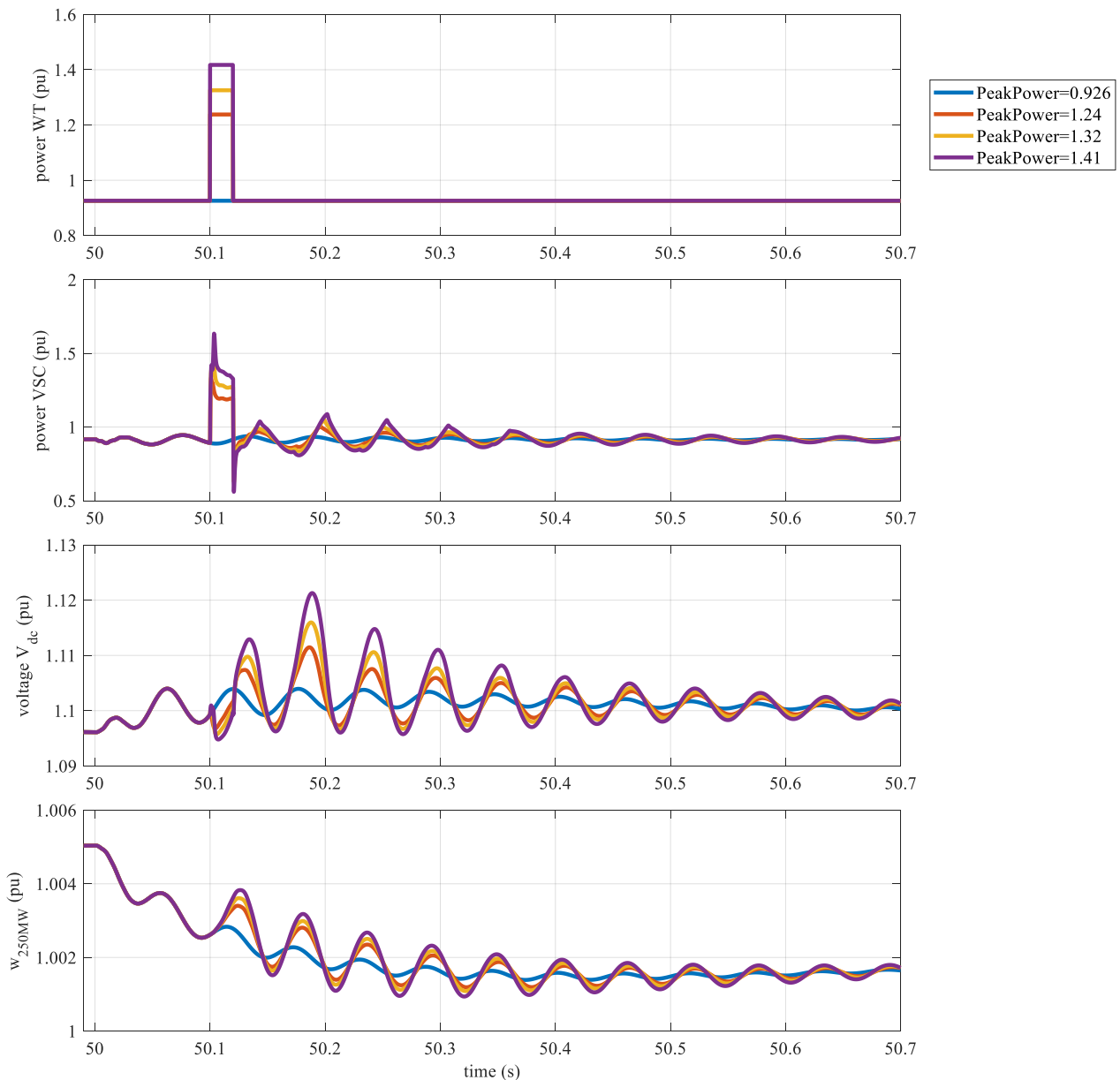
FIGURE 72 OVERPOWERING WITH FEEDFORWARD AFTER LOAD STEP AT 50 S, WITH ΔT= 20 MS AND T0=100 MS DELAY.

To see the effect on frequency more clearly without the oscillations due to the load step, the simulations have been repeated without the load step, but still with the same overpowering injection as before. As expected, the overpowering now generates a frequency increase, as seen in Figure 73. The base case with no extra power injected is the blue curve (PeakPower=0.926). The frequency support is clearly visible, especially in the case without feedforward. However, the impact in absolute terms is very small, less than 0.001 pu. In the case with the feedforward term included, the overpower injection generates an oscillation. The integrated effect is a positive contribution to the frequency, acting more rapidly than the case without the feedforward term. This was indeed the reason for introducing the feedforward term. But again, the magnitude of the actual contribution is very small.
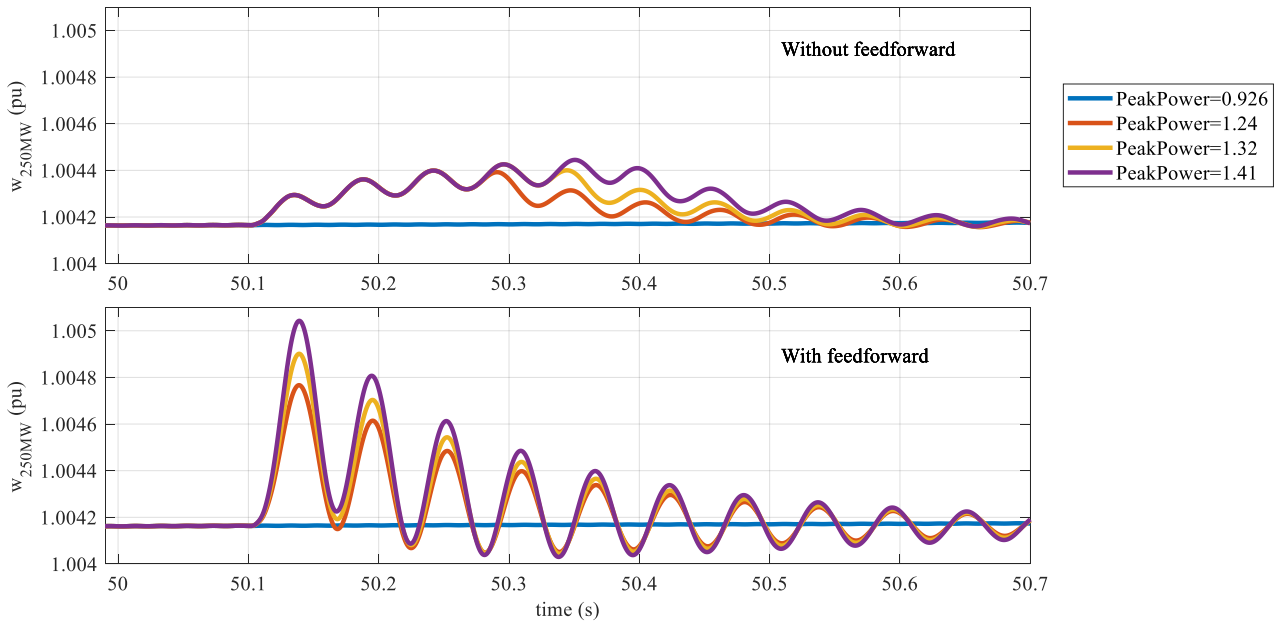
FIGURE 73 FREQUENCY RESPONSE WITH NO LOAD STEP AND ONLY OVERPOWERING INJECTION (ΔT=20 MS), WITHOUT (TOP) AND WITH (BOTTOM) FEEDFORWARD TERM IN THE CONTROLLER.

8.2 DISCUSSION

The strict safety limits on power electronics components means that little energy can be pushed through the converters if they are already operating at the rated value. As discussed above, converter overloading is only possible for very short time intervals. Of course, the maximum duration is dependent on the amount of power, but 20 ms is clearly at the upper end of what is permissible.

The frequency deviation seen in Figure 73 for the PeakPower=1.41 case, imagining that the oscillations are filtered out, is about 0.0004, or 0.02 Hz in absolute terms. This is about one tenth of the 0.2 Hz deviation caused by the load step. For comparison, we can make an order-of-magnitude estimate of the frequency impact using the swing equation: The energy injection in per units is $\Delta E = 0.41 \cdot 50/250 \cdot 20$ ms, giving $\Delta\omega/\omega_s = 0.0008$, again a factor two above the observation in the simulation. It should be noted that the simulated grid equivalent with S=250 MVA and H = 1 in fact corresponds to a low inertia grid, likely a considerably weaker grid than what is the case for most offshore wind power plant connections. That is, the simulation results likely overestimate the frequency impact of wind farm frequency support. In terms of overall *extra* energy injection into the grid, the overpowering cases provide up to $0.41 \cdot 50$ MW $\cdot 20$ ms = 0.41 MJ. This is very likely more than wat is realistically possible within converter safety limits.

For comparison, the VSM scheme depicted in Figure 59 ($\tau = 8$s), provides in the first 100 ms about $0.06 \cdot 50$ MW $\cdot 100$ ms = 0.3 MJ, and in the first 500 ms about 1.7 MJ. However, it makes little sense to compare the two control functions as they do not have the same purpose. The VSM frequency support is almost immediate and designed to limit the rate of change of the frequency (inertia support). The overpowering scheme needs to be explicitly activated and can then provide a short burst of energy when needed.

The two overpowering schemes (with or without feedforward term to the converter current controller) both provide grid frequency support by allowing a temporary over-rated power boost from the wind turbine to be fed through the converter into the grid. The dc-link capacitor buffers this energy injection and smooths the energy out over an extended time. A faster frequency support can be achieved with a feedforward term to the converter current controller that pushes the extra power directly to the grid. Such a sudden energy injection is akin to knocking the grid with a hammer, and as evident from the simulations, may produce power oscillations. We believe the necessary controller adjustments to be possible but requires more work that falls outside the scope of the present study.

At a more fundamental level, the potential benefit of converter overpowering is strictly limited by its safety margins, as discussed in the introduction to this chapter. To allow more substantial overpowering from the wind turbine, a converter with higher power rating could be selected. In that way, over-rated power from the turbine could be allowed for a longer time, overpowering cables and transformers without severe impacts whilst keeping within converter rated power. The benefit of such improved overpowering capability needs of course to be considered together with the added cost of the larger converter.

9 CONCLUSIONS

Two derating strategies have been developed by DTU and tested using a HAWC2 model of the 7 MW Levenmouth turbine. The strategies have been run at various power set-points with normal operation, and the loading implications for the two strategies have been compared. The mean tower loads generally decrease for both strategies with the produced power. However, fatigue loading is increased when the "constant rotation" is used. The "maximum rotation" strategy generally shows reductions of fatigue and extreme loads.

Different behaviour is found for the blades. The "constant rotation" de-rate strategy reduces both flapwise and edgewise fatigue while the "maximum rotation" strategy has barely an impact. The mean and extreme loads are reduced by both strategies. Both strategies also present a decrease on mean and fatigue shaft torsion loading with an increase in pitch activity.

Based on the HAWC2 model of the 7MW Samsung turbine coupled with the open-source DTU controller and considering the modelling limitations DTU had during this time it is possible to conclude that, both control strategies can be used without increasing extreme or fatigue loading when de-rate percentages of 90% and 80% are used. On the other hand, the 70% de-rate for the constant rotation strategy increase the tower loading because of the coupling between the 3P excitation and tower natural frequencies.

Both strategies were then implemented into the actual controller software of the 7 MW Levenmouth turbine, and tested using Bladed simulations, to demonstrate that the strategies are suitable for field testing in the coming year. This is important to ensure the integration of the strategy with other controller features not present in the DTU open-source controller used for the HAWC2 simulations. These include, for example, a generator speed exclusion zone to avoid the 3P forcing exciting the tower first fore-aft mode when operating the turbine in the variable speed mode, a fine pitch schedule to reduce thrust forces around rated wind speed, and individual pitch control to reduce asymmetrical hub / blade / yaw loads. There is also a noise reduction mode, but the power reduction strategies will only be used when the noise reduction mode is off.

A number of Bladed simulations were run in both steady and turbulent wind conditions to demonstrate the correct operation of both strategies, with a full range of de-rating setpoints, and confirm successful integration with the speed exclusion zone and other controller features mentioned above. The strategies can therefore be considered ready to be included in the schedule of field tests to be run on the Levenmouth turbine during the coming year.

In the second part of the report, the use of the virtual synchronous machine (VSM) concept for inverter control was investigated as means to provide fast frequency response to help stabilise grid frequency, as well an 'overpowering' strategy to provide a very short-duration injection of active power if needed by the grid. Although it will not be possible to implement these strategies in the Levenmouth turbine inverter, the feasibility of the concept was confirmed, and different options compared using simulations.

Inertia support using VSM depends on have some stored energy to inject into the grid. If the dc voltage is controlled by the grid-side VSM converter, the dc-link capacitor serves this purpose. However, simulation results demonstrated the need for a large dc-link capacitance or increased dc voltage level to allow significant inertia support by the VSM, and this may not be straightforward. Much more stored energy is available from the kinetic energy of the turbine rotor, however, and for the turbine inertia to participate in grid support, the dc voltage can instead be controlled on the generator side. This approach allows the VSM to support the frequency deviation with more freedom, and it can use normal design circuit and operating point parameters at the dc link. However, tighter coupling between controllers could lead to unwanted interactions, so careful parameter tuning is required.

Two overpowering schemes (with or without feedforward) were investigated as a way to provide a temporary over-rated power boost from the wind turbine to be fed through the converter into the grid. The dc-link capacitor buffers this energy injection and smooths the energy out over a longer period. Faster frequency support can be achieved with a feedforward term to the converter current controller. This gives a very sudden energy injection which may produce power oscillations, as evident from the simulations. Controller adjustments to avoid this may be possible, but further work would be required. However, the potential benefit of converter overpowering is strictly limited by its safety margins, so to allow more substantial overpowering from the wind turbine, a converter with higher power rating could be selected, if the extra cost justifies the benefit.

REFERENCES

[1]   S D'Arco, J Suul, "Virtual synchronous machines – Classification of implementations and analysis of equivalence to droop controllers for microgrids", IEEE Grenoble Conference, June 2013, https://doi.org/10.1109/PTC.2013.6652456

[2]   S. Wang, J. Hu and X. Yuan, "Virtual Synchronous Control for Grid-Connected DFIG-Based Wind Turbines," in IEEE Journal of Emerging and Selected Topics in Power Electronics, vol. 3, no. 4, pp. 932-944, Dec. 2015. https://doi.org/10.1109/JESTPE.2015.2418200

[3]   Y. Zhao, J. Chai and X. Sun, "Virtual synchronous control of grid-connected DFIG-based wind turbines," 2015 IEEE Applied Power Electronics Conference and Exposition (APEC), Charlotte, NC, 2015, pp. 2980-2983. https://doi.org/10.1109/APEC.2015.7104775

[4]   Y. Ma, W. Cao, L. Yang, F. Wang and L. M. Tolbert, "Virtual Synchronous Generator Control of Full Converter Wind Turbines With Short-Term Energy Storage," in IEEE Transactions on Industrial Electronics, vol. 64, no. 11, pp. 8821-8831, Nov. 2017. https://doi.org/10.1109/TIE.2017.2694347

[5]   Qing-Chang Zhong, Zhenyu Ma, Wen-Long Ming, George C. Konstantopoulos, Grid-friendly wind power systems based on the synchronverter technology, Energy Conversion and Management, Volume 89, 2015, Pages 719-726, ISSN 0196-8904, https://doi.org/10.1016/j.enconman.2014.10.027.

[6]   Zhong Q-C, Weiss G. Synchronverters: inverters that mimic synchronous generators. IEEE Trans Ind Electron 58 (4) 1259–67, 2011. https://doi.org/10.1109/TIE.2010.2048839

[7]   L. Huang et al., "A Virtual Synchronous Control for Voltage-Source Converters Utilizing Dynamics of dc-Link Capacitor to Realize Self-Synchronization," in IEEE Journal of Emerging and Selected Topics in Power Electronics, vol. 5, no. 4, pp. 1565-1577, Dec. 2017. https://doi.org/10.1109/JESTPE.2017.2740424

[8]   S. D'Arco, JA Suul, OB Fosso, "A Virtual Synchronous Machine implementation for distributedcontrol of power converters in SmartGrids", Electric Power Systems Research 122 (2015) 180–197, https://doi.org/10.1016/j.epsr.2015.01.001

[9]   O Mo, S D'Arco, JA Suul, " Evaluation of Virtual Synchronous Machines With Dynamic or Quasi-Stationary Machine Models", IEEE Trans. on Ind. Electronics 64 (2017) 7, https://doi.org/10.1109/TIE.2016.2638810

[10]   S. Andersen, et al., "Reference Wind Power Plant", TotalControl project report 1.3, April 2018.

[11]   A. Holdyk, K. Kölle, K. Merz, "An Electromechanical model of the TotalControl Reference Wind Power Plant", TotalControl project report D1.5, March 2019.

[12]   A. Shafiu, O. Anaya-Lara, G. Bathurst, and N. Jenkins; Aggregated Wind Turbines Models for Power System Dynamics Studies; Wind Engineering; Vol. 30; No. 3; 2006; pp. 17-186.

[13]   Mirzaei, M., Soltani, M., Poulsen, N. K., & Niemann, H. H. (2014). Model based active power control of a wind turbine. In 2014 American Control Conference (pp. 5037–5042). IEEE. https://doi.org/10.1109/ACC.2014.6859055

[14]   Lio, W. H., Mirzaei, M., & Larsen, G. C. (2018). On wind turbine down-regulation control strategies and rotor speed set-point. Journal of Physics: Conference Series, 1037, 032040. https://doi.org/10.1088/1742-6596/1037/3/032040

[15]   Hansen, M. H., & Henriksen, L. C. (2013). Basic DTU Wind Energy controller. DTU Wind Energy.

APPENDIX A

The polar plots for all wind speeds are provided in the appendix excluding 5 and 6 m/s where the de-rating strategies have the same response as the normal operation case.

CONSTANT ROTATION PLOTS
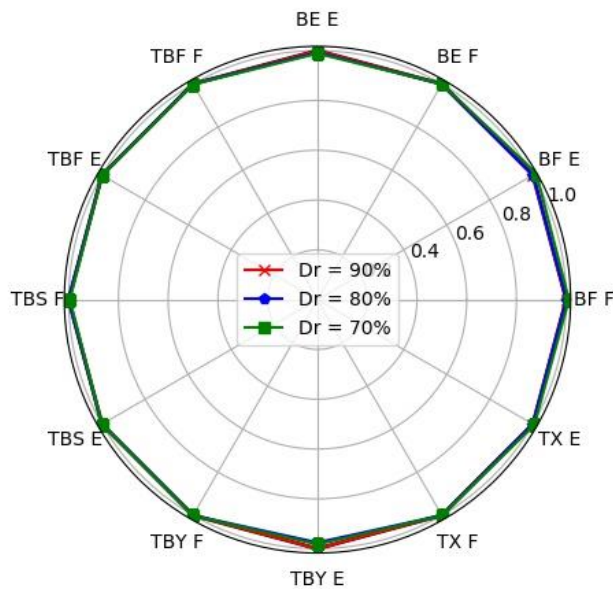
FIGURE 74: COMPARISON EXTREME AND FATIGUE CONSTANT ROTATION WSP = 7M/S
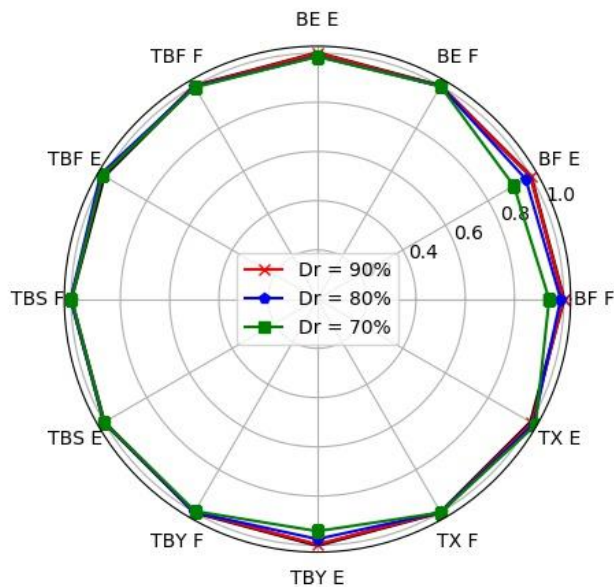
FIGURE 75: COMPARISON EXTREME AND FATIGUE CONSTANT ROTATION WSP = 8M/S
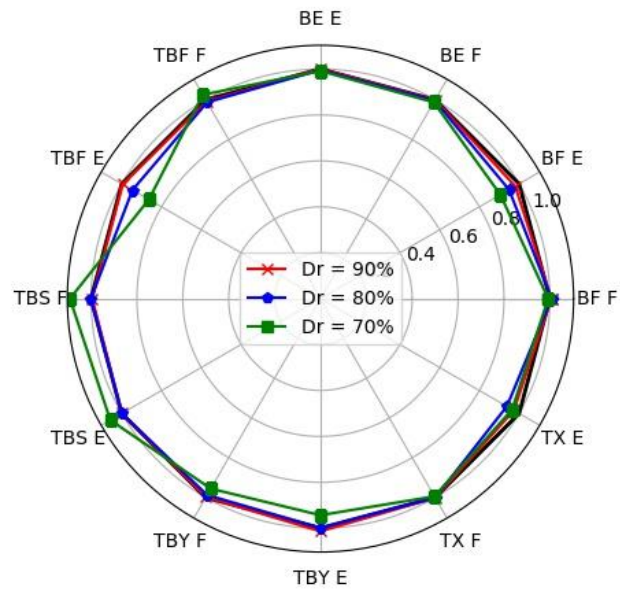
FIGURE 76: COMPARISON EXTREME AND FATIGUE CONSTANT ROTATION WSP = 9M/S
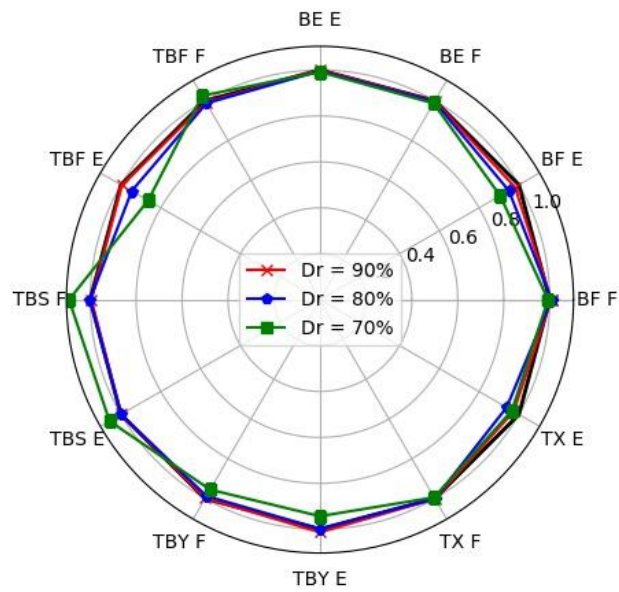
FIGURE 77: COMPARISON EXTREME AND FATIGUE CONSTANT ROTATION WSP = 10M/S
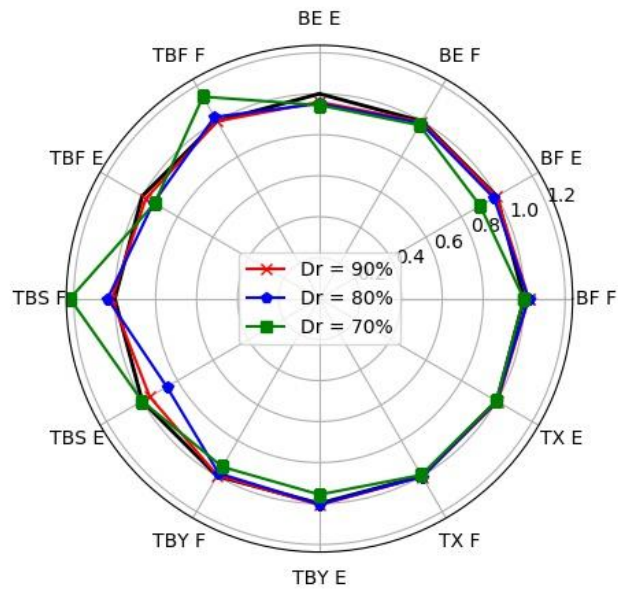
FIGURE 78: COMPARISON EXTREME AND FATIGUE CONSTANT ROTATION WSP = 11M/S
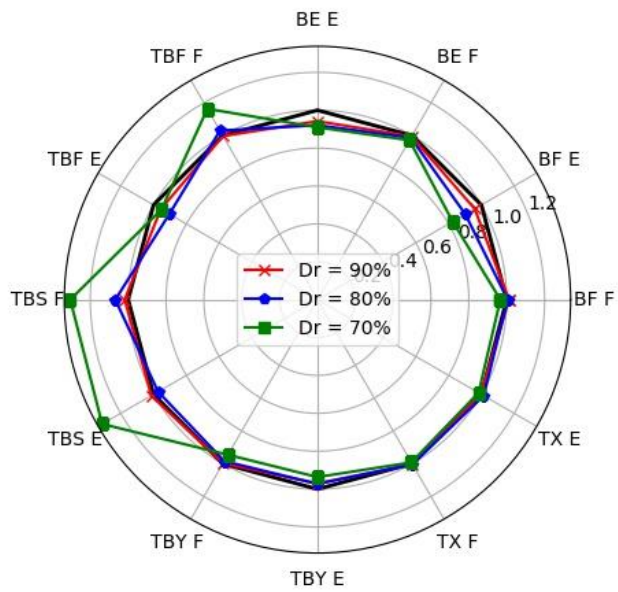
FIGURE 79: COMPARISON EXTREME AND FATIGUE CONSTANT ROTATION WSP = 12M/S
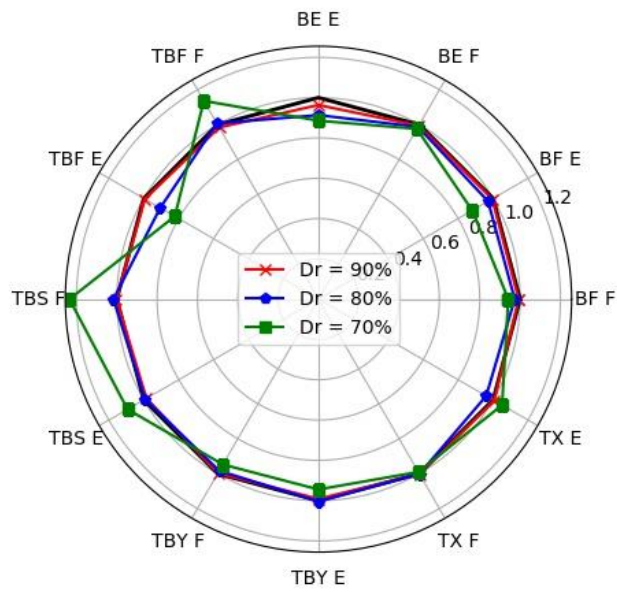
FIGURE 80: COMPARISON EXTREME AND FATIGUE CONSTANT ROTATION WSP = 13M/S
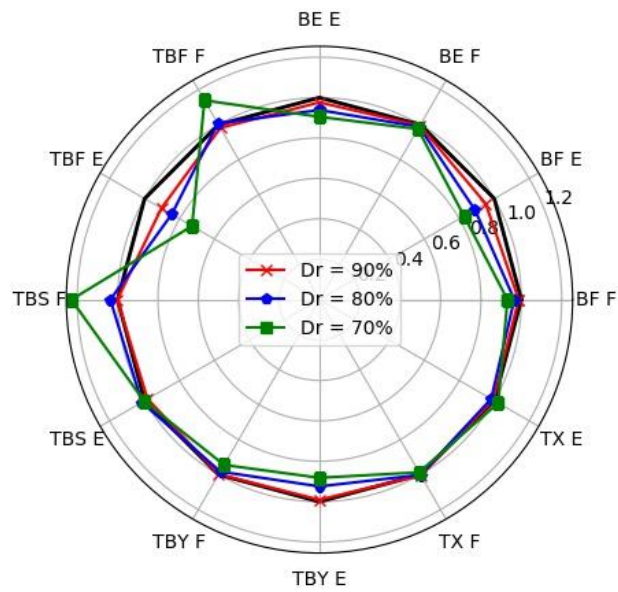
FIGURE 81: COMPARISON EXTREME AND FATIGUE CONSTANT ROTATION WSP = 14M/S
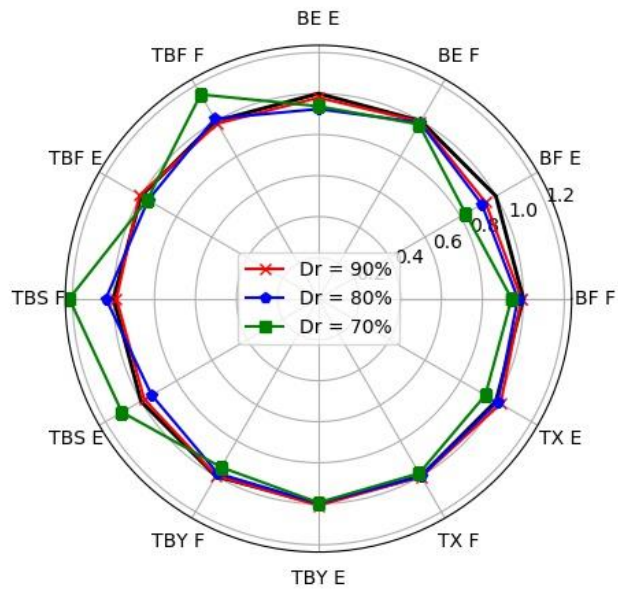
FIGURE 82: COMPARISON EXTREME AND FATIGUE CONSTANT ROTATION WSP = 15M/S
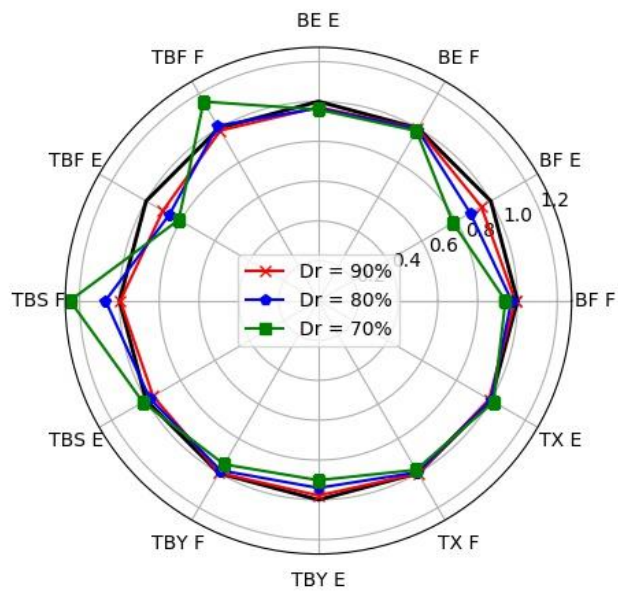
FIGURE 83: COMPARISON EXTREME AND FATIGUE CONSTANT ROTATION WSP = 16M/S
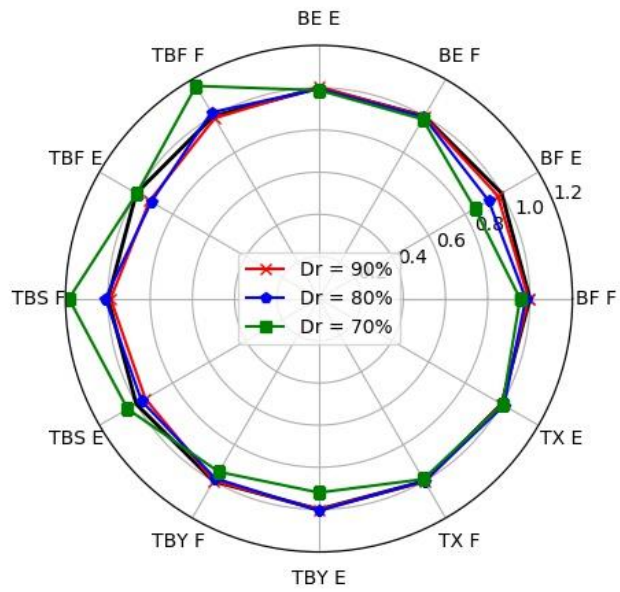
FIGURE 84: COMPARISON EXTREME AND FATIGUE CONSTANT ROTATION WSP = 17M/S
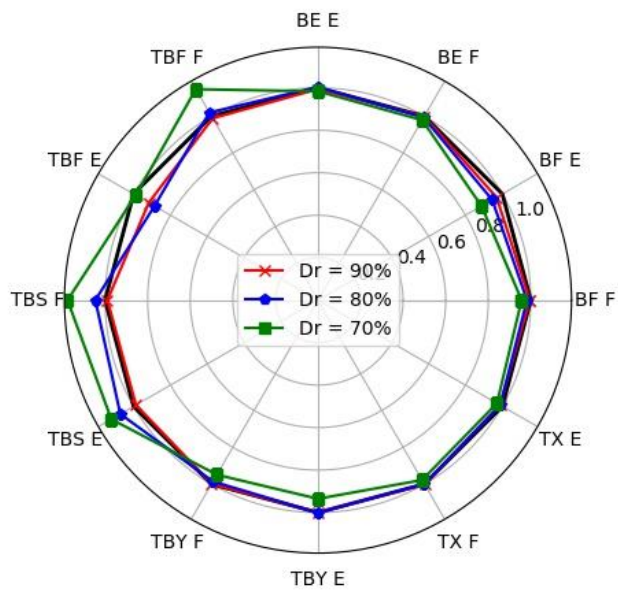
FIGURE 85: COMPARISON EXTREME AND FATIGUE CONSTANT ROTATION WSP = 18M/S
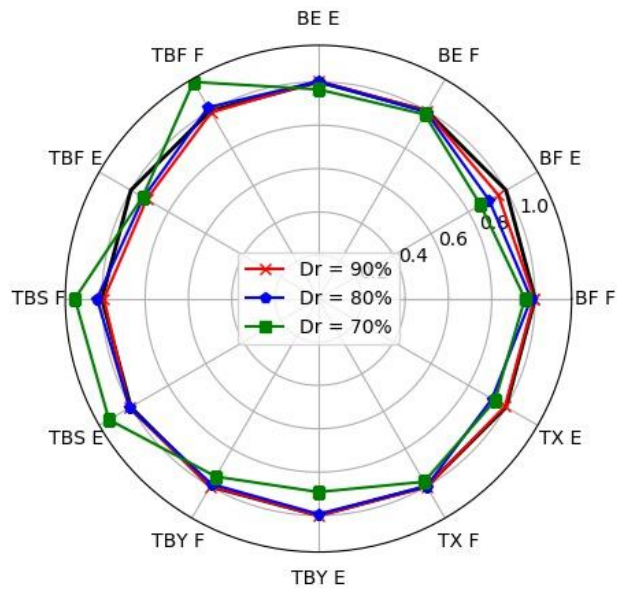
FIGURE 86: COMPARISON EXTREME AND FATIGUE CONSTANT ROTATION WSP = 19M/S
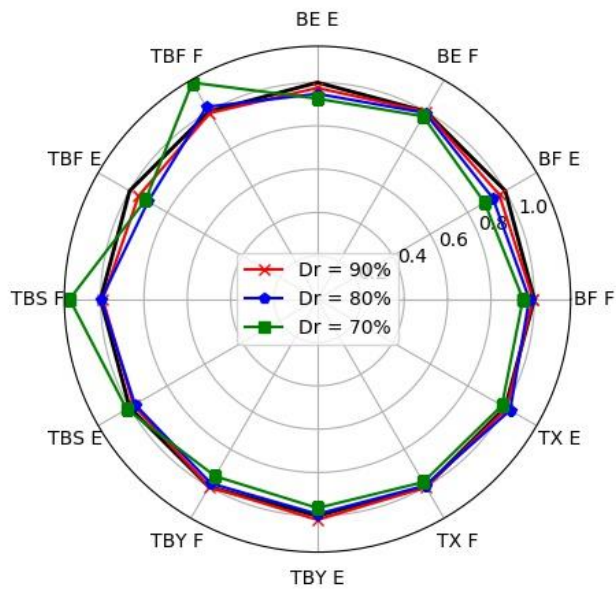
FIGURE 87: COMPARISON EXTREME AND FATIGUE CONSTANT ROTATION WSP = 20M/S
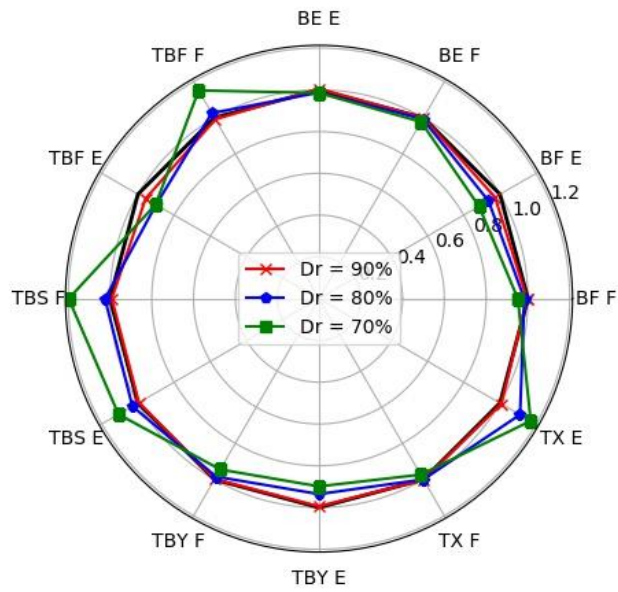
FIGURE 88: COMPARISON EXTREME AND FATIGUE CONSTANT ROTATION WSP = 21M/S
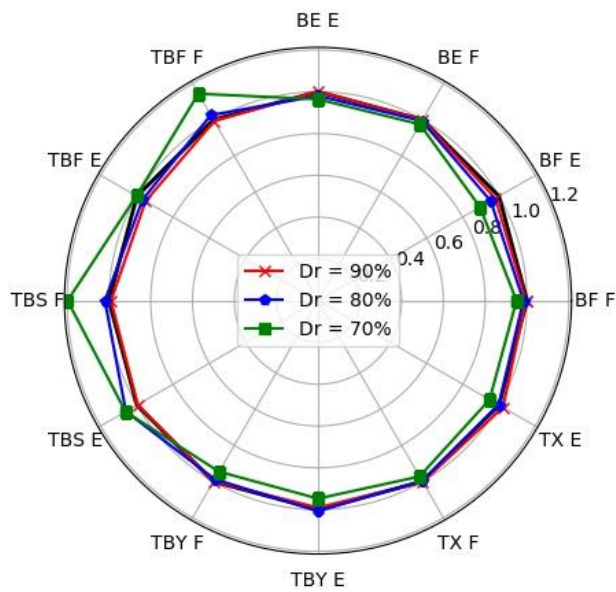
FIGURE 89: COMPARISON EXTREME AND FATIGUE CONSTANT ROTATION WSP = 22M/S
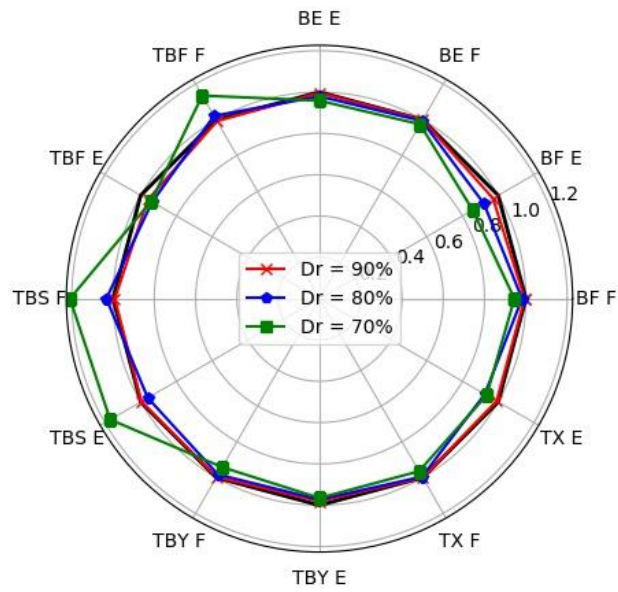
FIGURE 90: COMPARISON EXTREME AND FATIGUE CONSTANT ROTATION WSP = 23M/S
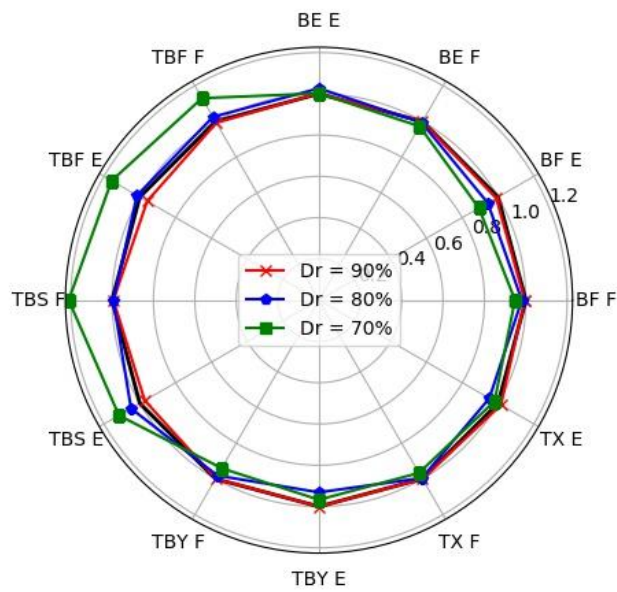
FIGURE 91: COMPARISON EXTREME AND FATIGUE CONSTANT ROTATION WSP = 24M/S
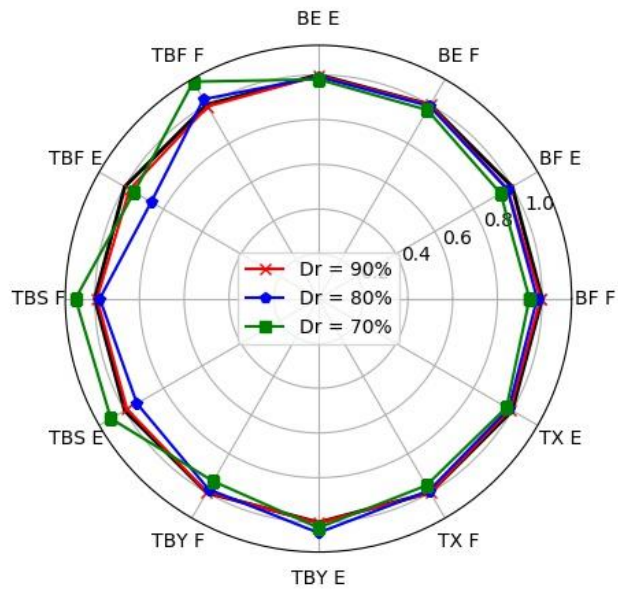
FIGURE 92: COMPARISON EXTREME AND FATIGUE CONSTANT ROTATION WSP = 25M/S

MAXIMUM ROTATION PLOTS
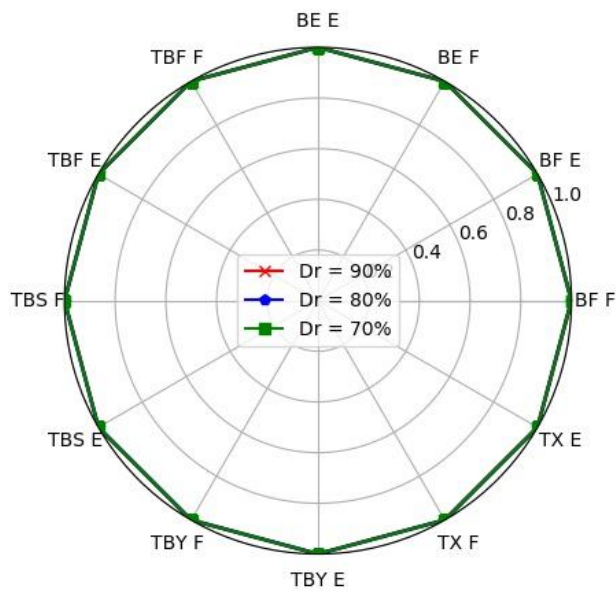
FIGURE 93: COMPARISON EXTREME AND FATIGUE MAXIMUM ROTATION WSP = 7M/S
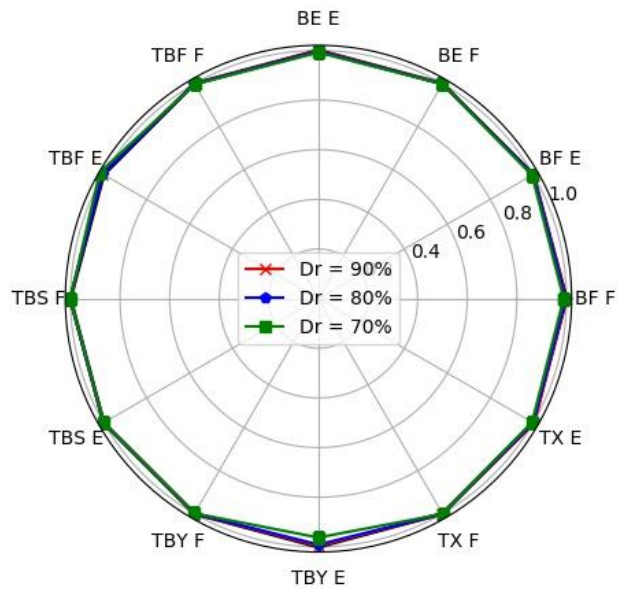
FIGURE 94: COMPARISON EXTREME AND FATIGUE MAXIMUM ROTATION WSP = 8M/S
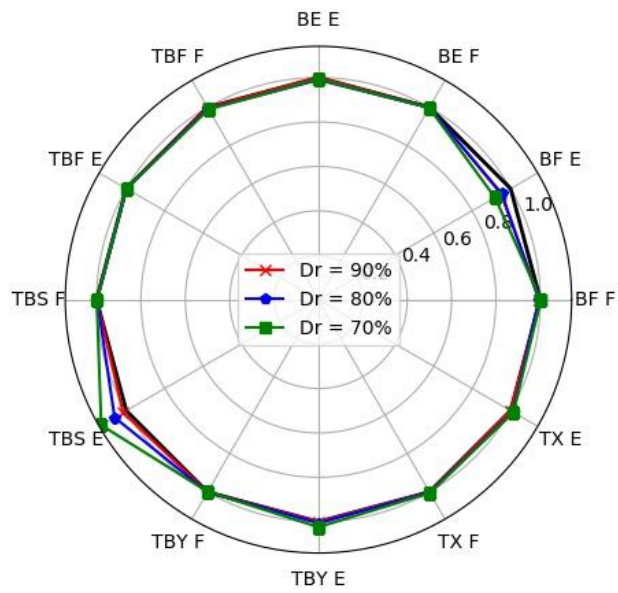
FIGURE 95: COMPARISON EXTREME AND FATIGUE MAXIMUM ROTATION WSP = 9M/S
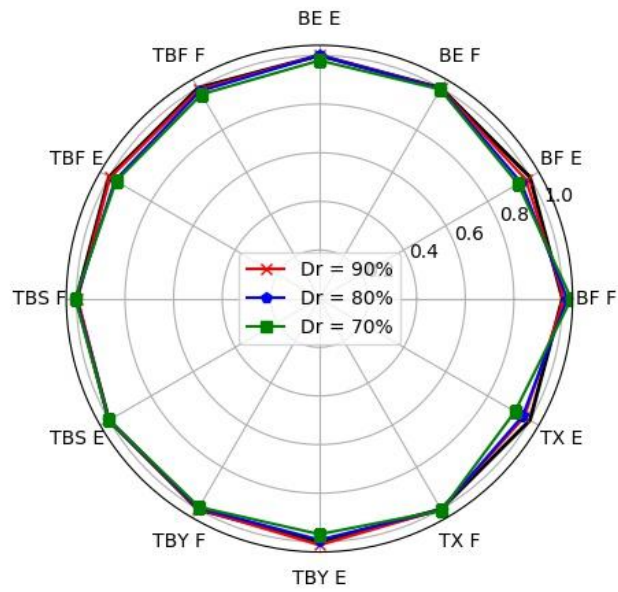
FIGURE 96: COMPARISON EXTREME AND FATIGUE MAXIMUM ROTATION WSP = 10M/S
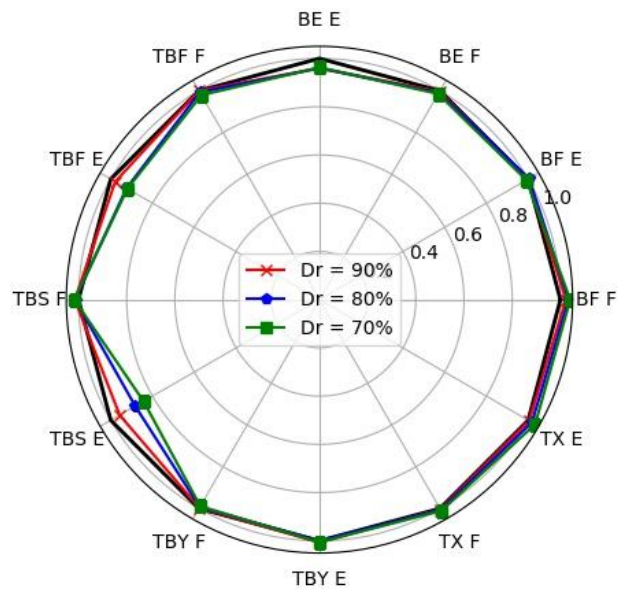
FIGURE 97: COMPARISON EXTREME AND FATIGUE MAXIMUM ROTATION WSP = 11M/S
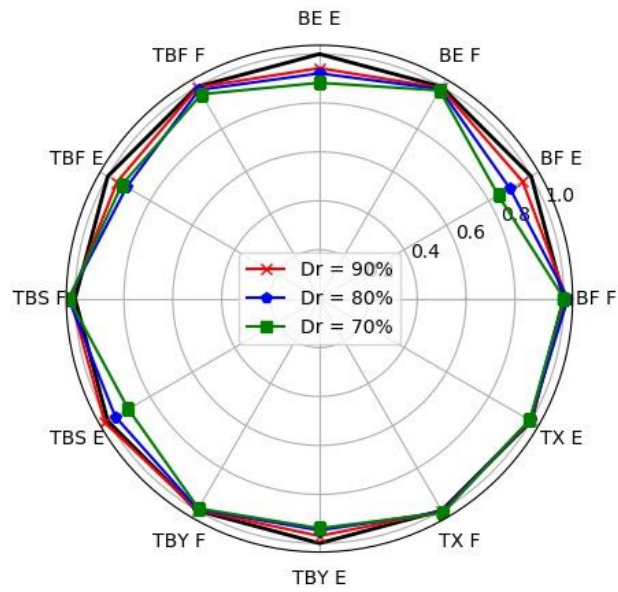
FIGURE 98: COMPARISON EXTREME AND FATIGUE MAXIMUM ROTATION WSP = 12M/S
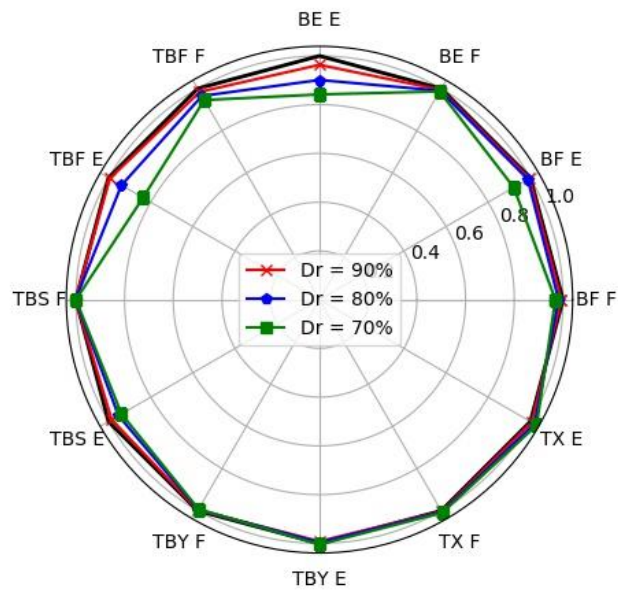
FIGURE 99: COMPARISON EXTREME AND FATIGUE MAXIMUM ROTATION WSP = 13M/S
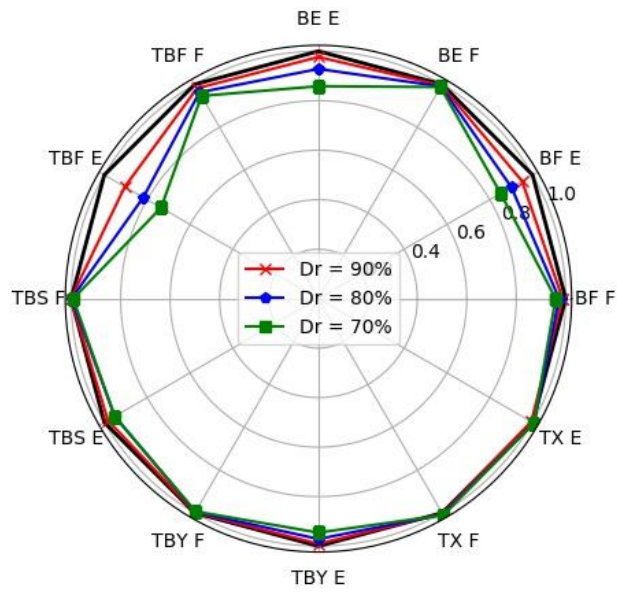
FIGURE 100: COMPARISON EXTREME AND FATIGUE MAXIMUM ROTATION WSP = 14M/S
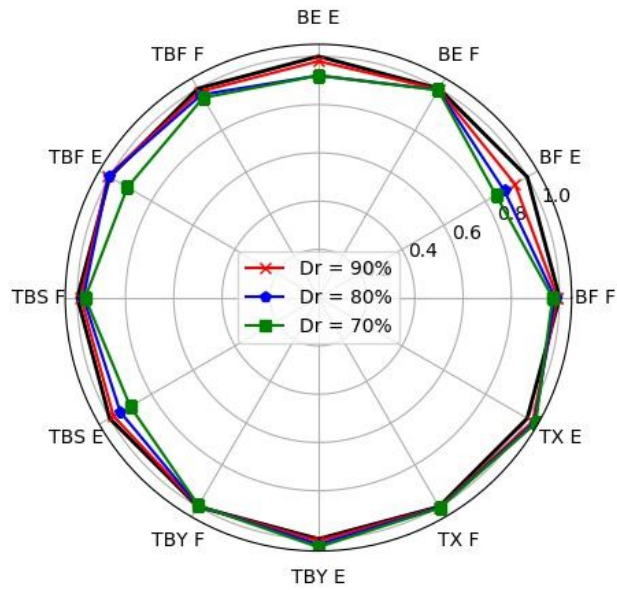
FIGURE 101: COMPARISON EXTREME AND FATIGUE MAXIMUM ROTATION WSP = 15M/S
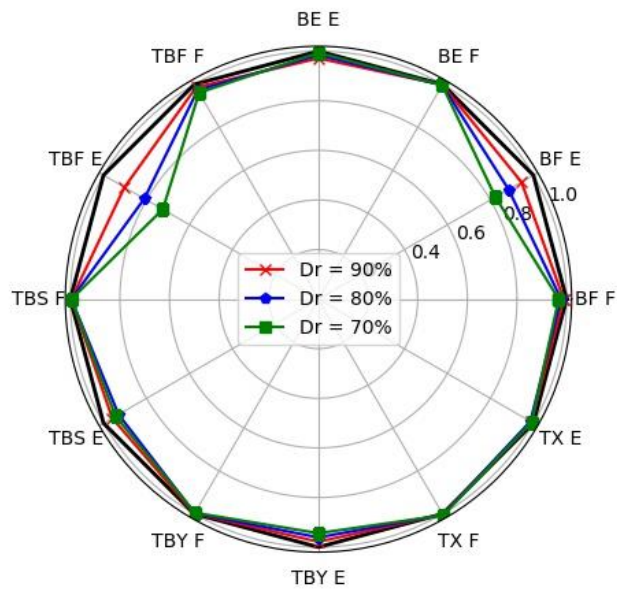
FIGURE 102: COMPARISON EXTREME AND FATIGUE MAXIMUM ROTATION WSP = 16M/S
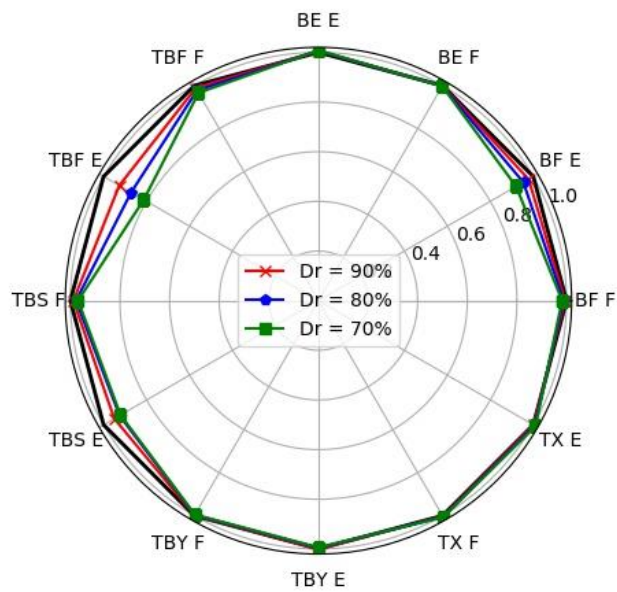
FIGURE 103: COMPARISON EXTREME AND FATIGUE MAXIMUM ROTATION WSP = 17M/S
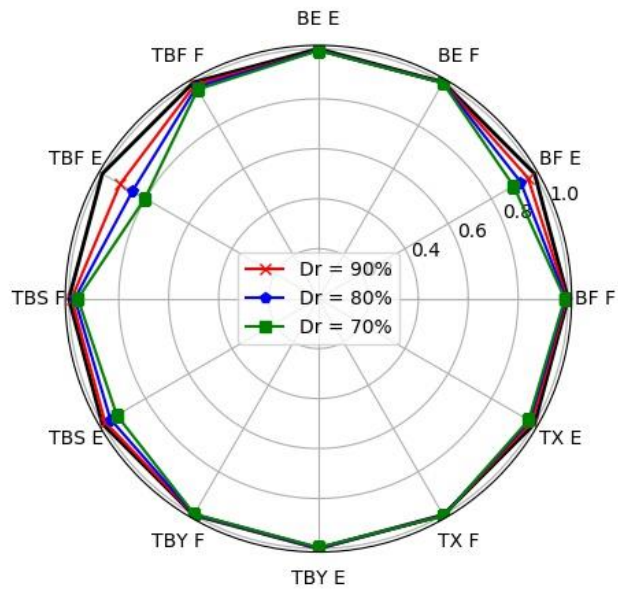
FIGURE 104: COMPARISON EXTREME AND FATIGUE MAXIMUM ROTATION WSP = 18M/S
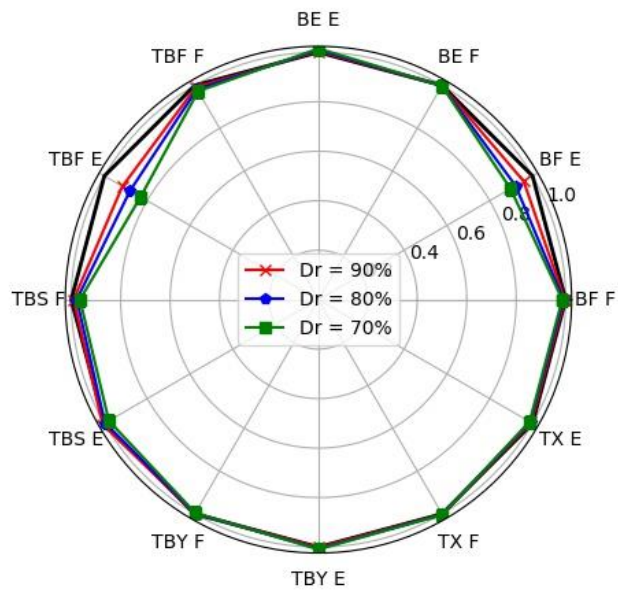
FIGURE 105: COMPARISON EXTREME AND FATIGUE MAXIMUM ROTATION WSP = 19M/S
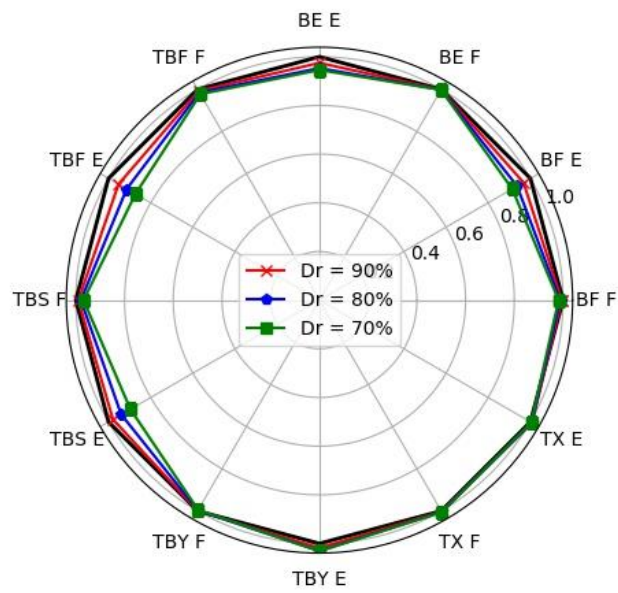
FIGURE 106: COMPARISON EXTREME AND FATIGUE MAXIMUM ROTATION WSP = 20M/S
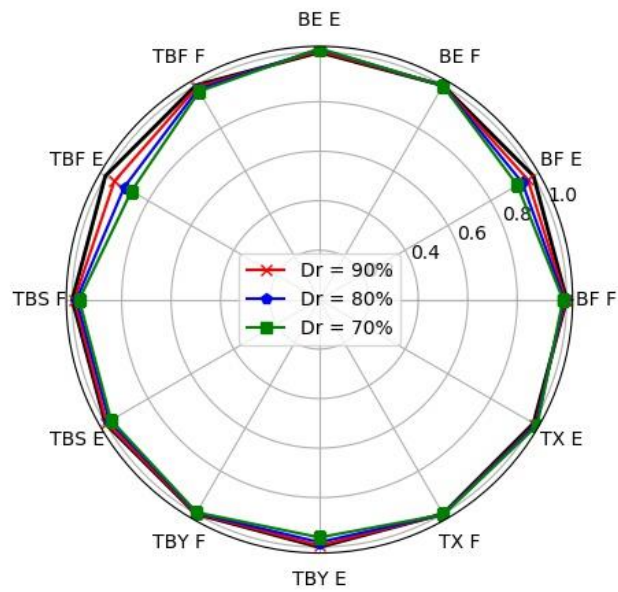
FIGURE 107: COMPARISON EXTREME AND FATIGUE MAXIMUM ROTATION WSP = 21M/S
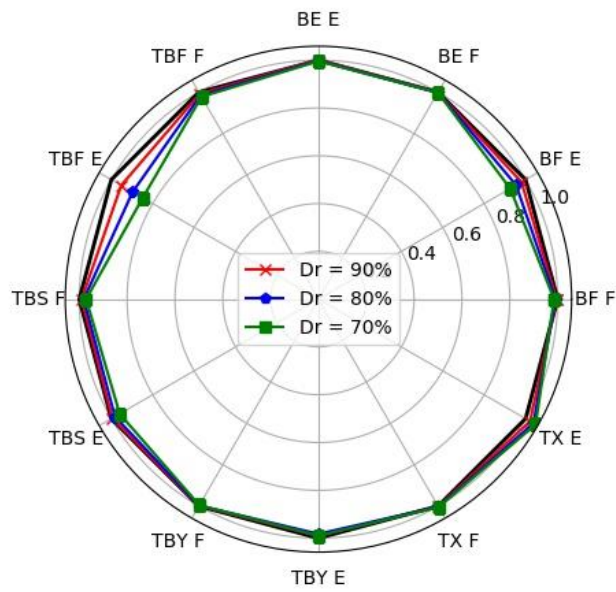
FIGURE 108: COMPARISON EXTREME AND FATIGUE MAXIMUM ROTATION WSP = 22M/S
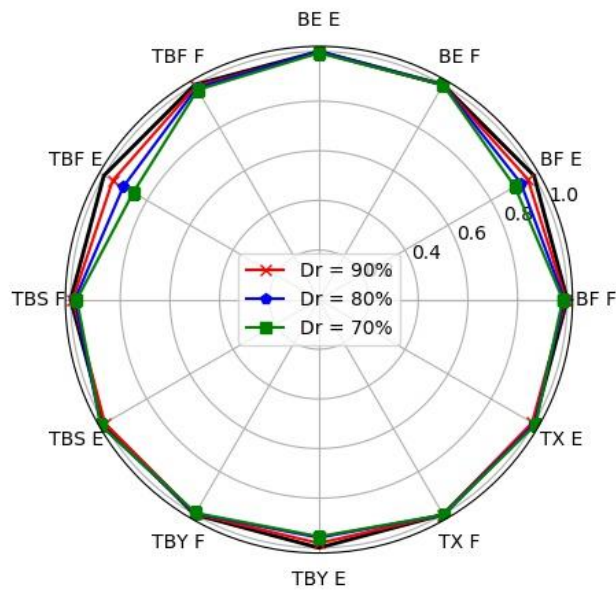
FIGURE 109: COMPARISON EXTREME AND FATIGUE MAXIMUM ROTATION WSP = 23M/S
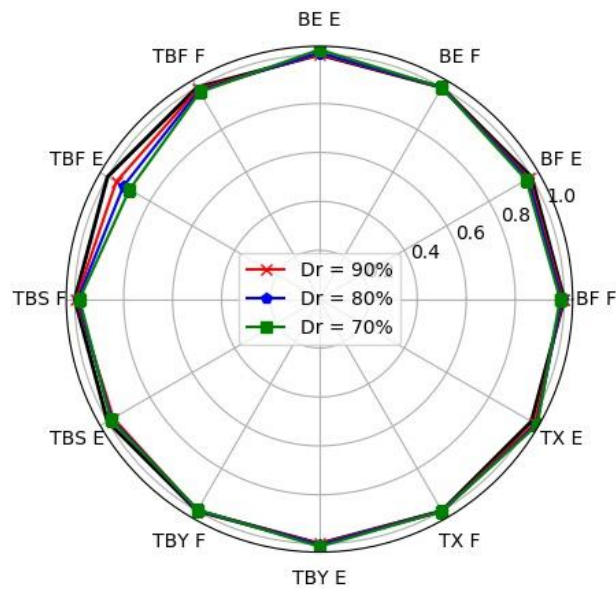
FIGURE 110: COMPARISON EXTREME AND FATIGUE MAXIMUM ROTATION WSP = 24M/S
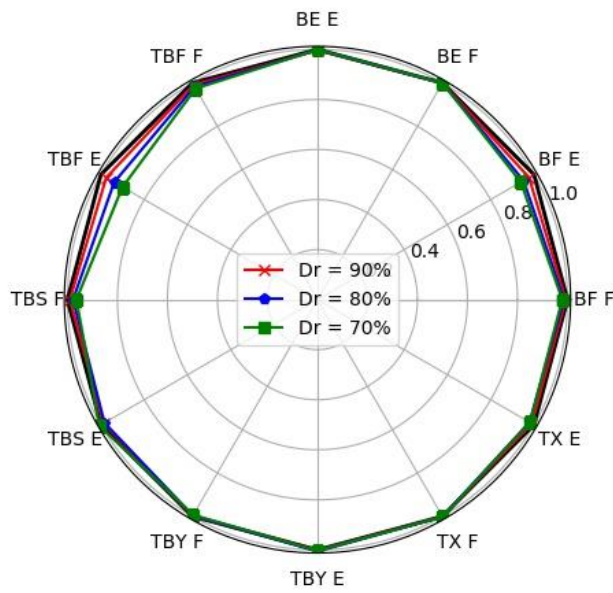
FIGURE 111: COMPARISON EXTREME AND FATIGUE MAXIMUM ROTATION WSP = 25M/S